Sektion für Sportorthopädie, Klinikum rechts der Isar
Prof. Dr. med. Sebastian Siebenlist

Schulterarthrose

Neue Entwicklungen in der Endoprothetik und 3-dimensionale Klassifikation

Kumulative Habilitationsschrift zur Erlangung der Venia Legendi

für das Fach Orthopädie und Unfallchirurgie an der Medizinischen Fakultät
der Technischen Universität München

vorgelegt von

Dr. med. Benjamin Daniel Kleim, MBBS, MRes

München, Oktober 2023

Fachmentorat:

1. **Prof. Dr. med. Sebastian Siebenlist**

   Sektionsleiter der Sektion für Sportorthopädie
   Klinikum rechts der Isar, Technischen Universität München

2. **Univ.-Prof. Dr. med. Peter Bieberthaler**

   Direktor der Abteilung für Unfallchirurgie
   Klinikum rechts der Isar, Technischen Universität München

3. **Prof. Dr. med. Stefan Buchmann**

   Facharzt für Orthopädie und Unfallchirurgie
   Orthopädisches Fachzentrum Weilheim | Garmisch | Starnberg | Penzberg

Meiner Familie.

Inhaltsverzeichnis

Abkürzungsverzeichnis

2D	Zweidimensional
3D	Dreidimensional
AHI	Acromiohumerales Intervall
AP	Anteroposterior (Röntgenaufnahme)
A-P	Anteroposterior (Subluxationsrichtung)
aTEP	Anatomische Totalendoprothese
AVN	Avaskuläre Nekrose
CT	Computertomographie
DA	Defektarthropathie
DSA	Degenerative Schulterarthrose
FR	Filling-Ratio
HP	Hemiprothese
HSA	Humeroscapuläre Ausrichtung
IA	Instabilitätsarthrose
iTEP	Inverse Totalendoprothese
KI	Konfidenzintervall
KoCr	Kobalt-Chrom
MCID	Minimaler für den Patienten bedeutsamer Unterschied
MRT	Magnetresonanztomographie
OA	Primäre Omarthrose
PTA	Posttraumatische Arthrose
PyC	Pyrocarbon
RA	Rheumatoide Arthritis
RM	Rotatorenmanschette
RSA	Reverse shoulder arthroplasty
SD	Standardabweichung
S-I	Superoinferior (Subluxationsrichtung)
TSA	Total shoulder arthroplasty
VAS	Visuelle Analogskala

1. Einleitung

Arthrose am Glenohumeralgelenk der Schulter entsteht sowohl durch primären Verschleiß der Knorpeloberflächen (primäre Omarthrose; OA), als auch durch chronische Rupturen der Rotatorenmanschette (Defektarthropathie; DA), chronische Instabilität (Instabilitätsarthrose; IA), rheumatoide Arthritis (RA), Avaskuläre Nekrose des Humeruskopfes (AVN) und nach intraartikulärer Fraktur (Posttraumatische Arthrose; PTA) [43]. Bei Versagen von konservativen Maßnahmen werden diese Erkrankungen mit zunehmender Häufigkeit durch Implantation von Schulterendoprothesen versorgt [22, 34]. Mit 14,5 Prothesenoperationen pro 100,000 Personenjahren ist das Schultergelenk, nach Hüfte und Knie, inzwischen das dritthäufigste Gelenk welches endoprothetischem Ersatz unterzogen wird [19, 22]. Bei steigender Inzidenz hat die Schulterendoprothetik in vergangenen Jahren an Bedeutung gewonnen und ist zunehmend (Verbesserung der Indikationsstellung, Prothesenmodelle, Planung und resultierenden Ergebnisse) in den Fokus der Wissenschaft gerückt [63, 72]. Diese Habilitation widmet sich Entwicklungen im Prothesendesign, resultierenden radiologischen und klinischen Ergebnissen, sowie der Entwicklung und Validierung einer neuartigen 3-dimensionalen Klassifikation zur degenerativen Schulterarthrose.

Zur verbesserten anatomischen Implantatpositionierung und Schonung der Knochensubstanz des proximalen Humerus, im Vergleich zu herkömmlichen diaphysär verankerten Schäften, wurden in den letzten Jahren metaphysär verankerte Kurzschaftprothesen entwickelt [10, 53]. Im Vergleich zu diaphysär verankerten Prothesen, weisen Kurzschaftprothesen eine physiologischere Kraftverteilung im proximalen Humerus auf [9, 57]. Hierdurch sollte auch das Problem des „Stress Shielding“ vermindert werden [9, 53, 67]. Stress Shielding beschreibt einen reaktiven Knochenumbauprozess, welcher entsprechend des Wolff’schen Gesetzes, bei Umleitung von Kräften durch den Prothesenschaft an die Diaphyse und dadurch resultierende Minderbelastung des metaphysären Knochens zum metaphysären Substanzverlust führt [51, 67]. Bei Kurzschaftprothesen der ersten Generation wurde jedoch eine hohe Lockerungsrate festgestellt, weshalb eine proximale poröse Beschichtung eingeführt wurde, um ein verbessertes Einwachsen des Knochens zu ermöglichen [3,

31, 50, 68]. Vorige Autoren hatten bereits begonnen Einwachseigenschsaften und knöcherne Umbauvorgänge (Lockerung, Implantat-Sinterung; Knochenresorption oder Sklerosebildung) bei diesen Schäften der 2. Generation zu beschreiben, jedoch blieb unklar wie diese im Zusammenhang stehen und welche Risikofaktoren diese beeinflussen [50, 56, 61]. In einer radiologischen Studie von Kurzschaftschulterprothesen der 2. Generation wurden diese Aspekte weiter analysiert (Teil 2.1.) [36].

Diese Kurzschaftprothesen der 2. Generation können durch Modularität sowohl als anatomische Totalendoprothese (aTEP), als auch inverse Totalendoprothese (iTEP) oder Hemiprothese (HP) konfiguriert und implantiert werden. Bei DSA werden aTEP bei Patienten mit intakter Rotatorenmanschette (RM), in Abwesenheit von hoher glenoidaler Retroversion (welche nicht auf <10° korrigiert werden kann) und in Abwesenheit von hoher posteriorer Subluxation (> 80% des Humeruskopfdurchmessers), präferentiell implantiert [27, 45]. Inverse Prothesen, welche mechanisch teilgekoppelt sind, kommen dahingegen bei rupturierter oder insuffizienter RM, bei hoher Retroversion, oder hoher Subluxation des Humeruskopfes, zum Einsatz [14, 28, 74]. Bei jungen Patienten (unter 50-60 Jahren) ist die Implantation einer aTEP, trotz intakter RM jedoch problematisch, da diese ein hohes Risiko von Lockerung der Glenoidalen Komponente als Komplikation tragen [11, 62, 66]. Daher werden bei Jungen Patienten HP bevorzugt [52]. Die Modularität der untersuchten Kurzschaftprothesen hat unter anderem zum Vorteil, dass bei Revisionsoperationen, falls der Schaft stabil eingeheilt sein sollte, lediglich ein modularer Austausch der Kopfkomponente, von anatomischer auf inverse Konfiguration, unter Belassung des Schaftes möglich ist [4, 58]. Klinische Ergebnisse nach Primärimplantation der jeweiligen Prothesenkonfigurationen mit diesem neuartigen Kurzschaft, für diverse Indikationen, fehlten jedoch. Eine Studie zur Nachuntersuchung des klinischen Erfolgs im kurz- bis mittelfristigen Nachuntersuchungszeitraum, wurde daher durchgeführt (Teil 2.2.) [37].

Bei dieser klinischen Auswertung wurde als HP ein Model mit neuartiger Pyrocarbon (PyC) Beschichtung der Kopfkomponente untersucht [37]. Herkömmliche HP verwenden einen Kobalt-

Chrom (KoCr) beschichteten Kopf. Ergebnisse hiermit sind jedoch wegen schmerzhaftem glenoidaler Knochenerosion, welche auch Revisionsoperationen erschwert, eingeschränkt [30, 55, 62, 66, 76]. PyC ist ein Kohlenstoffmaterial, das sich aus gasförmigen Kohlenwasserstoffverbindungen bei Temperaturen von 1000 bis 2500 Kelvin auf Trägermaterialien abscheidet [46]. Aufgrund von knorpelähnlichen biomechanischen Eigenschaften und einer extrem glatten Oberfläche, wird das Material zum einseitigen Gelenksersatz zur Schonung der gegenüberliegenden Gelenksfläche eingesetzt [17, 60]. Biomechanische Kadaverstudien am Glenohumeralgelenk und in vitro Laborstudien konnten bereits einen verminderten glenoidalen Abrieb und verbessertes biologisches Zusammenspiel mit Chondrozyten hinsichtlich Kollagenformation, im Vergleich zu herkömmlichen KoCr Prothesen, belegen [1, 21, 35]. An der Schulter werden PyC HP seit 2013 eingesetzt und kurzfristige Nachuntersuchungen konnten bereits eine gute klinische Funktion erweisen [6, 17]. Mittelfristig wurde durch eine Registerstudie ebenfalls eine niedrigere Revisionsrate mit PyC im Vergleich zu KoKr HP dargelegt [49]. Mittelfristige klinische und radiologische Daten fehlen jedoch weiterhin, bis wir diese im Sinne einer Kohortenstudie publizierten (Teil 2.3.) [40].

Degenerative Schulterarthrose (DSA) wird bisher entweder als OA in der axialen Ebene oder DA in der coronaren Ebene beschrieben. Die weit verbreitete Walch-Klassifikation und dessen Modifikationen (durch Bercik 2016 und Iannotti 2017) beschreibt Glenoidmorphologie und Glenohumerale Subluxation in der axialen Ebene [2, 25, 73]. Dahingegen beschreiben die Klassifikationen nach Hamada, Visotsky-Seebauer und Favard die DA mit glenohumeraler Subluxation und resultierender exzentrischer Glenoiderosion in der coronaren Ebene (anteroposteriore [AP] Röntgenaufnahme) [15, 20, 71]. Bei der vorausgegangenen Klassifizierung für die klinische Auswertung von Kurzschaftschulterprothesen (Teil 2.2.), ist mir jedoch aufgefallen, das ein Anteil der Patienten in beiden Ebenen eine Exzentrizität aufweisten [37]. In den letzten Jahren wurde in der Literatur zudem zunehmend von biplanarer Exzentrizität von glenoidaler Erosion berichtet [29, 41, 54, 65, 69]. Es ist gezeigt worden, dass eine degernerative Verfettung der zentrierenden dorsalen oder ventralen RM-Muskulatur der jeweils posterioren oder anterioren Dezentrirung des Glenohumeralgelenks vorausgeht [12, 23, 75]. Des Weiteren ist eine sekundäre Degeneration und

Insuffiziens der RM bei fortschreitender OA bekannt [13]. OA und DA sind daher am ehesten nicht als eindeutig abgrenzbare Pathologien anzusehen, sondern es besteht ein Schnittpunkt zwischen beiden formen der DSA. Keine der bestehenden 2-dimensionalen (2D) Klassifikationen beschreiben biplanare Exzentrizität bei DSA [2, 15, 20, 25, 71, 73]. In einer Computertomographie (CT) Studie mit 3-dimensionaler (3D) Rekonstruktion, bei einem Patientenkollektiv mit DAS, erfolgte zunächst die Einteilung nach etablierten 2D Klassifikationen (Hamada, Favard und modifizierte Walch) [2, 15, 20, 25, 38]. Hierbei konnte eindeutig eine unzureichende Erfassung, der in vielen Fällen bestehenden, biplanaren Subluxation, festgestellt werden [38]. Daraufhin wurde die biplanare humeroscapuläre Ausrichtung und begleitende glenoidale Erosion, gemessen und für Klassifikationsnutzen kategorisiert (Teil 2.4.) [38].

Bereits etablierte Klassifikationen zur Schulterarthrose weisen eine mittelmäßige bis beachtliche Intra-Beobachter Übereinstimmung, aber nur geringfüfgig bis mittelmäßige Inter-Beobachter Übereinstimmung auf (Tabelle 1) [24, 26, 32, 59, 64]. Der zeitliche Aufwand sowie die unklare Reproduzierbarkeit der vergleichsweise komplexeren neuen 3D Klassifikation warfen Fragen zum Nutzen dieser auf. Die publizierte 3D Klassifikation zu DSA wurde daher in einer Folgestudie hinsichtlich Validität und Reproduzierbarkeit unter zeitlich eingeschränkter Anwendung untersucht (Teil 2.5.) [39].

Tabelle 1: Zusammenfassung einer PubMed-Suche nach Studien zur Untersuchung der Intraobserver- und Interobserver-Übereinstimmung für die Walch- oder modifizierte Walch-Klassifikation, die in den letzten 5 Jahren veröffentlicht wurden, sowie für die Hamada-, Visotsky-Seebauer- und Favard-Klassifikationen, die in den letzten 15 Jahren veröffentlicht wurden

Study	Classifications investigated	Imaging modality	Intraobserver agreement	Interobserver agreement
Ricchetti et al. 2021 [59]	**Modified Walch**	CT using 3D image viewer	Moderate to substantial (κ = 0.51 – 0.61)	Moderate (κ = 0.43)
Hopkins et al. 2021 [24]	**Walch**	CT and MRI	CT: Substantial (κ = 0.71) MRI: Substantial (κ = 0.71)	CT: Fair (κ = 0.29) MRI: Fair (κ = 0.34)
Shukla et al. 2019 [64]	**Modified Walch**	X-ray and CT	CT: Substantial (κ = 0.73) X-ray: Substantial (κ = 0.73)	CT: Moderate (κ = 0.52) X-ray: Moderate (κ = 0.55)
Kappe et al. 2011 [32]	**Hamada**, **Visotsky-Seebauer** and **Favard**	X-ray	Hamada: Substantial (κ = 0.75) V-S: Substantial (κ = 0.73) Favard: Substantial (κ = 0.76)	Hamada: Moderate (κ = 0.41) V-S: Moderate (κ = 0.55) Favard: Fair (κ = 0.31)
Iannotti et al. 2010 [26]	**Visotsky-Seebauer**, **Favard** and **Hamada**	X-ray	V-S: Substantial (κ = 0.69) Hamada: Almost perfect (κ = 0.87) Favard: Moderate (κ = 0.59)	V-S: Fair (κ = 0.39) Hamada: Moderate (κ = 0.42) Favard: None to slight (κ = 0.13)

2. Hauptteil

2.1. Kurzschaftschulterprothesen: Radiologische Einwachseigenschaften und Risikofaktoren für Knochenumbauvorgänge

Originalarbeit:
Kleim BD, Garving C, Brunner UH. Cementless curved short stem shoulder prostheses with a proximal porous coating: ingrowth properties at 2-5 years of radiological follow-up with clinical correlation. JSES 2020. 29(11):2299-2307. PMID: 32666922.

2.1.1. Methodik

Studiendesign

Konsekutive Kohortenstudie von 74 aus 103 möglichen Patienten, welche zwischen Mai 2013 und Juni 2015 mit einer modularen Kurzschaftschulterprothese der zweiten Generation mit proximaler poröser Beschichtung (Aequalis Ascend flex™, Fa. Tornier) im Krankenhaus Agathariedoperiert wurden. Implantiert wurden diese Prothesen als aTEP, iTEP oder PyC Hemiprothesen. Alle 103 Patienten wurden zu Nachuntersuchungen eingeladen, für 76 dieser Patienten waren klinische Nachuntersuchungsdaten verfügbar, für 74 dessen waren zusätzlich Röntgenaufnahmen von adäquater Qualität und Projektion vorhanden. Der Nachuntersuchungszeitraum betrug 2-5 postoperative Jahre (Mittelwert 35 Monate). Neun der möglichen 103 Patienten hatten Komplikationen welche zur Revision führten oder diese Patienten nicht mehr vergleichbar mit dem Rest des Kollektivs machten, weshalb sie ausgeschlossen wurden (in Teil 2.2. detailliert aufgeführt). Die anderen 18 Patienten waren für die Nachuntersuchung verloren (wegen Altersschwäche, Tod (in keinem Fall in Zusammenhang mit der Schulteroperation) oder nicht Erscheinen zu den Nachuntersuchungen in unserer Klinik wegen weiter Anreise.

Prothesendesign und Operationstechnik

Der gekrümmte Titan-Kurzschaft mit proximaler poröser Beschichtung welcher modular in drei Konfigurationen (aTEP, iTEP und PyC Hemiprothese) eingesetzt wurde wird „Press-Fit“ implantiert. Der ovalförmige Schaft verfolgt hierbei den Weg des geringsten Widerstandes, wodurch eine naturgemäße Retrotorsion erreicht wird. Die Prothesen wurden durch einen deltoideopektoralen Zugang mit Ablösen der Subscapularissehne in „peel-off“ Technik. Der Humeruskopf wurde entsprechend des Prothesentyps reseziert (siehe unten). Der proximale Humerus wurde sequenziell

mit einem Kompaktor von aufsteigender Größe präpariert und kompaktiert, und daran abgeleitet die Schaftgröße bestimmt. Die Stabilität des Schaftes wurde mit dem Twist-Test bestätigt. Alle Schäfte in dieser Serie wurden unzementiert implantiert. Nach Implantation der Prothese wurde die Subscapularissehne in transossärer doppelreihiger Nahttechnik refixiert.

iTEP Technik

Für inverse Prothesen wurde die Resektion mit einer 132,5° Inklination, durch Nutzen eines Zielinstrumentariums, durchgeführt. Hierdurch wird eine finale Inklination von 145°, nach Anbringen des 12,5° Inlays, erzielt. Die Höhe der Resektion sollte so vorgenommen werden das der höchste Punkt der Pfanne auf Höhe der Spitze des Tuberculum majus zu liegen kommt. Die Glenoid Basisplatte wurde inferior abschließend mit dem Glenoidrand und mit 0-10° Inklination und < 10° Retroversion implantiert. In Fällen, in denen die Retroversion mehr als 10° betrug wurde diese mit Benutzen eines keilförmigen autologen Knochentransplantats (aus dem resezierten Humeruskopf) unter der Basisplatte korrigiert (4 Fälle). Zusätzlich wurde in 2 Fällen mit hochgradiger konzentrischer Glenoid Erosion eine Lateralisierung mittels autologer Knochentransplantation unter der Basisplatte vorgenommen. Die Größe der Glenoidkomponente (25 oder 29 mm Durchmesser) wurde entsprechend dem nativen Glenoiddurchmesser ausgewählt. Bei Frauen wurde eine metaglenen Größe von 36 mm und bei Männern von 42 mm gewählt und diese wurde mit einem inferioren Überhang von mindestens 5 mm implantiert. Die humeralen Probekomponenten wurden reponiert und die Stabilität und Vorspannung des Musculus deltoideus kontrolliert, die Höhe des Inlays gegebenenfalls in Abhängigkeit davon angepasst. Letztlich wurde die definitive Prothese zusammengesetzt und implantiert.

aTEP Technik

Für die anatomische Prothese wurde eine Freihandresektion entlang des anatomischen Halses des Humerus, nach Entfernung von Osteophyten, durchgeführt. Die den Patienten eigene Inklination wurde dann mit entweder 127,5°, 132,5° oder 137,5° Konfiguration nachgebildet. Ein so gering wie mögliches Fräsen des Glenoids zur Herstellung einer monokonkaven Fläche, unter Belassen des harten kortikalen Knochens, wurde entsprechend des gemessenen nativen Krümmungsradius durchgeführt. Ein gekieltes zementiertes Polyäthylenglenoid wurde daraufhin implantiert. Die

femorale Probeprothese mit der nötigen Kopfkomponente um eine adäquate Delta-Vorspannung und Stabilität zu erreichen wurden reponiert und klinisch untersucht. Daraufhin wurde die definitive humerale Prothese zusammengesetzt und implantiert.

PyC. Hemiprothese

Die Technik zur Präparation der humeralen Komponente entsprach der welche bereits für die aTEP beschrieben wurde. Die Gelenkskapsel wurde reseziert, das Labrum, sofern vorhanden, belassen. In Fällen mit exzentrischer wegkonkaver Erosion des Geräts wurde eine sparsame konzentrische Fräsung, zur Wiederherstellung einer konzentrischen Gelenkspaarung, durchgeführt. Verbliebene Sklerosezonen wurden durch Bohrungen mit einem 1,2 mm Kirschnerdraht unterbrochen. Die Größe und Ausrichtung der humeralen Kopfkomponente gegebenenfalls mit Exzentrizität) wurden daraufhin zur maximalen Deckung der resezierten Oberfläche, unter Vermeidung von Überhang, gewählt und Probe-reponiert. Daraufhin wurde der definitive Schaft implantiert und die PyC Kopfkomponente mit dem Federimpaktor aufgesetzt.

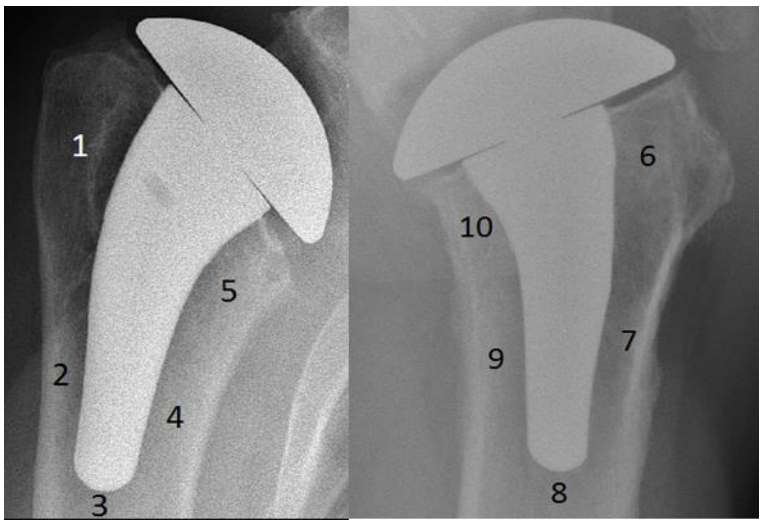

Abbildung 1: Die 10 Zonen im AP (links) und axialen (rechts) Röngenbild, anhand wessen die Lokalisierung von Knochenumbauvorgängen beschrieben wurde [36].

Radiologische Auswertung

Die Analyse der Einwachseigenschaften des Schaftes anhand der Röntgenbilder in 3 Ebenen wurde am Befundungsmonitor von 2 wissenschaftlich und orthopädisch erfahrenen Beobachtern (BDK und CG) unabhängig voneinander durchgeführt, und daraufhin ein Konsens gefunden. Die Methodik welche von Denard et al. publiziert wurde diente als Basis des Bewertungsprotokolls[10]. Die Lokalisation in welcher sich Umbauvorgänge ereigneten wurde anhand von 10 vorbeschriebenen

Zonen kategorisiert (Abbildung 1)[10]. Das Filling-Ratio (FR) wurde als Mittelwert von vier Messungen des Knochen- versus Prothesendurchmessers an 4 Stellen (zwei im AP und zwei im axialen Röntgenbild) ermittelt (Abbildung 2). Um eine bessere Trennung der Knochenresorption zu ermöglichen wurde eine neuartige Punkte Bewertung angewandt: Diese kategorisierte Resorptionszonen als partiell (Osteopenie) oder komplett (Kollaps der Knochensubstanz um den Prothesenschaft) und bewertete diese mit 1 bzw. 2 Punkten pro Zone, in welcher Resorption vorgefunden wurde. Zudem wurden knöcherne Hypermineralisierungen im Sinne von Sklerosezonen sowie die Schaftausrichtung (Varus, Valgus oder zentriert) notiert.

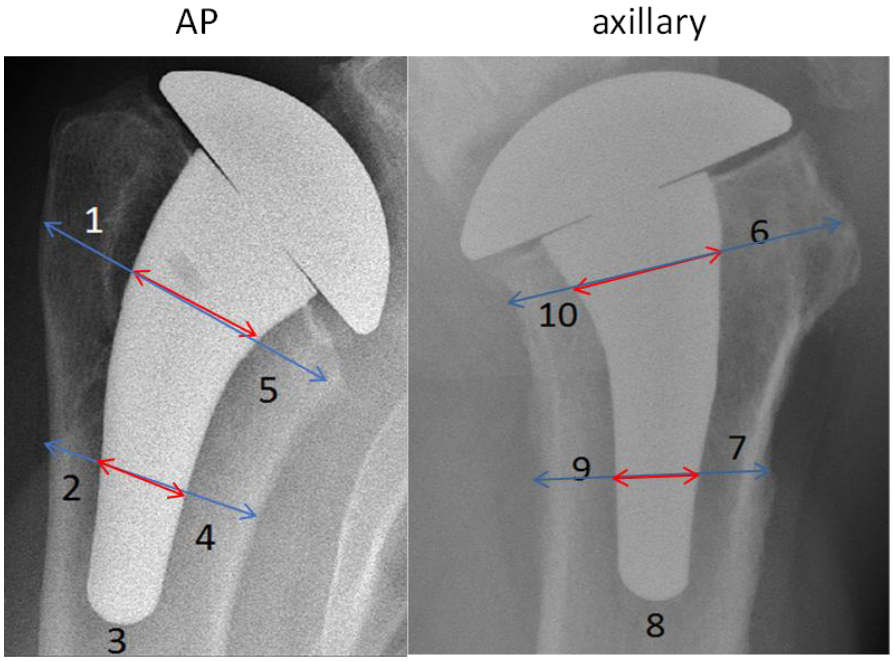

Abbildung 2: Methode zur Ermittlung des FR in zwei Ebenen. Der Mittelwert der vier Verhältnismessungen (rot/blau) wird genommen [36].

Klinische Evaluation

Der umfangreiche und validierte Constant Score (CS) wurde präoperativ und bei letzter Nachuntersuchung ermittelt um das klinische Ergebnis zu quantifizieren[7]. Um die vorhandenen Unterschiede in der Patientendemografie zu berücksichtigen wurden bei Vergleichen zwischen Patienten und Prothesentypen Deltawerte (postoperativer – präoperativer Wert) verwendet.

Statistik

Da alle Patienten in der Kohorte in Betracht gezogen wurden wurde auf eine Powerkalkulation verzichtet. Multiple lineare Regressionsmodelle, sowie hierarchische multiple lineare Regressionsmodelle, wurden zur Bewertung der Effektgröße und Signifikanz von möglichen

interagierenden Einflussfaktoren angewandt. Dies wurde unter Anwendung der Statistiksoftware SPSS V25.0 (IBM) durchgeführt.

2.1.2. Ergebnisse

Demografie

Die Demografie-Daten zu der Studienkohorte sind in Tabelle 2 abgebildet.

Tabelle 2: Demografie der Patientenkohorte

	Number	Age (years)	Sex	Diagnoses	Follow-up (months)
TSA	21	71.1 (range 62-84)	14 Female	21 primary osteoarthritis	34 (range 23-52)
RSA	32	74.1 (range 65-84)	26 Female	7 primary osteoarthritis, 24 cuff tear arthropathy, 1 irreparable rotator cuff tear	39 (range 23-60)
PyC	21	58.3 (range 22-84)	4 Female	14 primary osteoarthritis, 1 fracture sequelae, 3 avascular necrosis, 3 arthritis resulting from instability	29 (range 23-48)

Prothesensitz

55 der Prothesenschäfte waren zentriert, 14 mit Valgus- und 5 mit Varusausrichtung implantiert. Das FR betrug im Mittelwert 0,54 (Bereich 0,36-0,75). Im gesamten Kollektiv wurden weder Einsinken noch Dislokation des Schaftes beobachtet.

Tabelle 3: Frequenz von Knochenumbauvorgängen

Bony adaptation	Number of cases
Periprosthetic lucency	2 (each 1 mm in zone 1)
Reactive bony sclerosis	14
Partial thickness resorption	30
Full thickness resorption	8

Knochenumbauvorgänge

Die beobachteten Knochenumbauvorgänge sind in Tabelle 3 aufgeführt. Abbildung 3 zeigt ein Beispiel von reaktiver knöcherner Sklerose distal um einen großen Schaft. Zehn Patienten wiesen Sklerosierung in Zone 3, vier in Zone 2 und drei in Zone 4 auf. Vier Patienten hatten zudem reaktive Sklerose in den proximalen Zonen: Drei Patienten in Zone 1 und eine Patientin in Zone 6. Diese standen jeweils im Zusammenhang mit Sklerosierung in der zentralen distalen Zone (drei Fälle) oder

in Zone 2 (lateral distal, ein Fall). Alle Fälle mit Sklerosierung in den proximalen Zonen hatten eine zentrierte Ausrichtung des Schaftes. Patienten mit Sklerose in Zone 3 hatten in neun von zehn Fällen eine zentrierte Schaftausrichtung. Sklerose in Zone 2 ereignete sich nie bei Valgusausrichtung des Schaftes, sondern immer bei zentrierter oder bei Varusausrichtung. Zwei der Patienten mit knöcherner Sklerosebildung hatten eine Valgus-Schaftausrichtung und in beiden Fällen befand sich die Sklerose ausschließlich in Zone 4.

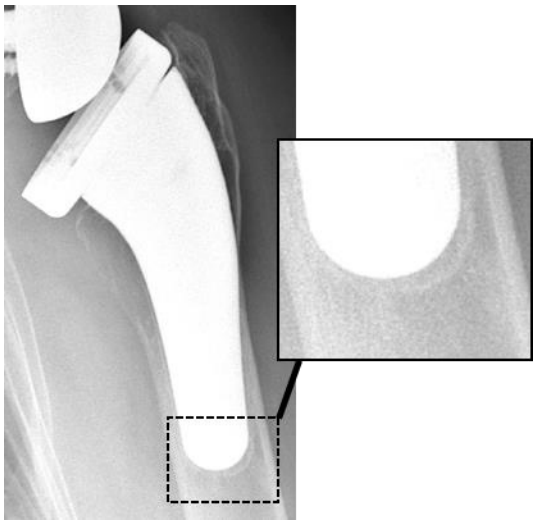

Abbildung 3: Reaktive knöcherne Sklerose distal um einen großen Schaft. Proximal medial zeigt sich eine partielle Knochenresorption [36].

Knochenresorption wurde in 30 Patienten (40,5%) festgestellt. Von diesen hatten 22 mindestens eine Zone mit partieller Knochenresorption und 8 (10,8%) zusätzlich eine oder mehr Zonen mit kompletter Knochenresorption. Die Anzahl von Patienten mit Knochenresorption (partiell oder komplett) in den 10 Zonen wird in Abbildung 5 gezeigt. Partielle Resorption wurde radiologisch erstmals nach durchschnittlich 16,6 Monaten (Bereich 3 - 40 Monate) gesehen. Der durchschnittliche Resorptionsscore (siehe Methodik) betrug 0,84 Punkte (Bereich 0 - 6). Abbildung 4 zeigt ein Bespiel von kompletter zonenbezogener periprothetischer Knochenresorption.

Abbildung 4: Beispiel eines Falles mit kompletter Knochenresorption in der proximalen Zone 1 sowie im Übergang von Zone 1 zu Zone 2. Zusätzlich partielle Resorption in Zone 5 [36].

Der Übergang von partieller zu kompletter Knochenresorption ergab sich im Mittelwert nach 32 Monaten (Bereich 10 - 49).

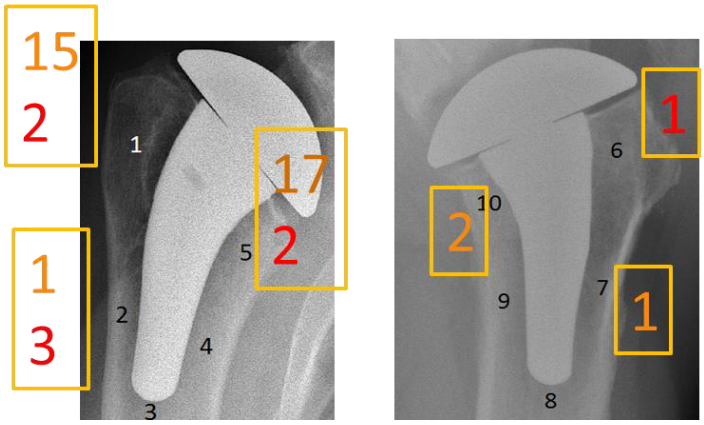

Abbildung 5: Anzahl der Fälle mit partieller (orange, obere Zahl) und kompletter (rot, untere Zahl) Knochenresorption in den entsprechenden Zonen.

Es wurde beobachtet das im Verlauf die Knochendensität abnahm und sich eine Osteopenie mit Ausdünnung der Kortikalis entwickelte. Daraufhin kollabierte die Knochenstruktur vollständing auf den Prothesenschaft, wie in Abbildung 6 gezeigt.

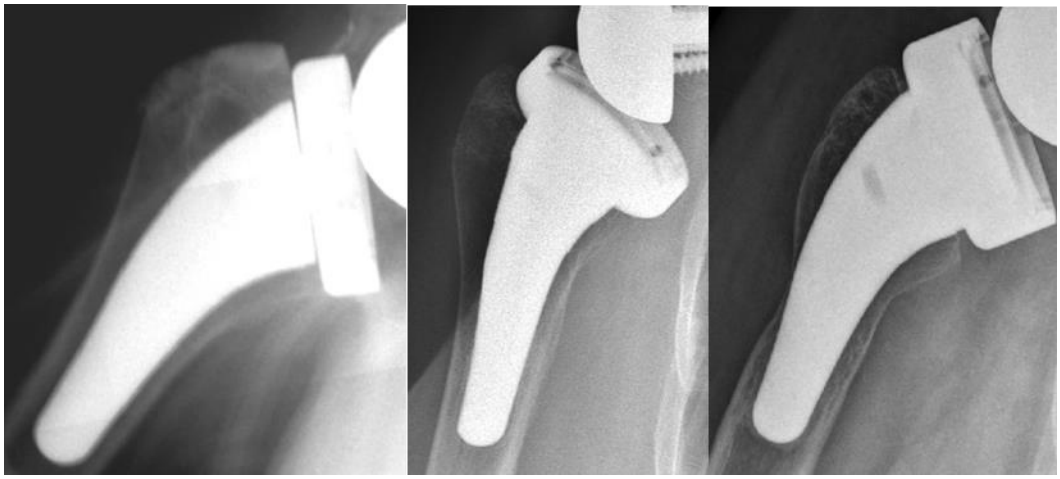

Abbildung 6: Chronologischer Verlauf des Knochenumbaus bei einer 69-jährigen Patientin mit iTEP. Direkt postoperativ (linkes Bild) zeigt sich ringsherum eine gute Knochensubstanz. Nach 24 Monaten (mittleres Bild), zeigt sich eine Osteopenie proximal und nach 37 Monaten der Kollaps der Kortikalis auf den Prothesenschaft. Derweil entwickelt sich distal um die Schaftspitze eine Hyperdensität der Spongiosa [36].

Korrelation der Einflussfaktoren

Die Ergebnisse der multiplen linearen Regressionsanalyse sind in Tabelle 4 aufgeführt. Es ergab sich eine starke Korrelation zwischen FR und Knochenresorption ($p < 0{,}001$), besonders wenn das FR über 0,55 lag (siehe Abbildung 7).

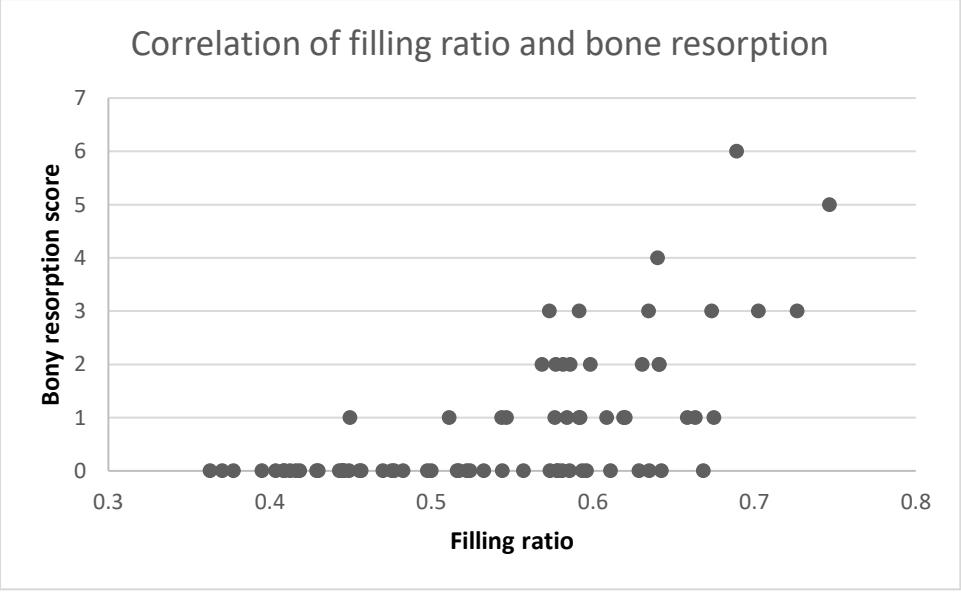

Abbildung 7: Graphik zum Verhältnis zwischen FR und Knochenresorption. Bei einem FR von über 0,55 kommt es zunehmend zu hochgradiger Resorption [36].

Alter und Geschlecht beeinflussten 51% der Verteilung im FR ($p < 0{,}001$). Knochenresorption hatte keinen Einfluss auf die Funktion im CS ($p = 0{,}17$). Die Operationsdiagnose hatte keinen Einfluss auf das FR ($p = 0{,}59$) oder auf die Knochenresorption ($p = 0{,}69$). Die Prothesenart zeigte keine Korrelation mit der Knochenresorption ($p = 0{,}47$). Varus- oder Valgusausrichtung des Schaftes

bedingte weder die Formation von knöcherner Sklerosierung (p = 0.93) noch beeinflusste es Knochenresorption (p = 0,42). Ein höheres FR war prädiktiv für Sklerosierung der Spongiosa und war für 8,1% der Verteilung dessen verantwortlich (p = 0,019).

In einem hierarchischen linearen Regressionsmodell, in welchem zuerst für den Einfluss von FR korrigiert wird, hatten Alter (p = 0,22) und Geschlecht (p = 0,95) keinen unabhängigen Einfluss auf die Knochenresorption. Die Entwicklung von reaktiver knöcherner Sklerose schien, wenn unabhängig getestet, einen Einfluss auf die Knochenresorption zu haben (p = 0,003). Wenn aber zuerst für die Kollinearität mit FR korrigiert wurde, bedingte Sklerose nur 3% der Verteilung des Knochenresorptionsscore und war statistisch insignifikant (p = 0,058). Ein direkter Vergleich zwischen aTEP- und iTEP-Patienten hinsichtlich Knochenresorption in Zone 1, welche sich bei Abwesenheit von Krafteinleitung durch die fehlende RM in iTEP-Patienten möglicherweise unterscheiden würde, zeigte keinen signifikanten Unterschied (p = 0,081).

Tabelle 4: Zeigt die Auswirkung unabhängiger Variablen auf abhängige Variablen. Das Ausmaß, in dem die unabhängigen Variablen die Verteilung der abhängigen Variablen beeinflussten, wird in % angezeigt, die Signifikanz in Form eines p-Werts. Alter und Geschlecht wurden in Kombination getestet, da sie in unserer Kohorte kollinear waren (Männer waren jünger).

Correlation	variability influenced	p-value
Filling ratio with bone resorption score	39%	<0.001
Age and sex with filling ratio	51%	<0.001
Age and sex with bone resorption score	18%	0.00067
Bone resorption score with constant score	2.6%	0.17
Diagnosis with filling ratio	0.39%	0.59
Diagnosis bone resorption score	0.22%	0.69
Filling ratio with reactive sclerosis	8.1%	0.019
Varus/valgus alignment with reactive sclerosis	0.0016%	0.93
Varus/valgus alignment with bone resorption score	0.89%	0.42
Prosthesis type with bone resorption	0.71%	0.47
Reactive sclerosis with bone resorption score	11%	0.003
RSA vs TSA on resorption score	9.8%	0.021
RSA vs TSA on filling ratio	36%	<0.001
RSA vs TSA on resorption score in zone 1	5.7%	0.081
When correcting for the effect of filling ratio first:		
Age and sex with bone resorption score	1.3%	0.22 and 0.95 respectively
Reactive sclerosis with bone resorption score	3.0%	0.058
RSA vs TSA on resorption score	0.19%	0.70

2.1.3. Schlussfolgerung

Unzementierte Kurzschaftschulterprothesen mit einer proximalen porösen Beschichtung sind nach 2 bis 5 Jahren fest verankert, was scheinbar eine Verbesserung zu dem Vorgängermodell darstellt. Insgesamt verankern große Schäfte (mit einem FR von > 0,55) distal und dies wird oft von einer hyperdensen reaktiven Sklerosierung der Spongiosa in den distalen Zonen begleitet. Die Entwicklung von solcher Sklerosierung kann bei der Nachuntersuchung als Anzeichen von hohem FR interpretiert werden. Die resultierende Minderbelastung des proximalen Knochens führt in der Folge auch zu Knochenresorption hier. Ältere Patienten weiblichen Geschlechts haben ein erhöhtes Risiko für ein hohes FR und dadurch indirekt ein höheres Risiko für Knochenumbauvorgänge. Besonders bei diesen Patienten sollte also darauf geachtet werden, dass entweder eine adäquate Stabilität mit einem

ausreichend kleinen Schaft erlangt wird, ggf. durch autologe Spongiosatransplantation aus dem abgesetzten Humeruskopf. Falls dies nicht möglich ist, sollte eine Zementierung des Schaftes in Erwägung gezogen werden.

2.2. Klinische Ergebnisse nach Implantation einer modularen Kurzschaftschulterprothese in drei Konfigurationen

Originalarbeit:
Kleim BD, Garving C, Brunner UH. RSA, TSA and PyC-Hemiprostheses: Comparing indications and clinical outcomes using a second-generation modular short stem shoulder prosthesis. AOTS 2020. DOI: 10.1007/s00402-020-03529-w. PMID: 33025070.

2.2.1. Methodik

Studiendesign

Monozentrische Kohortenstudie von 103 Patienten, welche zwischen Mai 2013 und Juni 2015 im Krankenhaus Agatharied eine modulare Kurzschaftschulterprothese mittels gebogenen unzementierten Titanschaft mit proximaler poröser Beschichtung (Aequalis Ascend flex™, Fa. Tornier), erhielten. Alle Patienten wurden zu regelmäßigen Nachuntersuchungen einbestellt. Die Operationen wurden jeweils von einem von 2 erfahrenen Schulterchirurgen über einen deltopectoralen Zugang mit anschließender doppelreihiger Refixation der Subscapularissehne durchgeführt. Präoperativ wurden sowohl Röntgenaufnahmen in 3 Ebenen, als auch eine Magnetresonanztomografie (MRT) und Computertomografie (CT) angefertigt. Die glenoidale Retroversion wurde anhand der Friedmann-Linie und die Inklination entsprechend des Maurerwinkels berechnet [16, 48]. Die Glenoidmorphologie wurde entsprechend der modifizierten Klassifikation nach Walch beschrieben [2].Die modulare Prothese wurde in 3 verschiedenen Konfigurationen, entsprechend der vorliegenden Pathologie, als PyC Hemiprothese, aTEP oder iTEP implantiert: Patienten mit primärer Omarthrose, intakter Rotatorenmanschette und glenoidaler Retroversion von < 10°, sowie posteriorer glenohumeraler Subluxation < 80° wurden mit aTEP versorgt; Patienten mit intakter Rotatorenmanschette, jungem Alter oder erhöhtem Risiko eines mechanischen Versagens einer anatomischen Glenoidkomponente (z.B. Walch Typ B2 Morphologie) erhielten die PyC Hemiprothese; bei Patienten mit Rotatorenmanschettenrupturen, glenohumeraler Subluxation von mehr als 80° oder Retroversion von mehr als 10° wurde eine iTEP implantiert. In Fällen, in denen die Retroversion mehr als 10° betrug, wurde diese mittels autologem Knochenaufbau (keilförmig) unter der Basisplatte korrigiert (4 Fälle). In 2 weiteren Fällen mit hochgradiger Glenoiderosion wurde ein biologischer Glenoidaufbau mittels autologem Knochentransplantat zur Lateralisierung durchgeführt.

Zehn Patienten aus der initialen Kohorte wurden ausgeschlossen: Ein Patient erhielt eine Hemiprothese mit Titankopf anstatt von PyC (aufgrund einer Nickelallergie) und wurde ausgeschlossen; 9 Patienten wurden aufgrund von Komplikationen (siehe Komplikationen in Ergebnisteil) ausgeschlossen, wodurch eine potenzielle Studienpopulation von 93 Patienten verblieb. Hiervon konnten 76 Patienten (82 %) nachuntersucht und eingeschlossen werden. Gründe weshalb Patienten zur Nachuntersuchung verloren wurden waren: Hohes Alter und schlechter gesundheitlicher Allgemeinzustand, Patiententod (ohne Zusammenhang mit der Operation) oder Nichtteilnahme an den Nachuntersuchungen aufgrund von weiter Anreise.

Klinische Evaluation

Präoperativ und während Nachuntersuchungen wurde der Bewegungsumfang, Schmerzen auf der visuellen Analogskala (VAS) von 0-10, sowie der validierte Constant Score erhoben [7]. Zusätzlich wurden demografische Daten wie Patientenalter, Diagnose und Geschlecht aus der Patientenakte erhoben. Die Innenrotation wurde entsprechend der Kategorisierung in Tabelle 5 quantifiziert.

Tabelle 5: Quantifizierung der Innenrotation mit Punktesystem

Internal rotation score	Level reached
0	Thigh
1	Gluteal
2	Iliosacral joint
3	Lumbar spine
4	Thoracic spine
5	Scapula

Statistik

Zur Auswertung wurde die Statistik Software SPSS V25.0 (IBM) verwendet. Die Signifikanz zwischen Veränderungen von prä- und postoperativen Ergebnissen wurde mittels gepaartem t-test kalkuliert. Delta-Werte wurden mittels Students t-test verglichen. Es wurde jeweils ein Signifikanzniveau von $p < 0,05$ festgelegt.

2.2.2. Ergebnisse

Patientendemografie

Die demografische Zusammenfassung des Patientenkollektivs sowie die zur Operation führenden Diagnosen sind in Tabelle 6 aufgeführt. Im Vergleich zum Gesamtkollektiv waren die Patienten in der PyC Subgruppe jünger und überwiegend männlich. Die Patienten der iTEP-Subgruppe hatten das höchste Durchschnittsalter.

Tabelle 6: Patientendemografie

	Total	TSA	RSA	PyC
Number	76	23	32	21
Age	68.5 (22-84)	70.0 (58-84)	74.1 (65-84)	58.3 (22-84)
Sex	45 Female	15 Female	26 Female	4 Female
Follow-up (months)	31.4 (23-55)	31.6 (23-51)	34.3 (23-55)	26.7 (23-38)
Primary Osteoarthritis	44	23	6	14
Cuff tear arthropathy	24	0	25	0
Irreparable rotator cuff tear	1	0	1	0
Fracture sequelae	1	0	0	1
Avascular necrosis	3	0	0	3
Arthritis resulting from instability	3	0	0	3

Tabelle 7 zeigt die präoperative Glenoidmorphologie nach Walch, unterteilt nach Subgruppen [2].

Tabelle 7: Glenoidmorphologie nach der modifizierten Walch-Klassifikation [2]

Glenoid Type (Walch)	Total	TSA	RSA	PyC Hemi
A1	14	0	9	5
A2	28	13	11	4
B1	19	6	7	6
B2	11	4	2	5
B3	0	0	0	0
C	0	0	0	0
D	4	0	3	1

Komplikationen

In der Studienkohorte von 76 Patienten entwickelten 2 Patienten Stressfrakturen: Eine Spina scapulae Fraktur, welche erfolgreich mit Plattenosteosynthese versorgt werden konnte, eine Acromionfraktur, welche konservativ ausbehandelt werden konnte. Zwei Patienten hatten im kurzfristigen Verlauf eine Revision zur Hämatomausräumung bei postoperativem Hämatom. Zwei Patienten hatten eine postoperative Anämie welche transfusionspflichtig war (2,7 %). Und 4 Patienten hatten eine postoperative Neuropraxie, welche in den Monaten nach der Operation jeweils spontan rückläufig war.

Komplikationen welche zum Ausschluss führten

Bei 9 Patienten der initialen Kohorte von 103 Patienten führten Komplikationen zum Ausschluss aus dem Studienkollektiv, da diese nicht mehr vergleichbar mit dem Gesamtkollektiv waren. Vier Patienten hatten im postoperativen Verlauf eine low-grade Infektion (3,88 %) und mussten revidiert werden. Zwei von diesen hatten eine iTEP erhalten, von diesen war eine Patietin 88 Jahre alt, die andere war wegen Psoriasis vulgaris unter Methotrexat Therapie. Zudem gab es jeweils eine Infektion bei PyC- und aTEP-Patienten. Bei dem PyC Patienten handelte sich um eine posttraumatischen Fall mit Voroperation zur Osteosynthese. Zwei von den vier Infektionen wurden durch Cutibacterium acnes verursacht. Ein Patient entwickelte eine Rotatorenmanschettenruptur nach aTEP und wurde zur iTEP konvertiert. Zwei Patienten hatten periprothetische Humerusfrakturen (1,9 %), eine hiervon wurde ex domo weiterbehandelt. Die andere stürzte zweimal, das erste Mal konnte sie konservativ behandelt werden, das zweite Mal wurde sie mit einer Cerclage operativ versorgt, mit einem guten Ergebnis. Eine iTEP Patientin mit schwerer Osteoporose erlitt einen knöchernen Ausbruch der

Glenoidkomponente, trotz Nutzen einer long Peg Basisplatte und 4 Schrauben. Diese wurde revidiert, die Glenoidkomponente entfernt und als Notlösung ein modularer Austausch mit anatomischer Kopfkomponente auf den bestehenden Schaft. Ein Patient wurde einer HWS-Operation in den Monaten nach der Schulterprothese unterzogen und dieser erlitt daraufhin eine neurologisch bedingte Parese des Musculus deltoideus, welche rezidivierende Luxationen der iTEP verursachte.

Klinische Ergebnisse

Tabelle 8 zeigt die prä- versus postoperativen klinischen Ergebnisse. Alle Patientengruppen zeigten im Durchschnitt eine signifikante Besserung in allen gemessenen Parametern.

Tabelle 8: Prä- vs postoperative klinische Ergebnisse, in Subgruppen unterteilt.

Outcome	Total pre-OP	Total post-OP	TSA pre-OP	TSA post-OP	RSA pre-OP	RSA post-OP	PyC pre-OP	PyC post-OP
CS	38.2	78.3	34.5	84.0	36.9	72.9	44.2	80.3
Pain VAS	6.6	1.0	6.7	0.37	6.8	1.1	6.4	1.5
Abduction°	88.2	129.4	84.3	138.3	88.1	121.7	92.6	131.4
Flexion°	92.5	137.1	87.6	144.3	91.4	128.0	99.5	143.1
Internal rotation (score)	1.4	2.6	1.0	3.1	1.7	2.3	1.2	2.7
External rotation°	21.1	39.6	6.1	40.0	19.8	36.3	17.6	44.3

Um den Konfundierungseffekt der unterschiedlichen Patientendemografie der Subgruppen entgegenzuwirken wurden Deltawerte der Ergebnisse zwischen den Subgruppen verglichen. Dieser Vergleich wird in Abbildung 8 zusammengefasst. Insgesamt erfuhren die Patienten der aTEP-Subgruppe im Nachuntersuchungszeitraum die größten Funktionsgewinne, im Vergleich zu iTEP gewannen sie mehr Innenrotation und im Vergleich zu PyC Hemiprothesen berichteten sie mehr Schmerzlinderung.

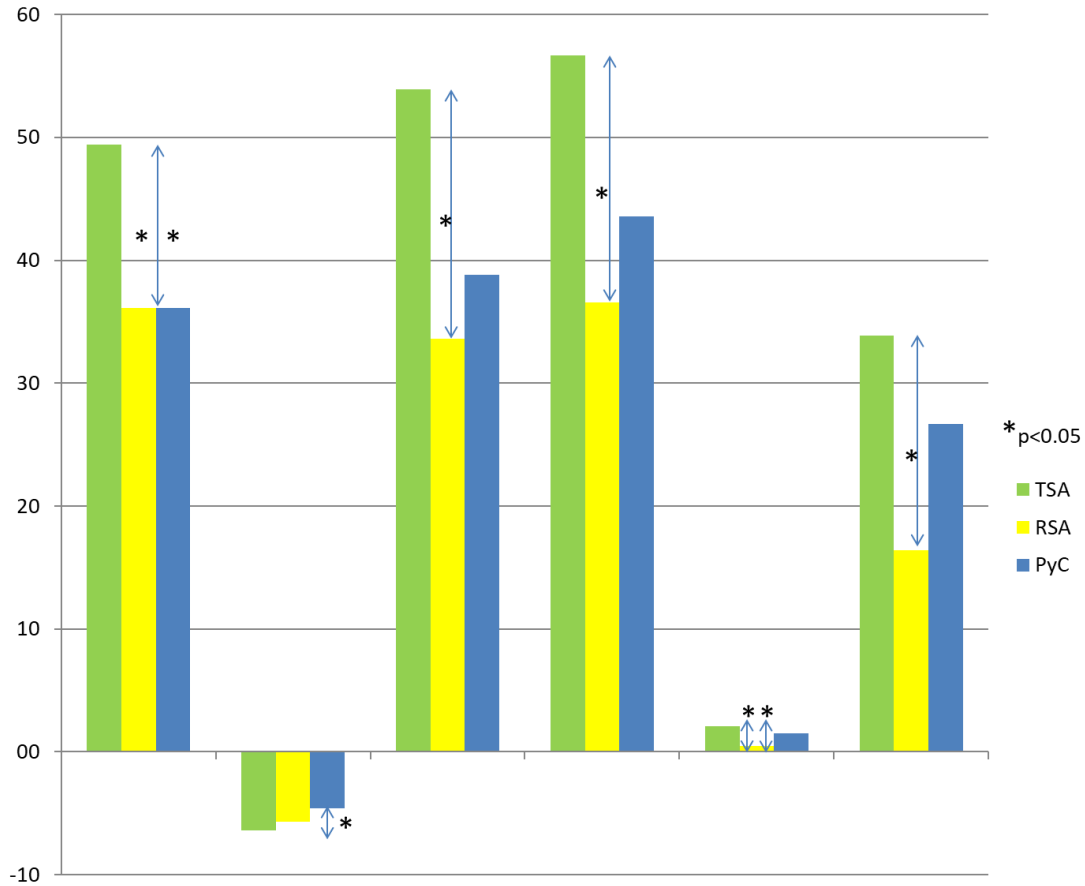

	Constant score	Pain VAS	Abduction°	Flexion°	Internal rotation score	External rotation°
TSA	49.4	-6.4	53.9	56.7	2.1	33.9
RSA	36.1	-5.7	33.6	36.6	0.5	16.4
PyC	36.1	-4.6	38.8	43.6	1.5	26.7

Abbildung 8: Verglich der prä- und postoperativen Deltawerte der Ergebnisse zwischen den Prothesentypen.

Eine Unterteilung der Ergebnisse der Prothesentypen entsprechend der präoperativen Glenoidmorphologie wird in Tabelle 9 angezeigt. Patienten mit Walch Typ B-Morphologie hatten nach Implantation einer PyC Hemiprothese einen größeren Zuwachs im CS als solche die Typ A-Morphologie hatten. Walch Typ B-Patienten hatten ein vergleichbares Ergebnis nach PyC Hemiprothese oder aTEP, bei Typ A-Morphologie jedoch, ergab sich eine größere Besserung nach aTEP.

Tabelle 9: Vergleich der Mittelwerte im CS zwischen verschiedenen Typen der Glenoidmorphologie und Prothesentypen [2]

Glenoid Type (modified Walch)		Prosthesis Type		
		TSA	**RSA**	**PyC**
A	Preoperative CS	28.9	30.4	52.7
	Postoperative CS	83.5	71.5	81.7
	Delta CS	53.7	41.1	29.0
B	Preoperative CS	40.6	47.8	39.5
	Postoperative CS	84.5	76.6	82.8
	Delta CS	43.9	28.8	43.3
D	Preoperative CS	-	49.7	18.0
	Postoperative CS	-	74.0	39.0
	Delta CS	-	24.3	21.0

Tabelle 10 unterteilt die Ergebnisse im CS der drei Prothesentypen nach Diagnosen. Bei primärer OA zeigte sich die aTSA-Gruppe in den Deltawerten (bei schlechtester präoperativer Funktion) im Vergleich zu den andren beiden Prothesentypen überlegen. Während der erreichte CS zwischen sTEP und PyC Patienten vergleichbar war, war die aTEP der iTEP auch in dieser Hinsicht überlegen.

Tabelle 10: Ergebnisse im CS der drei Prothesentypen nach Diagnosen

Diagnosis		Prosthesis Type		
		TSA	**RSA**	**PyC**
Primary Osteoarthritis	Preoperative CS	34.5	42.5	45.6
	Postoperative CS	84.0	74.7	83.8
	Delta CS	49.5	32.2	38.2
Cuff tear arthropathy	Preoperative CS	-	34.8	-
	Postoperative CS	-	72.4	-
	Delta CS	-	37.6	-
Irreparable rotator cuff tear	Preoperative CS	-	53	-
	Postoperative CS	-	75	-
	Delta CS	-	22	-
Fracture sequelae	Preoperative CS	-	-	50
	Postoperative CS	-	-	61.5
	Delta CS	-	-	11.5
Avascular necrosis	Preoperative CS	-	-	41.7
	Postoperative CS	-	-	68
	Delta CS	-	-	26.3
Arthritis resulting from instability	Preoperative CS	-	-	38.3
	Postoperative CS	-	-	82.3
	Delta CS	-	-	44

2.2.3. Schlussfolgerung

Diese Studie ergab einen Einblick in die guten klinischen Ergebnisse welche mit modernen modularen Schulterprothesen erzielt werden können. Wenn die Prothese in den jeweiligen Konfigurationen für die Indikationen für welche sie bestimmt sind implantiert werden, zeigt sich das Patienten nach aTEP im Vergleich zur iTEP und PyC den größten Zuwachs an klinischer Schulterfunktion haben. Während die iTEP den beiden anderen Prothesentypen hinsichtlich der Innenrotation unterlegen war,

berichteten die jüngeren PyC-Patienten subjektiv weniger Schmerzlinderung als aTEP-Patienten. Die Ergebnisse nach PyC-Hemiprothesen waren jedoch, bei Patienten mit OA und posteriorer Subluxation (Walch Typ B), in unserem Kollektiv mit denen nach aTEP vergleichbar. Daher sollte in diesen Fällen, aufgrund des bekannterweise erhöhten Risikos einer Lockerung der Glenoidkomponente bei aTEP, die PyC Hemiprothese präferenziell in Erwägung gezogen werden.

2.3. Mittelfristige Ergebnisse nach Implantation von Pyrocarbon Hemiprothesen

Originalarbeit:
Kleim BD, Zolotar A, Hinz M, Nadjar R, Siebenlist S, Brunner UH. Pyrocarbon hemiprostheses show little glenoid erosion and good clinical function at 5.5 years of follow up. Journal of Shoulder and Elbow Surgery. June 2023. PMID: 37385424. DOI: 10.1016/j.jse.2023.05.027.

2.3.1. Methodik

Studiendesign

Wir führten eine konsekutive Kohortenstudie mit 31 von möglichen 34 Patienten (91%), welche zwischen September 2013 und Juni 2018 eine PyC Hemiprothese im Krankenhaus Agatharied erhalten hatten, durch. Implantiert wurden Aequalis Ascend Flex Prothesen™ (Wright Medical, Bloomington, USA) mit PyC-Kopfkomponente. Alle Patienten wurden zu regelmäßigen Nachuntersuchungen eingeladen.

Ausschlusskriterien waren a) weniger als 3 Jahre klinische und radiologische Nachuntersuchungen und b) inadequate Qualität der Röntgenaufnahmen, was von 2 Untersuchern im Konsensus bewertet wurde (siehe unten bezüglich Qualitätsmerkmale der radiologischen Auswertung). Ein Patient, der in diesem Zeitraum mittels Hemiprothese versorgt wurde, erhielt aufgrund einer Nickelallergie eine traditionelle Kobalt-Chromium Kopfkomponente und wurde folglich ausgeschlossen. Drei Patienten wurden vor der Mindestzeit von 3 Jahren zur Nachuntersuchung verloren (2 sind wegen Ursachen, die nicht mit der Operation in Verbindung stehen verstorben, und 1 wurde wegen entwickelter Demenz nicht mehr vorstellig). Die restlichen 31 Patienten (91%) wurden in die Studienpopulation eingeschlossen.

Die Operationstechnik erfolgte wie bereits in Abschnitt 2.1.1. beschrieben. In 11 Fällen mit bikonkaver Glenoiderosion (neun posteriore und zwei anteriore Neoglenoide) wurde zusätzlich eine konzentrische Glenoidfräsung, zur Wiederherstellung einer monokankaven Gelenkspaarung (auch „ream-and-run“ genannt), durchgeführt[47].

Patientendemografie

Das durchschnittliche Patientenalter betrug 59 Jahre (Bereich 22 bis 87 Jahre). Das Durchschnittsalter von Patienten, welche zusätzlich mit Glenoidfräsung behandelt wurden, war 50 Jahre (22 bis 64). Patienten ohne Glenoidfräsung waren im Mittelwert 62 Jahre (45 bis 84 Jahre) alt. 11 der Patienten

waren weiblich, 20 waren männlich. Der kürzeste Nachuntersuchungszeiteraum war 3,5 Jahre (ein Patient) und der längste 7 Jahre (8 Patienten), der Durchschnitt betrug 5,5 Jahre. Revisionsoperationen wurden bei keinem der Patienten erforderlich („Survival“ 100%). Indikationen, welche zur Operation mit Hemiprothesenimplantation führten, sind in Tabelle 11 aufgeführt.

Tabelle 11: Zur Operation führende Diagnosen und klinisches Ergebnis im CS

Diagnosis	*n*	Preoperative Constant score	Constant score at final follow-up	Increase in Constant score
Osteoarthritis	20	46.7	79.9	33.3
- Type A (Walch)	9	51.8	80	28.2
- Type B (Walch)	11	40.3	79.8	39.4
▪ With reaming	8	50.6	86.7	36.1
▪ Without reaming	12	44.5	76.2	31.7
Arthritis of instability	3	35	86.3	51.3
Avascular necrosis of the humeral head	3	41.7	64.3	22.7
Post-traumatic arthritis	4	45	78.8	33.8
Psoriatic arthritis	1	52	78	26

Klinische Bewertung

Präoperativ und bei jeder Nachuntersuchung wurde das Bewegungsausmaß der Schulter mit einem Goniometer gemessen. Die Innenrotation wurde wie zuvor in Tabelle 5 beschrieben quantifiziert. Schmerzen wurden anhand der VAS von 0 bis 10 Punkten erfasst. Der CS wurde, wie von Constant und Murley beschrieben, bewertet [7]. Der in der Literatur berichtete, minimal für den Patienten bedeutsamen Unterschied (MCID) von 5,7 bis 9,4 Punkten im CS, wurde zur Bewertung der klinischen Relevanz angewandt [8].

Radiologische Bewertung

AP Röntgenaufnahmen nach Grashey, sowie laterale und axiale Aufnahmen, wurden präoperativ sowie zwei Tage postoperativ (ohne axiale Aufnahme) und bei jeder Nachuntersuchung, für welche die Patienten erschienen, in standardisierter Technik angefertigt [44]. Diese wurden unabhängig von zwei Fachärzten für Orthopädie und Unfallchirurgie (B.D.K. und A.Z.) bewertet. Zunächst wurde die Qualität und Projektion der Aufnahmen überprüft [44]. Medialer glenoidaler Knochenverlust wurde entsprechend einer vorbeschriebenen standardisierten Technik an den AP-Röntgenaufnahmen

gemessen [42, 76] (Abbildung 9). Gemessene Werte wurden anhand des aus den OP-Berichten bekannten Durchmessers der Kopfkomponente skaliert.

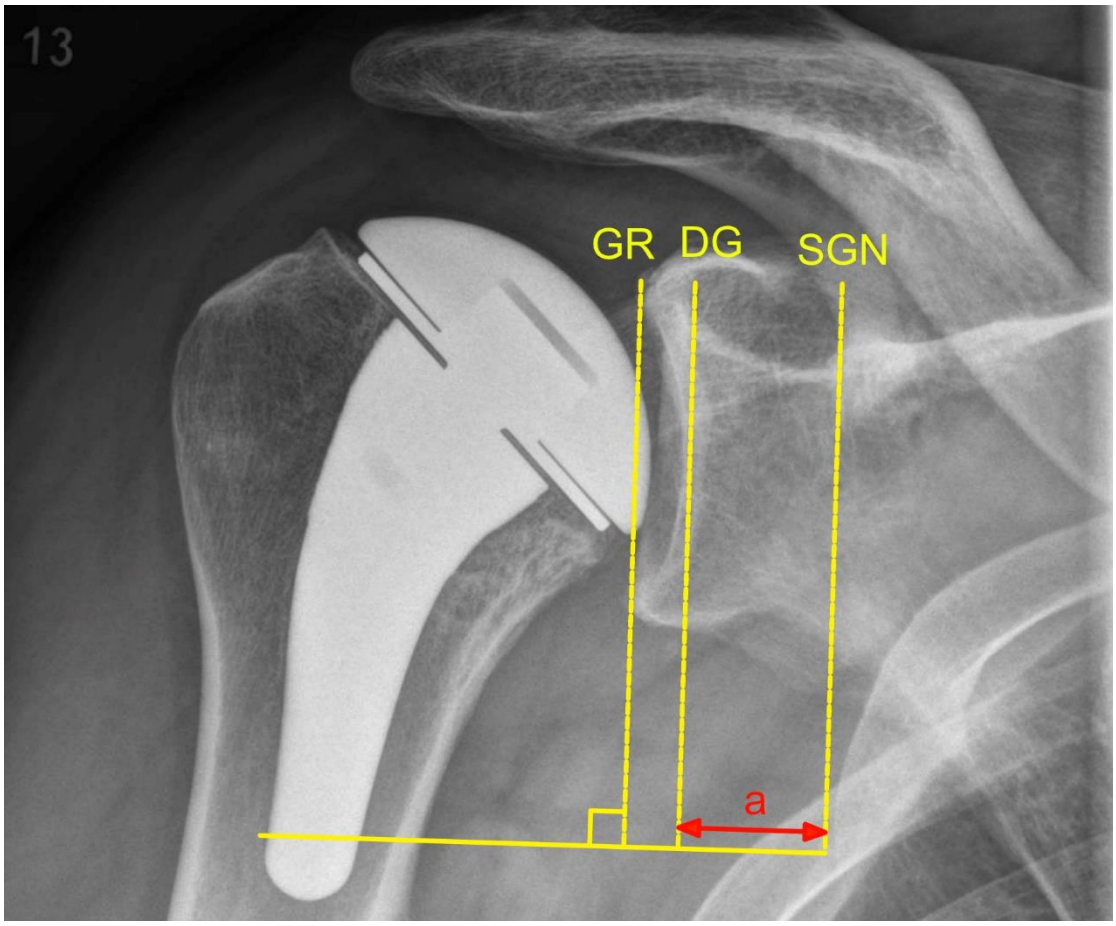

Abbildung 9: Messmethode für die mediale Glenoiderosion. Zuerst wird eine Linie durch den superioren und inferioren Glenoidrand (GR) gelegt. Diese wird dann nach medial über den tiefsten Punkt des Glenoids (DG) transponiert. Daraufhin wird eine parallele Linie durch die Incisura spinoglenoidalis (SGN) gelegt, der Abstand zwischen DG und SGN (a) gemessen und im Verlauf verglichen [40].

Um möglicherweise exzentrische Glenoiderosion zu erfassen wurden die AP und axialen Aufnahmen nach der modifizierten Klassifikation nach Walch (axial) und der Favard-Klassifikation (AP) im Konsensus bewertet [2, 15]. Bei 21 Patienten wurde die erste Nachuntersuchung drei Monate nach der Operation durchgeführt, die anderen Patienten stellten sich hierzu heimatnah bei ihrem niedergelassenen Facharzt vor. Bei Patienten, für welche Glenoidfräsung durchgeführt wurde, wurden die axialen Aufnahmen dieser Dreimonatskontrollen, sofern vorhanden (8 von 11), als Ausgangsbefund für die Walchklassifikation verwendet.

Das acromiohumerale Intervall (AHI; der Abstand zwischen dem Apex des Humeruskopfes und des Acromions) wurde gemessen und wie zuvor beschrieben skaliert.

Statistik

Der Durchschnittswert zwischen den gemessenen Werten der beiden Beobachter wurde zur Analyse verwendet und dieser wurde zu einer Kommastelle ± Standardabweichung angegeben. Die statistische Auswertung wurde mit dem SPSS Statistics software (Version 27.0; IBM, Armonk, NY, USA) durchgeführt. Die Normalverteilung wurde mit dem Shapiro-Wilk-Test bestätigt. Der Student t-Test und gepaarte t-Test wurden verwendet um signifikante Unterschiede zwischen Subgruppen und verschiedenen Zeitpunkten zu ermitteln. Der Pearson-Korrelationskoeffizient wurde verwendet um die Stärke von möglichen linearen Korrelationen zu beurteilen. Der Intraklassen-Korrelationskoeffizient wurde errechnet um die Reliabilität der Messungen zwischen den beiden Beobachtern zu untersuchen. Da wir alle zur Verfügung stehenden Patienten in die Studie eingeschlossen haben, wurde auf eine Poweranalyse verzichtet.

2.3.2. Ergebnisse

Glenoiderosion

Der Intraklassen-Korrelationskoeffizient der Messungen zeigte eine hohe Übereinstimmung (Bereich 0,94 - 0,97). Der Mittelwert des Abstandes zwischen dem tiefsten Punkt des Glenoids und der Incisura spinoglenoidalis betrug 17,1 mm (Bereich 9,6 - 27,5 mm) am 2. postoperativen Tag und 15,8 mm (Bereich 8,7 - 24,3 mm) bei der letzten Nachuntersuchung. Der Mittelwert des medialen Knochenverlusts betrug 1,4 mm (Standardabweichung ±1,20 mm) bei einem durchschnittlichen Nachuntzersuchungszeitraum von 5,5 Jahren. Die Entwicklung der Glenoiderosion über Zeit ist in Abbildung 10 dargestellt und wird in Abbildung 11 anhand eines Falles illustriert.

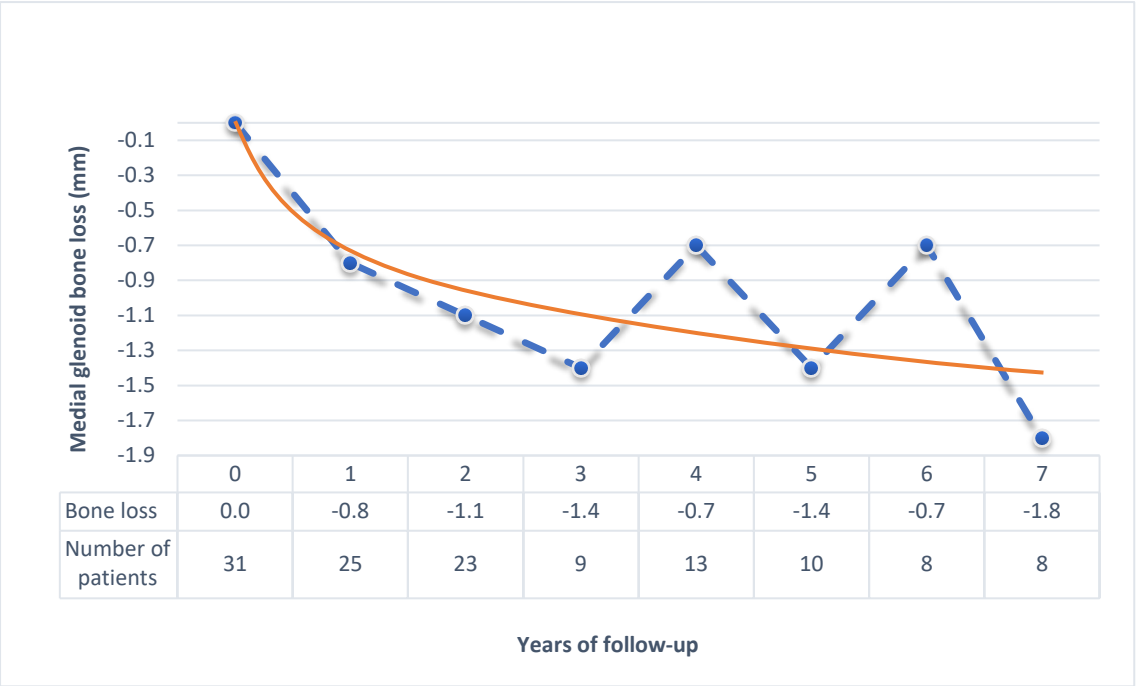

	0	1	2	3	4	5	6	7
Bone loss	0.0	-0.8	-1.1	-1.4	-0.7	-1.4	-0.7	-1.8
Number of patients	31	25	23	9	13	10	8	8

Abbildung 10: Entwicklung des medialen glenoidalen Knochenverlustes im Nachuntersuchungszeitraum. Die Deltawerte der Messungen für die pro Jahr vorhandenen Patienten werden angegeben. Bei den 9 Patienten mit 3-Jahres-Daten und den 10 Patienten mit 5-Jahres-Daten handelte es sich weitgehend um dieselbe Gruppe, ebenso wie bei den 13 Patienten mit 4-Jahres-Daten und den 8 Patienten mit 6-Jahres-Daten. Die rote Linie stellt eine Best-Fit-Linie dar [40].

Abbildung 11: Anteroposteriore und axiale Aufnahmen eines 52-jährigen männlichen Patienten drei Monate nach der PyC-Hemiprothese (a, c) und sieben Jahre postoperativ (b, d). Sieben Jahre nach der Operation ist der glenoidale Knochenverlust gering [40].

Die Messungen des medialen glenoidalen Knochenverlustes sind in Tabelle 12 aufgeführt. Der Knochenverlust im ersten Jahr war signifikant höher als der als der durchschnittliche Knochenverlust pro Jahr ($p < .001$).

Betrachtet man die Patienten ohne Glenoidfräsung, so hatten die jüngsten 10 Patienten (im Alter von 45-60 Jahren zum Zeitpunkt der Operation) einen durchschnittlichen Knochenverlust von 0,2 mm pro Jahr; bei den ältesten 10 Patienten (61-84 Jahre zum Zeitpunkt der Operation) waren es 0,3 mm pro Jahr ($p= 0.38$). Die Pearson Korrelationsanalyse zeigte keine signifikante Korrelation zwischen Patientenalter und Erosion pro Jahr ($r = 0,10$; $p = 0,68$).

Tabelle 12: Medialer glenoidaler Knochenverlust

Outcome	Measurement (mm)
Mean distance from glenoid surface to SGN	
- 2 days postoperatively	17.1 (± 3.83)
- At latest follow-up	15.7 (± 3.41)
Mean bone loss at latest follow-up	1.4 (± 1.20)
Mean bone loss per year	0.3 (± 0.26)
Mean bone loss after 1 year	0.8 (± 0.66)
Mean bone loss after 2 years	1.1 (± 1.08)

Präoperative Glenoidmorphologie und Fälle mit Veränderungen der Morphologie im postoperativen Verlauf nach der Favard- und modifizierter Walch-Klassifikation sind in Tabelle 13 dargestellt [2, 15]. Unter Außerachtlassung der iatrogenen Veränderungen der Glenoidmorphologie, die durch das Fräsen verursacht wurden, beobachteten wir, dass 6 Patienten eine Entwicklung der Morphologie aufwiesen, die durch die modifizierte Walch-Klassifikation beschrieben werden konnte und 3 eine Progression nach der Favard-Klassifikation. Das mittlere AHI betrug präoperativ 14,5 mm (SD, 4,10 mm) und war bei der letzten Nachuntersuchung 9,8 mm (SD, 2,96 mm) ($p < 0,001$). Dies entspricht einer durchschnittlichen Verringerung des AHI von 4,7 mm (SD 2,80 mm).

Tabelle 13: Präoperative Glenoidmorphologie und Evolution dessen im postoperativen Verlauf

Modified Walch [2]			
Preoperative glenoid morphology	Frequency	Glenoid evolution	Frequency
A1	7	B2 to B3	1
A2	11	A1 to D (antero-superior)	1
B1	1	B1 to A2 (without reaming)	3
B2	8	A1 to B1	1
B3	2	B2 to A2 **after reaming**	3
C	0	B2 to B1 **after reaming**	1
D	2	D (biconcave) to A2 **after reaming**	1
		A1 to A2 **after reaming**	1
Favard [15]			
Preoperative glenoid morphology	Frequency	Glenoid evolution	Frequency
E0	9	E0 to E1	1
E1	21	E0 to mild E2 after cranialisation	1
E2	1	E1 to E2	1
E3	0	E0 to E1 **after reaming**	2

Klinische Ergebnisse

Die durchschnittliche aktive Flexion stieg von 99° (SD 30,3°) präoperativ auf 140° (SD 19,6°) bei der letzten Nachuntersuchung; Abduktion, von 93° (SD 29,0°) auf 127° (SD, 19,8°); Außenrotation, von 16° (SD 17,9°) auf 38° (SD 13,3°); und Innenrotation, von 1,3 (SD 1,1) auf 2,8 (SD 0,80) Punkte (von Glutealregion präoperativ bis zur Lendenwirbelsäule bei letzter Nachuntersuchung erreicht). Die Verbesserungen waren in jedem Vergleich statistisch signifikant ($p < 0,001$).

Der Constant Score verbesserte sich sowohl aus klinischer als auch statistischer Perspektive signifikant 2-3 Jahre postoperativ (23 Patienten mit 2-Jahres-Nachuntersuchung, 8 Patienten mit 3-Jahres-Nachuntersuchung), und dieses gute Ergebnis blieb bei der letzten Nachuntersuchung im mittelfristigen Verlauf erhalten (Abbildung 12).

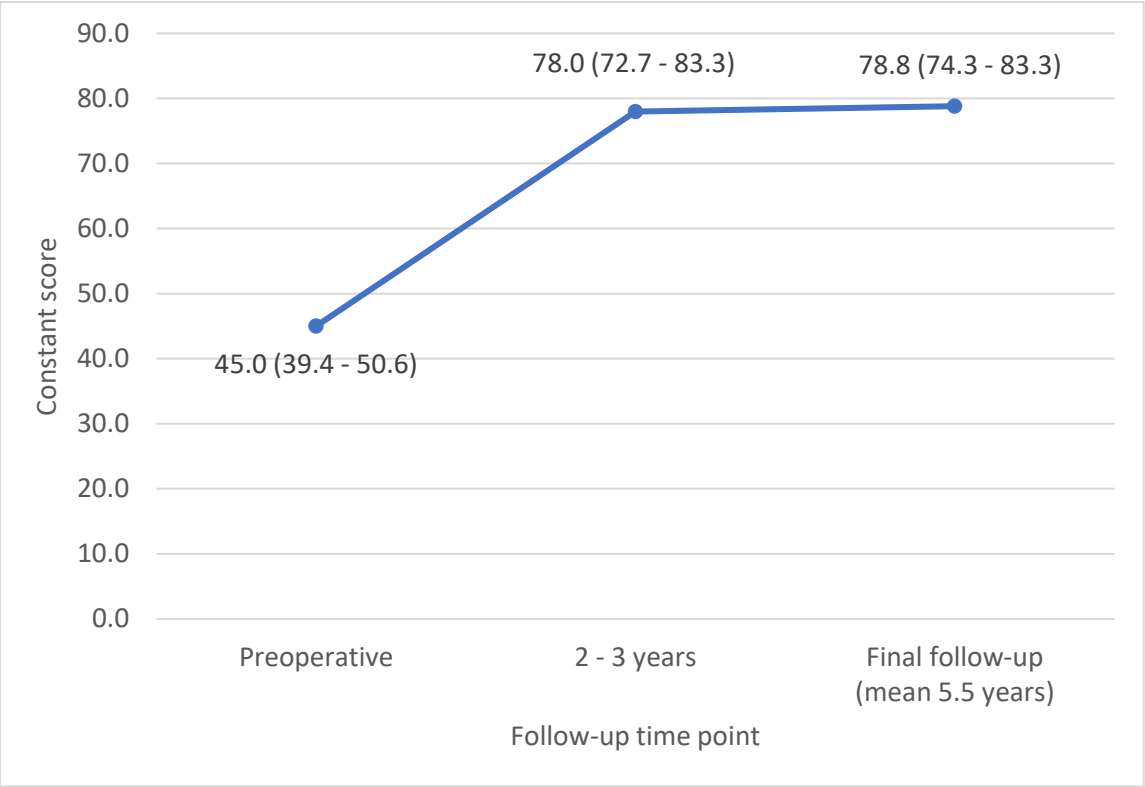

Abbildung 12: Klinische Funktion im Constant Score präoperativ, im kurzfristigen- und mittelfristigen Nachuntersuchungszeitraum [40].

Eine Untergruppenanalyse der klinischen Ergebnisse im Constant-Score für verschiedene Indikationen ist in Tabelle 11 dargestellt. Der MCID (5,7-9,4 Punkte) wurde jeweils übertroffen. Die acht Patienten mit Walch Typ B OA hatten eine signifikant größere Verbesserung im Constant-Score ($p = 0,036$) als Patienten mit Typ A, bei vergleichbaren Endergebnissen.

Präoperativ lag der mittlere VAS-Schmerzwert bei 6,7 (SD 1,64) Punkten; bei letzter Nachuntersuchung hatte sich dieser Wert auf 2,2 (SD 2,25; $p < 0,001$) verringert. Die mittlere Verbesserung des VAS-Schmerzwertes von präoperativ zu postoperativ betrug -4,5 (SD 2,09) Punkte. Von 31 Patienten hatten 23 (74 %) bei der letzten Nachuntersuchung einen VAS-Score von ≤3 Punkten; 10 von ihnen gaben an, überhaupt keine Schmerzen zu haben (VAS-Score von 0). Es bestand eine schwache Korrelation zwischen höherem glenoidalen Knochenverlust und stärkerer Schmerzreduktion ($r = 0,37$, $P = 0,039$), wie in Abbildung 13 dargestellt.

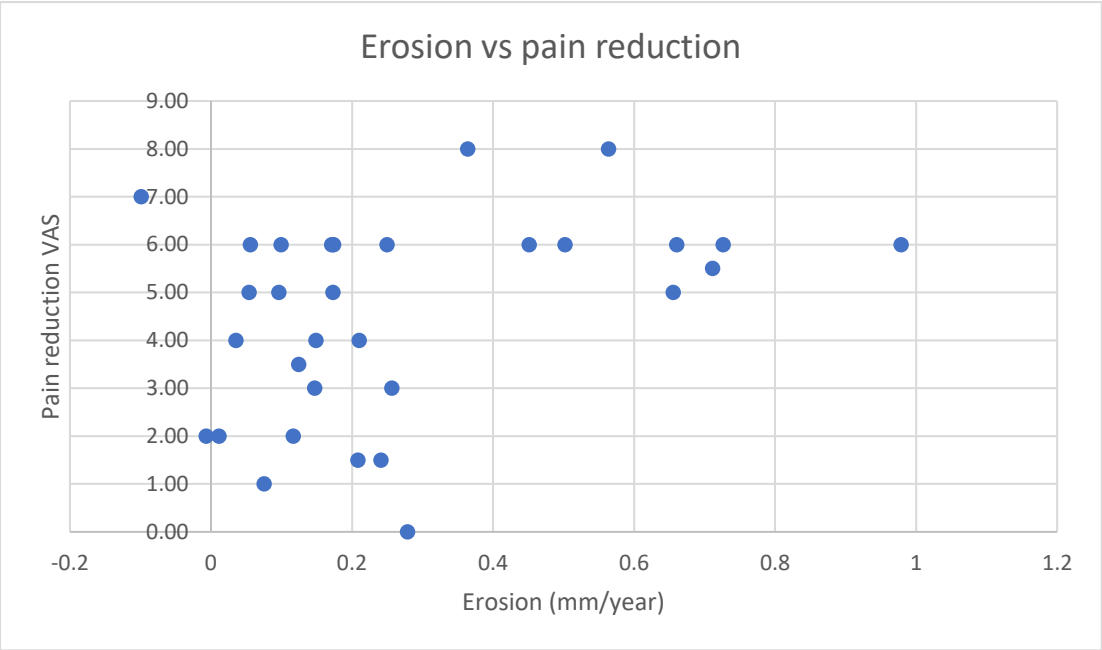

Abbildung 13: Verhältnis zwischen Schmerzreduktion und Glenoiderosion [40].

Es gab keine Korrelation zwischen Glenoiderosion und der Veränderung im CS (r = 0,06). Patienten mit einer Diagnose einer posttraumatischen Arthrose oder avaskulären Nekrose des des Humeruskopfes hatten mehr Restschmerzen als Patienten mit anderen Diagnosen (mittlerer VAS-Score 4,6 vs. 1,5; p < 0,001).

Glenoidfräsung

Der Vergleich zwischen den 11 Patienten mit Glenoidfräsung und den 20 Patienten ohne Glenoidfräsung hinsichtlich der Erosion des Glenoids ergab eine mittlere Erosion von 0,4 mm pro Jahr in der Gruppe mit Fräsung, und 0,2 mm in der Gruppe ohne Fräsung (p = 0,09). Im ersten Jahr betrug der mittlere Knochenverlust 1,0 mm (SD 0,56 mm) in der Fräsung-Gruppe gegenüber 0,6 mm (SD 0,68 mm) in der Gruppe ohne Glenoidfräsung (p = 0,13). Iatrogene Veränderungen der Morphologie des Glenoids nach konzentrischen Glenoidfräsen sind in Tabelle 13 aufgeführt. Abbildung 6 zeigt ein Beispiel, bei dem sich eine anhaltende Rezentrierung des Glenohumeralgelenks nach dem konzentrischen Aufbohren ergab. Die Patienten, bei denen eine Glenoidfräsung durchgeführt wurde, schienen über eine stärkere Schmerzreduktion (Veränderung des VAS-Scores, -5,2 Punkte; SD 1,8) als die Patienten ohne Aufbohren (Veränderung des VAS-Scores -4,2 Punkte; SD 2,2) zu berichten, aber dieser Unterschied war statistisch nicht signifikant (p = 0,19). Die

Verbesserung der Constant-Scores von OA-Patienten, die mit Fräsung behandelt wurden (bikonkave Walch Typen B und D) im Vergleich zu Patienten mit OA, die nicht gefräst wurden, war nicht signifikant unterschiedlich (p = 0,51) (Tabelle 11).

2.3.3. Schlussfolgerung

Im Vergleich zu Glenoiderosion, welche bei KoCr-beschichteten Prothesen bekannt ist, verursachte PyC wenig Erosion [30, 55, 76]. Zudem konnte eine anhaltende Verbesserung der klinischen Funktion in unserer Kohorte bei mittelfristiger Nachuntersuchung festgestellt werden. Nach Implantation einer PyC-Hemiprothese zeigte sich der geringe glenoidale Knochenverlust mit biphasischem Verlauf, wobei dieser nach einer Konsolidierungsphase im ersten Jahr deutlich verlangsamt. PyC-Hemiprothesen sollten daher als eine Alternative zu KoCr-Hemiprothesen und zu aTEP bei Patienten mit einem erhöhten Risiko von Komplikationen der Glenoidkomponente in betracht gezogen werden.

2.4. Neuartige Klassifikation zur degenerativen Schulterarthrose in 3 Dimensionen

Originalarbeit:
Kleim BD, Hinz M, Geyer S, Scheiderer B, Imhoff AB, Siebenlist S. A 3-Dimensional Classification for Degenerative Glenohumeral Arthritis Based on Humeroscapular Alignment. Orthopaedic Journal of Sports Medicine. August 2022. doi:10.1177/23259671221110512.

2.4.1. Methodik

Studienpopulation

Für diese deskriptive Querschnittstudie wurden Patienten identifiziert, die zwischen 2009 (seit Digitalisierung der Patientenakten) und 2020 an der Abteilung für Sportorthopädie des Universitätsklinikums Rechts der Isar in München mit einer primären Schulterprothese (aSTEP, iSTEP oder Hemiprothese) versorgt wurden, indem eine Datenbanksuche durchgeführt wurde. Die Operationsberichte wurden auf die Diagnose DSA (als Typ OA oder DA) geprüft. Schultern mit anderen Diagnosen als DA oder OA oder ohne Verfügbarkeit von CT-Bildern wurden von der Untersuchung ausgeschlossen. Von 299 Patienten, die sich einem primären Schultergelenksersatz unterzogen, wurde bei 243 die Diagnose DSA gestellt. Für 135 dieser Fälle lagen präoperative CT-Scans vor, die nach einem standardisierten hausinternen Protokoll (Schichtdicke, 0,9 mm; Pitch, 0,39; Röhrenstrom, 82 mA [Bereich, 50-115 mA]; Röhrenspannung, 120 kV) durchgeführt wurden, und für die Analyse verfügbar waren. Alle CT-Aufnahmen waren weniger als 6 Monate vor der Operation angefertigt worden. Fünf CT-Aufnahmen mussten von der Analyse ausgeschlossen werden: 2 wegen unzureichender Erfassung des Schulterblatts, 1 wegen Bewegungsartefakten und 2 wegen extremer Erosion, die eine zuverlässige Platzierung der anatomischen Orientierungspunkte für die Messung nicht zuließ. Die übrigen CT-Aufnahmen von 130 Schultern wurden in die Studie aufgenommen.
Die Patienten der Studie hatten ein Durchschnittsalter von 69,7 Jahren (Spanne: 38-88 Jahre), und 60 (46 %) waren männlich. Die Diagnose, die zu einer Endoprothese führte, war in 52 Fällen (40 %) als OA und in 78 Fällen (60 %) als DA dokumentiert worden.

Messmethode

Die Analyse der CT-Aufnahmen wurde von zwei orthopädischen Assistenzärzten (B.D.K. und M.H.) mit Interesse an der Schulterchirurgie durchgeführt, wobei ein standardisiertes, selbst entwickeltes Protokoll verwendet wurde, das an Methoden aus der Literatur angelehnt war[18, 29, 33, 77].

Zunächst wurde die Morphologie des Glenoids anhand der bestehenden Klassifikationen für Schulterarthrose (modifizierte Walch-, Favard-, und Hamada-Klassifikationen) beschrieben, wie bereits zuvor anhand CTs durchgeführt wurde [70]. Dies geschah im Konsens zwischen den beiden Beobachtern.

Als Nächstes verwendeten wir eine klinische 3D-Bildbetrachtungssoftware (IDS7 Workstation Version 22.2; Sectra), um das Glenoidzentrum, das Trigonum und den Angulus inferior in einer Ebene auszurichten. Diese Rekonstruktion wurde bereits zuvor als Scapulaebene beschrieben [29, 33, 65]. Zur Bestimmung des Glenoidzentrums wurde der Mittelpunkt in der axialen und in der koronalen Ebene definiert, wobei Osteophyten außer Acht gelassen wurden. Die Scapulaachse wurde als eine Linie definiert, die in der Scapulaebene durch das Trigonum und das Glenoidzentrum verläuft, was mit früheren Arbeiten übereinstimmt (Abbildung 14) [29, 33, 65]. Die Platzierung eines „best-fit"-Kreises auf dem Humeruskopf, der der Gelenkfläche (soweit intakt) folgte und erhaltene extraartikuläre Orientierungspunkte an den Rändern der Gelenkfläche zuverlässig schnitt, ermöglichte eine genaue Bestimmung des Rotationszentrums und der Größe des Humeruskopfes [77]. Das Rotationszentrum des Humeruskopfes wurde immer an der breitesten Stelle der Ellipse des Humeruskopfes in der Koronal- bzw. axialen Schicht der Scapularebene bestimmt, und dann auf die Ebene der Scapularachse übertragen. Dies war besonders wichtig, um das Rotationszentrum in Fällen mit einem hohen Grad an Subluxation genau zu bestimmen.

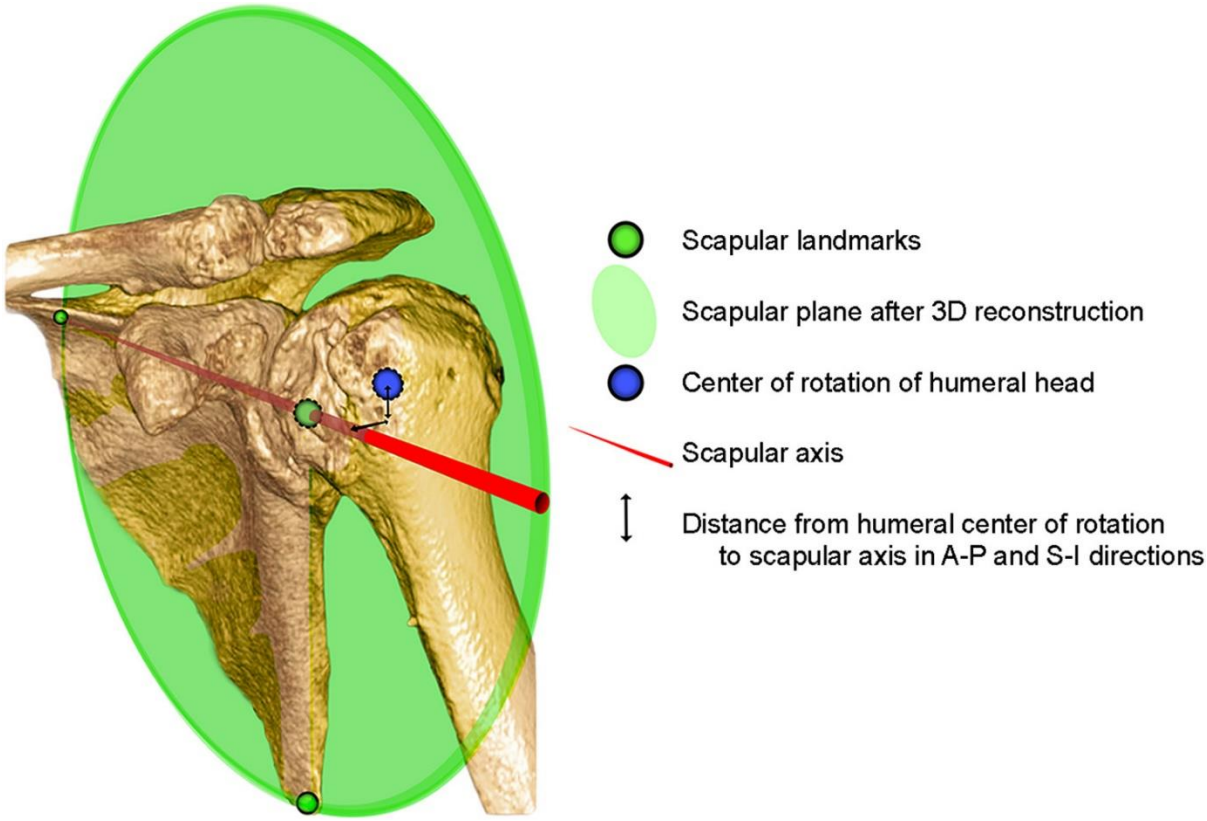

Abbildung 14: Eine dreidimensionale (3D) Computertomographie-Rekonstruktion, die die Scapulaebene unter Verwendung des Trigonums, des Glenoidzentrums und des Angulus inferior der Scapula als Orientierungspunkte darstellt. Die Scapulaachse ist die Linie, die vom Trigonum durch das Glenoidzentrum in dieser Ebene verläuft. Die Exzentrizität des Rotationszentrums des Oberarmkopfes wurde als Abstand zur Scapulaachse sowohl in anteroposteriorer (A-P) als auch in superoinferiorer (S-I) Richtung gemessen [38].

Das Ausmaß der Subluxation des Humeruskopfes wurde dann durch Messung des Abstands des Rotationszentrums des Humeruskopfes von der Scapulaachse sowohl in A-P- als auch in S-I-Richtung bestimmt, wie bereits zuvor beschrieben wurde (Abbildung 16) [33]. Um für die Größe des Patienten zu korrigieren, wurde dies als Prozentsatz des Radius des Humeruskopfes (ähnlich der Methode von Walch zur Beschreibung der Subluxation anhand des Durchmessers des Humeruskopfes [74]) (Abbildung 15) in der entsprechenden Ebene mit der folgenden Formel ausgedrückt:

$$\%\ \text{Subluxation} = \left(\frac{\text{Abstand Rotationszentrum des Humeruskopfes von Scapulaachse}}{\text{Humeruskopfradius}}\right) x\ 100$$

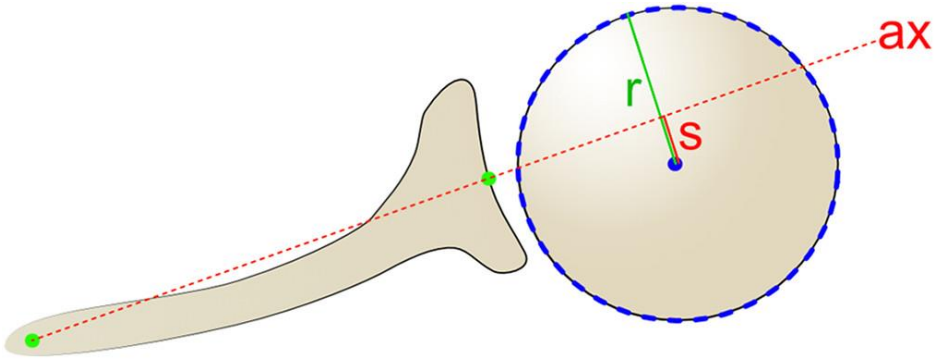

Abbildung 15: Methode zur Bestimmung des Prozentsatzes der Subluxation s des Rotationszentrums des Humeruskopfes von der Scapulaachse ax in Bezug auf den Radius r nach der angegebenen Formel [38].

Bei der Berechnung für jede Ebene entstehen so Vektorkoordinaten, bei denen (0%, 0%) der Mittelpunkt ist.

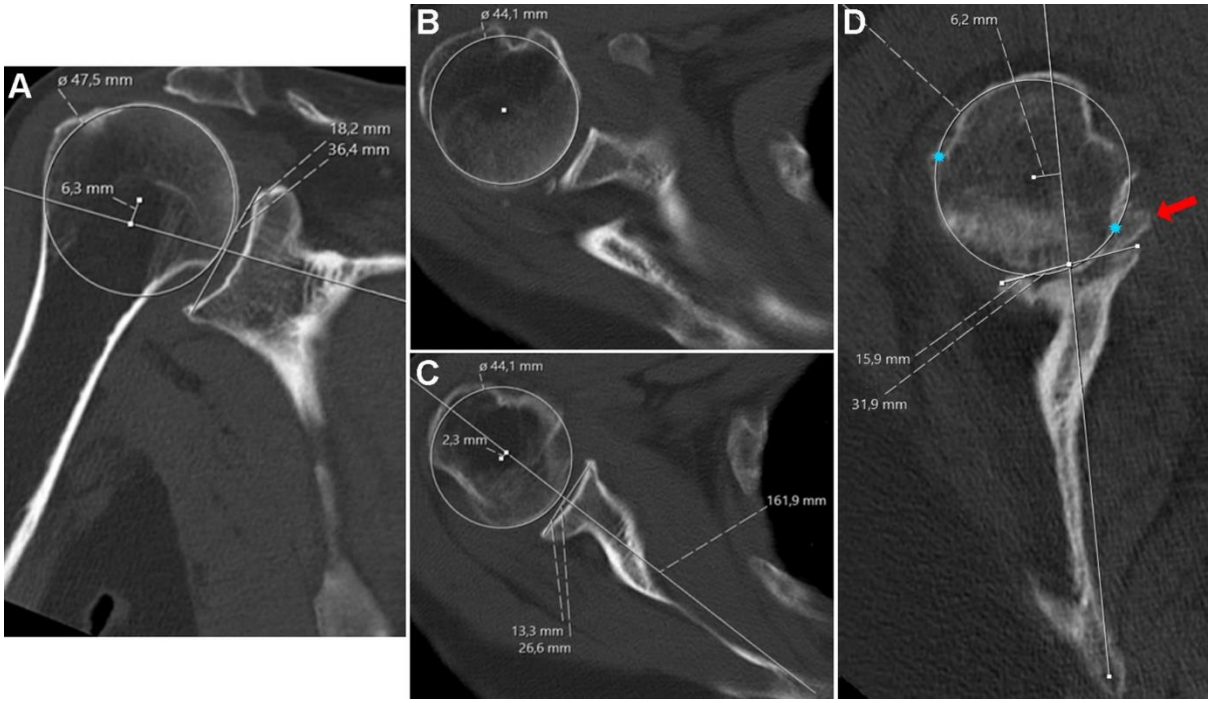

Abbildung 16: Messung der humeroscapulären Ausrichtung auf Computertomographien in (A) der Coronalebene und (B und C) in der Querschnittsebene, nach Rekonstruktion der Scapulaebene in 3 Dimensionen. (B) Das Rotationszentrum des Humeruskopfes wird an der breitesten Stelle des Kopfes bestimmt und (C) dann zur Messung der Subluxation auf die Ebene der Scapulaachse transponiert. (D) Bei höhergradiger Erosion mit partiellem Humeruskopfkollaps und Osteophyten ist die Messung schwieriger. Osteophyten (roter Pfeil), ob auf der Humerus- oder Glenoidseite, müssen außer Acht gelassen werden. Das Rotationszentrum wird mit Hilfe der intakten Übergänge der humeralen Gelenkfläche (blaue Sterne) bestimmt [38].

Beide Beobachter bewerteten alle CT-Scans unabhängig voneinander. Bei großen Unterschieden in den Messungen (>10 %) wurden die Fälle gemeinsam neu bewertet, bis ein Konsens erzielt wurde.

Schließlich wurden die rekonstruierten koronalen, axialen und sagittalen CT-Ebenen bewertet, um die Glenoid-Erosion (die dritte Dimension) zu klassifizieren. Dies geschah nach einem Klassifizierungssystem, das auf früheren Publikationen basierte und welches für das 3D-Konzept angepasst wurde [2, 15]. Nach unseren deskriptiven Beobachtungen wurde die Erosion in drei Typen eingeteilt: Grad 1, keine signifikante knöcherne Erosion; Grad 2, Erosion, die in exzentrischen Fällen eine Bikonkavität verursacht, oder in zentrierten Fällen einen zentralen Krater; und Grad 3, Neoglenoid, das die gesamte Glenoidoberfläche in einer Ebene eingenommen hat (oder schwere zentrale Erosion, mit Beteiligung des Glenoidrandes) (Abbildung 17). Alle Schultern wurden entsprechend eingeteilt, und der Grad der Erosion wurde mit der Art der Ausrichtung kombiniert, um die 3D-Klassifizierung zu vervollständigen.

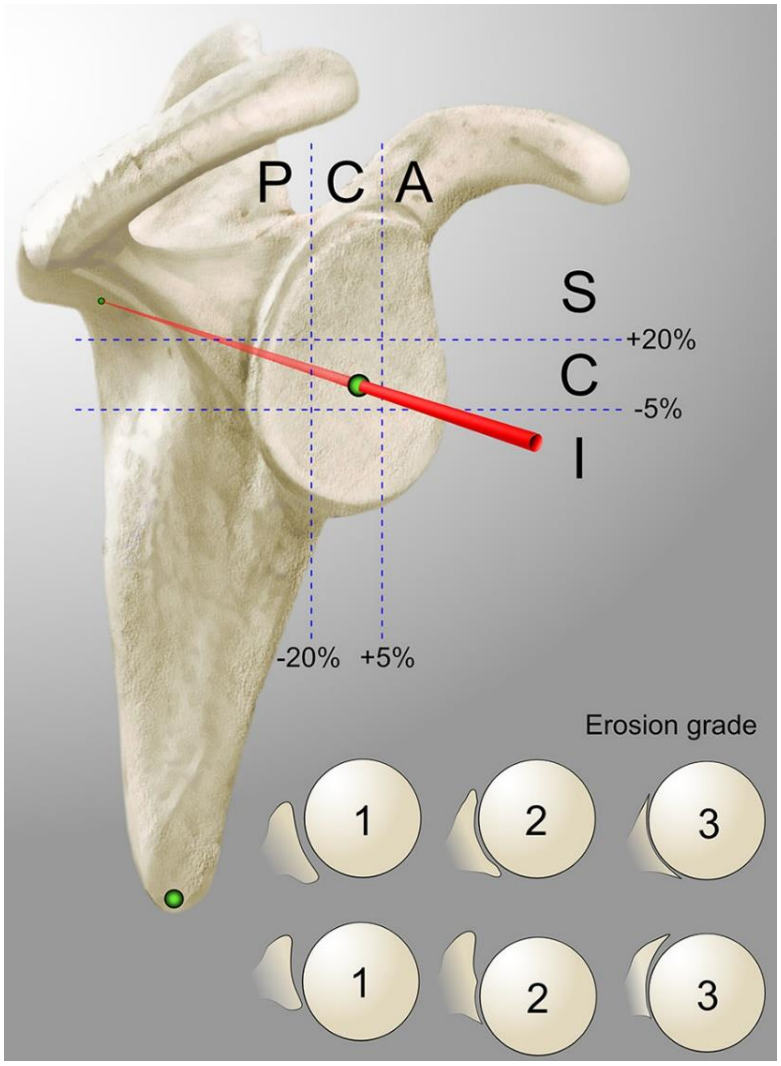

Abbildung 17: Schematische Darstellung der 3-dimensionalen Klassifikation für degenerative Arthrose der Schulter. Die humeroscapuläre Ausrichtung wurde in Form einer Subluxation des Rotationszentrums des Oberarmkopfes in anteroposteriorer Richtung (posterior [P]/central [C]/anterior [A]) und in superoinferiorer Richtung (superior [S]/central [C]/inferior [I]) beschrieben, was insgesamt 9 verschiedene Kombinationen ergab. Die Erosion wurde auf einer Skala von 1 bis 3 eingestuft, wobei 1 = keine signifikante knöcherne Erosion, 2 = fokale Erosion, die einen Krater oder eine Bikonkavität des Glenoids (an beliebiger Stelle) bildet, und 3 = schwere Erosion des Glenoids, die die gesamte Oberfläche des Glenoids in einer Ebene (zentral oder exzentrisch) betrifft [38].

Statistik

Die statistische Analyse wurde mit der Software SPSS Version 26.0 (IBM Corp) durchgeführt. Der Intraklassen-Korrelationskoeffizient wurde zur Messung der Reproduzierbarkeit der Messungen zwischen den beiden Beobachtern verwendet. Die Normalverteilung wurde mit dem Shapiro-Wilk-Test bestätigt. Der Student-t-Test wurde zur Messung der Signifikanz von Unterschieden in normalverteilten Datensätzen verwendet, wobei das Signifikanzniveau auf $p < 0,05$ festgelegt wurde. Die Werte für die Messwerte wurden auf 1 Dezimalstelle gerundet. Da alle verfügbaren CT-Scans, die den Einschlusskriterien entsprachen, einbezogen wurden, wurde auf eine Power-Analyse verzichtet.

2.4.2. Ergebnisse

Zweidimensionale Klassifikation

Die Ergebnisse der Klassifikation der 130 Schultern mit DSA nach der coronalen- (modifizierte Walch [2]) und axialen Ebene (Hamada [20] und Favard [15]) deuteten häufig auf eine biplanare Exzentrizität hin (Tabelle 14), die keines der bestehenden Klassifikationssysteme umfassend beschreiben konnte.

Tabelle 14: DSA eingeteilt nach der axialen (mod. Walch [2]) versus coronalen (Favard [15] und Hamada [20]) Ebene (N = 130 Schultern)

	Modified Walch						
	A1	**A2**	**B1**	**B2**	**B3**	**C**	**D**
Hamada							
1	2	12	4	11	10	0	3
2	11	3	4	4	4	0	1
3	10	2	7	1	1	0	2
4a	4	4	10	1	0	0	3
4b	0	2	2	7	3	0	1
5	0	0	0	0	0	0	1
Favard							
E0	15	0	5	2	0	0	3
E1	9	20	18	12	13	0	5
E2	3	1	4	7	2	0	2
E3	0	1	0	1	2	0	1
E4	0	1	0	2	1	0	0

Der mittlere Durchmesser des Humeruskopfes betrug 44,4 ± 4,05 mm (Bereich 36,1 - 55,8 mm) in der axialen Ebene und 47,0 ± 4,02 mm (Bereich 36,5 - 56,2 mm) in der Coronalebene der rekonstruierten CT-Scans. Ein gepaarter t-Test zeigte einen signifikanten Unterschied zwischen diesen Werten ($p < 0,001$), was eine elliptische Form des Humeruskopfes bestätigte. Die Intraklassen-Koeffizient-Werte zeigten einen hohen Grad an intra-Beobachter-Reproduzierbarkeit für alle gemessenen Variablen:

Humeruskopfdurchmesser (Querschnitt, 0,988; koronal, 0,981), A-P-Subluxation (0,901) und S-I-Subluxation (0,971).

Humeroscapuläre Ausrichtung

In der A-P-Ebene reichte die HSA von 74,1 % posterior bis 23,5 % anterior (SD 19,3 %), wenn sie relativ zum Radius des Humeruskopfes ausgedrückt wurde (absolute Werte, 16,9 mm posterior bis 5,2 mm anterior). Diese Werte wurden dann grafisch in aufsteigender Reihenfolge dargestellt (Abbildung 18). Anhand dieser Grafik sowie des bei der Messung gewonnenen Eindrucks wurde die HSA in der A-P-Ebene in drei Typen eingeteilt: anterior (>5 % anteriore Subluxation), zentral (zwischen 5 % anterior und 20 % posteriore Subluxation) und posterior (>20 % posteriore Subluxation). Eine posteriore Verschiebung des Bereichs für die zentrale Ausrichtung wurde sowohl durch die grafische Analyse als auch durch unseren subjektiven Eindruck unterstützt und ist wahrscheinlich auf die physiologische Retroversion des Glenoids zurückzuführen. Ein weiterer Subtyp (als extraposterior bezeichnet) für besonders schwere posteriore Subluxation wurde für Schultern mit >60 % posteriorer Subluxation definiert, was einem deutlichen Sprung in der Grafik entsprach (siehe Abbildung 18, grüner Pfeil).

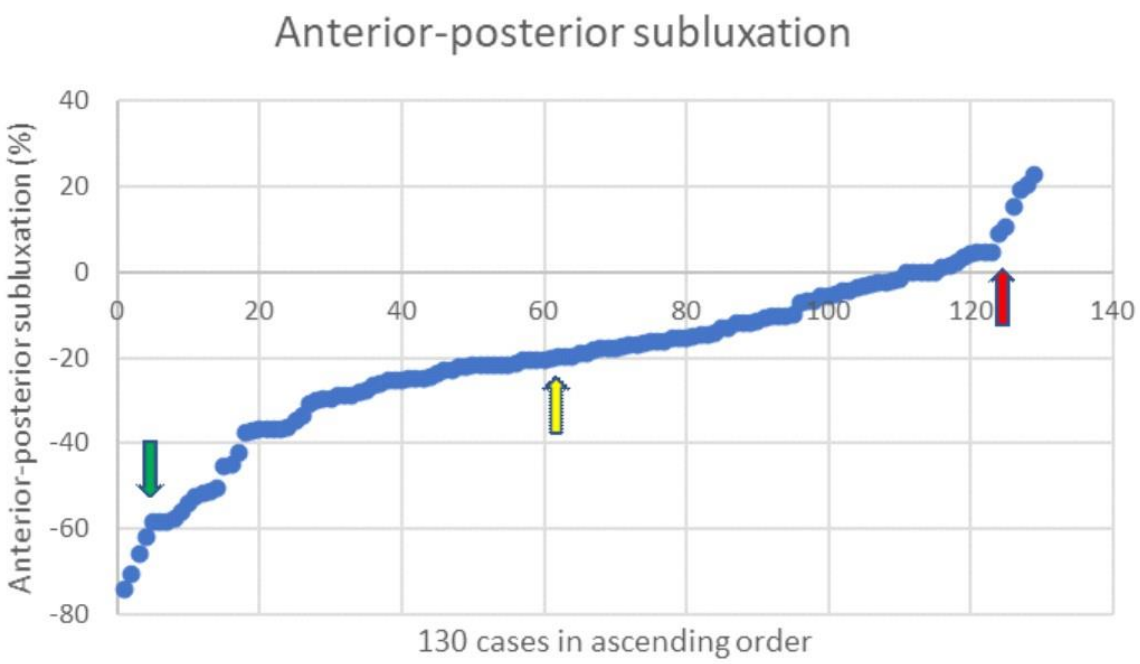

Abbildung 18: Die Werte für die anteroposteriore Subluxation sind in aufsteigender Reihenfolge dargestellt; negative Werte zeigen eine posteriore Subluxation an. Der rote Pfeil markiert den Schritt von der zentralen zur anterioren Ausrichtung, der grüne Pfeil (-60%) den Schritt von der posterioren zur extraposterioren Ausrichtung und der gelbe Pfeil den Wendepunkt der zunehmenden posterioren Subluxation, der bei -20 % liegt und als Grenzwert zwischen zentraler und posteriorer Ausrichtung angenommen wurde [38].

In der S-I-Ebene reichte die Subluxation von 17,2 % inferior bis 68,6 % superior (SD 17,1 %) relativ zum Radius des Humeruskopfes (absolute Werte, 4 mm inferior bis 16,8 mm superior). Diese Werte wurden auch grafisch in aufsteigender Reihenfolge dargestellt (Abbildung 19) und in drei Typen eingeteilt: superior (>20% superiorer Subluxation), zentral (zwischen 5% inferior und 20% superiorer Subluxation) und inferior (>5% inferiore Subluxation). Eine obere Verschiebung des Bereichs für die zentrale Ausrichtung wurde sowohl durch die grafische Analyse als auch durch unseren subjektiven Eindruck bestätigt und ist wahrscheinlich auf die physiologische Inklination des Glenoids sowie die Spannung des Deltamuskels zurückzuführen. Zusätzlich wurde ein weiterer Subtyp für Patienten mit extremer superiorer Subluxation (als extrasuperior bezeichnet) bei statischer Acetabularisation definiert. Alle Patienten mit >50 % superiorer Subluxation (ein bemerkenswerter Schritt in der Kurve (Abbildung 19) wurden in diesen Subtyp aufgenommen. Andere Fälle mit etablierter Acetabularisation, aber <50 % Subluxation, konnten sich aufgrund der knöchernen Obstruktion nicht

weiter nach oben verschieben, weshalb der absolute Wert der Subluxation nicht als Grenzwert für diese Gruppe herangezogen wurde.

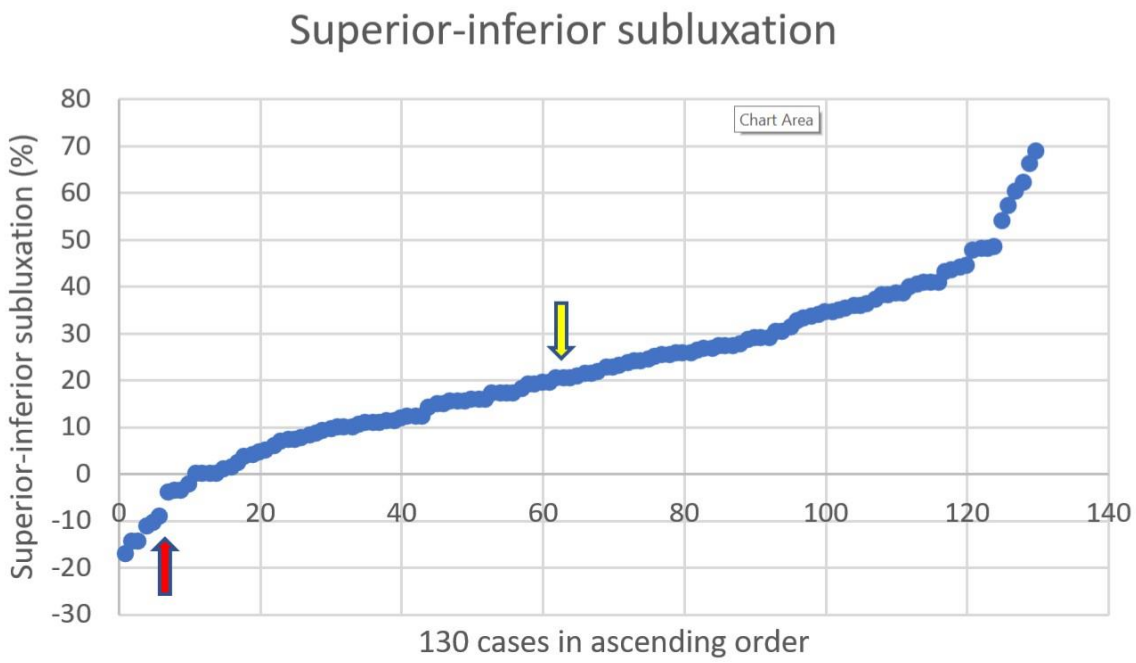

Abbildung 19: Die Werte für die superoinferiore Subluxation sind in aufsteigender Reihenfolge dargestellt; negative Werte bedeuten inferiore Subluxation. Der rote Pfeil markiert den Schritt von der zentralen zur inferioren Ausrichtung (-5%), und der gelbe Pfeil kennzeichnet den Wendepunkt der zunehmenden superioren Subluxation, der bei etwa 20 % liegt und als Grenzwert zwischen zentraler und superiorer Ausrichtung angenommen wurde [38].

Anhand dieser Werte zur Kategorisierung der HSA wurden die 130 Schultern in die 9 möglichen Kombinationen eingeteilt, wie in Tabelle 15 dargestellt. Nur 21 Schultern waren in beiden Ebenen zentriert. Eine biplanare Exzentrizität wurde bei 25 Patienten mit posterosuperiorer, bei 5 Patienten mit posteroinferiorer und bei 4 Patienten mit anterosuperiorer Ausrichtung festgestellt (34/130; 26 %).

Tabelle 15: Häufigkeit der Fälle nach dem Kategorisierungssystem der HSA

Alignment	Posterior (P)	Central (C)	Anterior (A)
Superior (S)	25 (1 XP, 6 XS)	40 (9 XS)	4 (2 XS)
Central (C)	31 (3 XP)	21	3
Inferior (I)	5	1	0

Die Mittelwerte der prozentualen A-P- und S-I-Subluxation für die einzelnen Ausrichtungsarten sind in Tabelle 16 aufgeführt. Es gab einen signifikanten Unterschied bei Patienten mit anteriorer versus

zentraler versus posteriorer A-P-Subluxation ($p < 0,001$; Students t-test) sowie bei Patienten mit superiorer versus zentraler versus inferiorer S-I-Subluxation ($p < 0,001$; Students t-test).

Tabelle 16: Durchschnittliche A-P- und S-I-Subluxation für jede Ausrichtungsart (Bereich, SD)

Alignment	Posterior (P)	Central (C)	Anterior (A)
Superior (S)	A-P subluxation -31.7% (-20.5 to -70.4, 12.8); S-I subluxation 36.1% (20.2 to 68.6, 13.2)	A-P subluxation -9.6% (-19.8 to 4.8, 7.70); S-I subluxation 32.0% (20.1 to 60.1, 9.39)	A-P subluxation 16.8% (9.1 to 23.5, 6.10); S-I subluxation 45.6% (29.0 to 62.0, 13.6)
Central (C)	A-P subluxation -37.4% (-20.3 to -74.1, 16.1); S-I subluxation 7.5% (-4.3 to 18.8, 7.12)	A-P subluxation -7.5% (-19.9 to 4.5, 7.88); S-I subluxation 12.3% (0.9 to 19.5, 5.17)	A-P subluxation 17.7% (10.5 to 22.6, 6.40); S-I subluxation 9.8% (3.8 to 14.9, 5.57)
Inferior (I)	A-P subluxation -37.6% (-25.1 to -58.3, 13.7); S-I subluxation -12.6% (-9.3 to -17.2, 3.33)	A-P subluxation -10.6%; S-I subluxation -14.4%	–

Glenoiderosion

Die Häufigkeit der verschiedenen Erosionsgrade des Glenoids je nach HSA-Ausrichtungstyp ist in Tabelle 17 dargestellt. Abbildung 20 zeigt Beispiele für eine Erosion des Grades 2, und Abbildung 21 zeigt ein Beispiel für eine Erosion des Grades 3.

Tabelle 17: Häufigkeit der Fälle je nach HSA-Typ und Erosionsgrad

	Posterior	Central	Anterior
Superior			
Grade 1	7	20	1
Grade 2	16	15	3
Grade 3	2	5	
Central			
Grade 1	5	4	
Grade 2	11	13	3
Grade 3	15	4	
Inferior			
Grade 1			
Grade 2	3	1	
Grade 3	2		

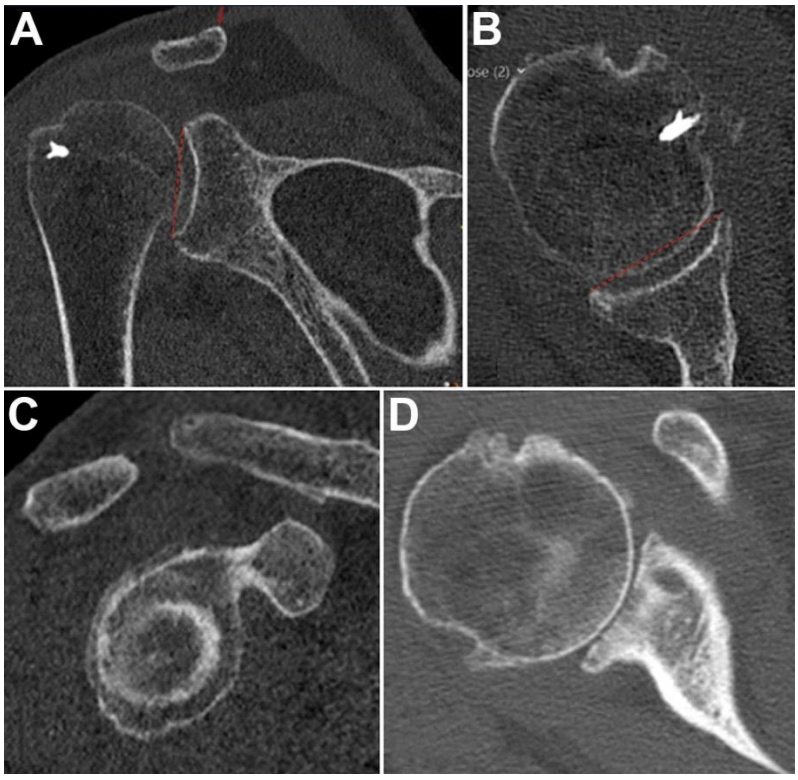

Abbildung 20: Beispiel einer zentral-zentralen Erosion des Grades 2 in der Computertomographie: (A) in der coronalen, (B) in der axialen und (C) in der Sagittalebene. Der Humeruskopf ist medialisiert und überragt eine Linie (gestrichelte rote Linie), die zwischen dem vorderen und hinteren bzw. zwischen oberem und unterem Glenoidrand gezogen wurde, wie zuvor

beschrieben [2]. (D) Ein Beispiel für eine Erosion Grad 2 mit einem zentralen Krater, aber ohne Beteiligung der gesamten Glenoidoberfläche [38].

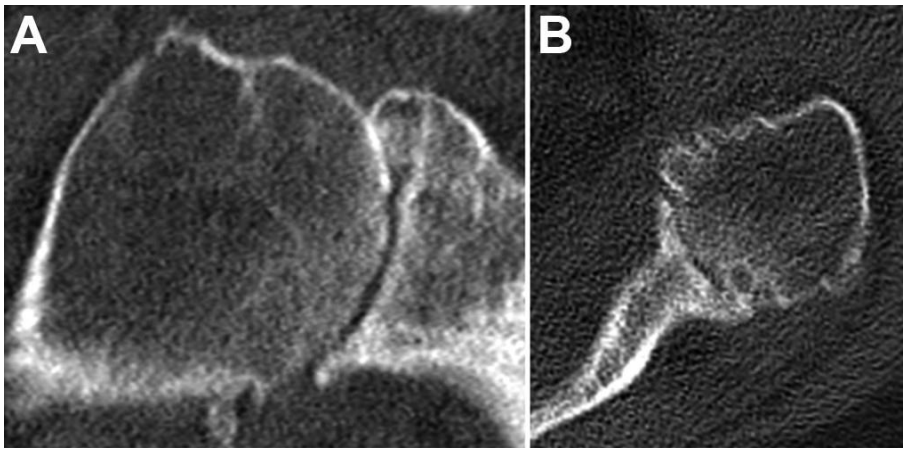

Abbildung 21: Beispiel einer zentral-zentralen Erosion des Grades 3, dargestellt in der Computertomographie: (A) coronal- und (B) axiale Eebene. Die gesamte Glenoidoberfläche, einschließlich des Randes, ist erodiert und der Humeruskopf ist eingebettet [38].

2.4.3. Schlussfolgerung

Diese Arbeit hat eine hohe Prävalenz von biplanarer Exzentrizität bei DSA gezeigt und Grenzwerte für die Unterteilung der zentrierten HSA in beiden Ebenen erarbeitet. Die Erkrankung wird durch bisher etablierte Klassifikationen nicht ausführlich dargestellt. Wir schlagen daher die Verwendung einer 3D-Klassifikation vor, die sowohl die kombinierte HSA als auch die glenoidale Erosion berücksichtigt, um DSA umfassend zu beschreiben. Die Reproduzierbarkeit und klinische Bedeutung dieser Klassifikation müssen noch ermittelt werden.

2.5. Validierung der 3-dimensionalen Klassifikation zur degenerativen Schulterarthrose

Originalarbeit:
Kleim BD, Lappen S, Kadantsev P, Degenhardt H, Fritsch L, Siebenlist S, Hinz M. Validation of a novel 3-dimensional classification for degenerative arthritis of the shoulder. Archives of orthopaedic and trauma surgery. 2023. PMID: 37308783. DOI: 10.1007/s00402-023-04890-2.

2.5.1. Methodik

Für diese Validierungsstudie wurde die zuvor untersuchte Kohorte von Patienten mit DSA identifiziert, die sich zwischen 2009 und 2020 einer primären Schulterendoprothese (Schulter-Totalendoprothese, Hemiprothese oder inverse Schulterendoprothese) an der Abteilung für Orthopädische Sportmedizin des Universitätsklinikums Rechts der Isar in München unterzogen hatten [38]. In diesem Zeitraum wurden 299 Schulterendoprothesen bei DAS implantiert. Bei 135 von ihnen standen präoperative CT-Aufnahmen nach einem standardisierten internen Protokoll (Pitch, 0,39; Schichtdicke, 0,9 mm; Röhrenspannung, 120 kV; Röhrenstrom, 82 mA [Bereich, 50-115 mA]) zur Analyse zur Verfügung. Die CT-Scans waren nicht länger als 6 Monate vor der Operation angefertigt worden. Fünf dieser Patienten wurden von der Analyse ausgeschlossen: In zwei Fällen war die Scapula nicht ausreichend freigelegt, in einem Fall aufgrund von Bewegungsartefakten und in zwei Fällen aufgrund starker Erosionen, so dass die anatomischen Orientierungspunkte für die Messung nicht zuverlässig gesetzt werden konnten. Von den verbleibenden 130 CTs wurden 100 nach dem Zufallsprinzip ausgewählt.
Das Durchschnittsalter der Patienten lag bei 70 Jahren (Spanne 38-88 Jahre), 49 waren männlich (49 %). Bei 59 Patienten wurde entsprechend der Operationsberichten präoperativ eine DA und bei 41 eine OA dokumentiert.

CT-Klassifikation
Es wurde eine klinische Bildbetrachtungssoftware, die zur 3D-Rekonstruktion fähig ist (IDS7 Workstation Version 22.2; Sectra), verwendet, um CT-Bilder gemäß der zuvor beschriebenen 3D-Klassifikation für DAS zu klassifizieren [38]. Zunächst wurde die Scapularebene in 3D unter Verwendung zweidimensionaler orthogonaler Ebenen (axial, koronal und sagittal) rekonstruiert: Das Glenoidzentrum, das Trigonum und der Angulus inferior scapulae wurden in einer Ebene ausgerichtet

(Abbildung 14). Anschließend wurde die anteroposteriore Ausrichtung als posterior, zentriert oder anterior klassifiziert; die superoinferiore Ausrichtung wurde als superior, zentriert oder inferior klassifiziert und mit einem Erosionsgrad (1-3) kombiniert (Abbildung 17). Die Subluxation des Humeruskopfzentrums von der Scapularachse (Linie, die vom Trigonum scapulae durch das Glenoidzentrum verläuft) wurde relativ zum Radius des Humeruskopfes beurteilt (Abbildung 15). Zentrierte Ausrichtung wurde, entsprechend der Primärstudie, definiert als: Zwischen 20% posteriorer und 5% anteriorer Subluxation in anteroposteriorer Richtung; zwischen 5% inferiorer und 20% superiorer Subluxation in superoinferiorer Richtung [38]. Zusätzlich konnte die Ausrichtung als extra-posterior beschrieben werden, wenn die posteriore Subluxation > 60 % des Humeruskopfradius (> 80 % des Durchmessers) betrug, oder als extra-superior, wenn eine statische Acetabularisierung vorlag [38]. Wenn die Ausrichtung offensichtlich war, mussten die Beobachter keine Messungen durchführen. In Grenzfällen wurden die Scapulaachse, der Humerusumfang mit Drehzentrum, der Radius und die Subluxation des Humeruskopfzentrums von der Scapulaachse bestimmt, um die Klassifizierung zu quantifizieren (Abbildung 16).

Nach einem 2-stündigen Trainingsseminar klassifizierten vier in der Schulterchirurgie erfahrene orthopädische Assistenzärzte (von denen keiner an den Messungen für die Primärstudie beteiligt war) unabhängig voneinander alle 100 CT-Aufnahmen. Es wurde eine Anleitung für die 3D-Rekonstruktion und Klassifizierungsmethode mit einer schematischen Darstellung der 3D-Klassifizierung (Abbildung 17) bereitgestellt. Vier Wochen nach der ersten Analyse klassifizierten die gleichen vier Beobachter die 100 CT-Scans ein zweites Mal. Die Beobachter waren gegenüber den Ergebnissen ihres vorherigen Versuchs verblindet. Die für die neue Klassifizierung benötigte Zeit wurde für jeden Beobachter gemessen. Um die in der klinischen Praxis verfügbare Zeit zu simulieren, wurden die Beobachter angewiesen, < 5 Minuten pro CT in Anspruch zu nehmen.

Die humeroscapuläre Ausrichtung aller 100 Schulter-CTs war zuvor für die Primärstudie von BDK und MH präzise gemessen und klassifiziert worden, wobei die Übereinstimmung zwischen den Beobachtern bei den Ausrichtungsmessungen nahezu perfekt war [38]. Die Erosion wurde im

Konsens zwischen den beiden Beobachtern klassifiziert. Diese bestehenden Klassifikationswerte (siehe Tabelle 17) wurden als Goldstandard herangezogen, mit dem die vorliegenden Werten der Beobachter zur Validierung verglichen wurden.

Statistik

Die statistische Analyse wurde mit der Software SPSS Version 29.0 (IBM-SPSS, New York, USA) durchgeführt. Die Klassifizierungswerte wurden umkodiert und als String-Variablen mit drei ordinalen Kategorien eingegeben. Intrabeobachter-Reliabilität, Interbeobachter-Reliabilität und Validität (im Vergleich zu bestehenden Goldstandard-Werten) wurden mit Hilfe von Cohens gewichtetem κ mit linearer Gewichtung berechnet. Die Mittelwerte der Vergleiche beider Versuche jedes Beobachters (vier Vergleiche für jeden einzelnen Intra-Beobachter-Vergleich) wurden für alle sechs individuellen Inter-Beobachter-Vergleiche zwischen den vier Beobachtern berechnet. Für jeden Wert wurde ein 95%-Konfidenzintervall (KI) ermittelt. Für die Interpretation der κ-Werte wurde Cohens Kategorisierung der Übereinstimmung (≤ 0 für keine Übereinstimmung, 0,01-0,20 für keine bis geringe Übereinstimmung, 0,21-0,40 für geringfügige Übereinstimmung, 0,41- 0,60 für mittelmäßige Übereinstimmung, 0,61-0,80 für erhebliche Übereinstimmung und 0,81-1,00 für nahezu perfekte Übereinstimmung) verwendet [5]. Die Tests waren zweiseitig und hatten ein Signifikanzniveau von 0,05.

2.5.2. Ergebnisse

Die Intrabeobachter-Zuverlässigkeit der 3D-Klassifizierung zeigte eine erhebliche Übereinstimmung mit einem gewichteten Cohen-κ von 0,71 (KI 0,63-0,79).

Die Übereinstimmung zwischen den Beobachtern war insgesamt mittelmäßig und reichte von mittelmäßig bis erheblich (Tabelle 18). Bei der Bewertung der Übereinstimmung nur für die biplanare Ausrichtung (ohne Berücksichtigung des Erosionsgrads) verbesserte sich die Übereinstimmung zwischen den Untersuchern bei jedem Vergleich und reichte von mittelmäßig bis erheblich, obwohl die Unterschiede statistisch nicht signifikant waren (Tabelle 18). Die Übereinstimmung zwischen den Beobachtern änderte sich nicht wesentlich, wenn die zusätzlichen Deskriptoren extra-posterior und extra-superior einbezogen wurden (κ = 0,44 [KI 0,33-0,55]).

Tabelle 18: Interbeobachter-Übereinstimmung unter Verwendung von Cohens gewichtetem Kappa (95% Konfidenzintervall) für biplanare humeroscapuläre Ausrichtung mit Erosionsgrad (obere Hälfte) und isoliert biplanare humeroscapuläre Ausrichtung (untere Hälfte).

Alignment with erosion	**Observer 4 (Attempts 1 and 2)**	**Observer 3 (Attempts 1 and 2)**	**Observer 2 (Attempts 1 and 2)**
Observer 1 (Attempts 1 and 2)	0.37 (0.26–0.48)	0.67 (0.61–0.73)	0.46 (0.34–0.57)
Observer 2 (Attempts 1 and 2)	0.40 (0.27–0.54)	0.49 (0.38–0.61)	
Observer 3 (Attempts 1 and 2)	0.38 (0.27–0.50)		
Overall mean average	**0.46 (0.36–0.57)**		
Alignment only	**Observer 4 (Attempts 1 and 2)**	**Observer 3 (Attempts 1 and 2)**	**Observer 2 (Attempts 1 and 2)**
Observer 1 (Attempts 1 and 2)	0.41 (0.30–0.54)	0.71 (0.64–0.78)	0.55 (0.42–0.68)
Observer 2 (Attempts 1 and 2)	0.47 (0.34–0.60)	0.61 (0.48–0.73)	
Observer 3 (Attempts 1 and 2)	0.46 (0.33–0.59)		
Overall mean average	**0.55 (0.42–0.65)**		

Die Validitätsanalyse, bei der die Klassifizierungen der Beobachter mit den Goldstandardwerten verglichen wurden, ergab eine mäßige Übereinstimmung (Tabelle 19). Wie schon zuvor in der Interbeobachter-Analyse beobachtet, änderte sich die Übereinstimmung für die Validität nicht wesentlich, wenn die zusätzlichen Deskriptoren extra-posterior und extra-superior einbezogen wurden (κ = 0,45 [KI 0,33-0,56]). Bei der Analyse nur des quantifizierbaren Aspekts (biplanare Ausrichtung) stieg der κ-Wert auf 0,53 (KI 0,41-0,65).

Tabelle 19: Ergebnisse der Validitätsanalyse, die den Mittelwert (95% KI) der beiden Versuche eines jeden Beobachters mit den Goldstandardwerten zeigen

	Agreement with gold standard
Observer 1	0.49 (0.37 – 0.61)
Observer 2	0.52 (0.41 – 0.63)
Observer 3	0.53 (0.41 – 0.64)
Observer 4	0.37 (0.25 – 0.48)
Total average	0.48 (0.36 – 0.59)

Die durchschnittliche Zeit, die für die Klassifizierung benötigt wurde, betrug 2 Minuten und 47 Sekunden (Bereich 45 Sekunden bis 4 Minuten und 1 Sekunde).

2.5.3. Schlussfolgerung

Die 3D-Klassifikation für DAS ist valide. Obwohl diese Klassifikation umfassender ist als frühere monoplanare (zweidimensionale) Klassifikationen, ist die Übereinstimmung der 3D-Klassifikation mindestens vergleichbar mit diesen (Tabelle 1). Dies ist wahrscheinlich auf den quantifizierbaren Charakter des Ausrichtungsaspekts dieser Klassifizierung zurückzuführen, der klare Grenzwerte ermöglicht. Außerdem waren die Beobachter in der Lage, die Klassifizierung in < 5 Minuten anzuwenden, was der in der klinischen Praxis verfügbaren Zeit entspricht. Da die neue 3D-Klassifikation quantifizierbar ist, hat sie das Potenzial, in Zukunft durch eine automatisierte, auf Algorithmen basierende Softwareanalyse, vereinfacht angewandt zu werden.

Abbildungsverzeichnis

Tabellenverzeichnis

Literaturverzeichnis

1. Ajdari N, Tempelaere C, Masouleh MI, Abel R, Delfosse D, Emery R, et al. (2020) Hemiarthroplasties: the choice of prosthetic material causes different levels of damage in the articular cartilage. Journal of Shoulder and Elbow Surgery 29:1019-1029
2. Bercik MJ, Kruse K, 2nd, Yalizis M, Gauci MO, Chaoui J, Walch G (2016) A modification to the Walch classification of the glenoid in primary glenohumeral osteoarthritis using three-dimensional imaging. J Shoulder Elbow Surg 25:1601-1606
3. Casagrande DJ, Parks DL, Torngren T, Schrumpf MA, Harmsen SM, Norris TR, et al. (2016) Radiographic evaluation of short-stem press-fit total shoulder arthroplasty: short-term follow-up. J Shoulder Elbow Surg 25:1163-1169
4. Castagna A, Delcogliano M, de Caro F, Ziveri G, Borroni M, Gumina S, et al. (2013) Conversion of shoulder arthroplasty to reverse implants: clinical and radiological results using a modular system. Int Orthop 37:1297-1305
5. Cohen J (1960) A Coefficient of Agreement for Nominal Scales. Educational and Psychological Measurement 20:37-46
6. Cointat C, Raynier JL, Vasseur H, Lareyre F, Raffort J, Gauci MO, et al. (2022) Short-term outcomes and survival of pyrocarbon hemiarthroplasty in the young arthritic shoulder. J Shoulder Elbow Surg 31:113-122
7. Constant CR, Murley AH (1987) A clinical method of functional assessment of the shoulder. Clin Orthop Relat Res 160-164
8. Dabija DI, Jain NB (2019) Minimal Clinically Important Difference of Shoulder Outcome Measures and Diagnoses: A Systematic Review. Am J Phys Med Rehabil 98:671-676
9. Denard PJ, Noyes MP, Walker JB, Shishani Y, Gobezie R, Romeo AA, et al. (2018) Proximal stress shielding is decreased with a short stem compared with a traditional-length stem in total shoulder arthroplasty. J Shoulder Elbow Surg 27:53-58
10. Denard PJ, Raiss P, Gobezie R, Edwards TB, Lederman E (2018) Stress shielding of the humerus in press-fit anatomic shoulder arthroplasty: review and recommendations for evaluation. J Shoulder Elbow Surg 27:1139-1147
11. Denard PJ, Raiss P, Sowa B, Walch G (2013) Mid- to long-term follow-up of total shoulder arthroplasty using a keeled glenoid in young adults with primary glenohumeral arthritis. J Shoulder Elbow Surg 22:894-900
12. Domos P, Checchia CS, Walch G (2018) Walch B0 glenoid: pre-osteoarthritic posterior subluxation of the humeral head. Journal of Shoulder and Elbow Surgery 27:181-188
13. Donohue KW, Ricchetti ET, Ho JC, Iannotti JP (2018) The Association Between Rotator Cuff Muscle Fatty Infiltration and Glenoid Morphology in Glenohumeral Osteoarthritis. J Bone Joint Surg Am 100:381-387
14. Farron A, Terrier A, Büchler P (2006) Risks of loosening of a prosthetic glenoid implanted in retroversion. J Shoulder Elbow Surg 15:521-526
15. Favard L, Lautmann S, Clement P. Osteoarthritis with Massive Rotator Cuff-Tear: The Limitation of its Current Definitions. *Shoulder Arthroplasty*;DOI: 10.1007/978-3-642-58365-0_28. Berlin, Heidelberg: Springer Berlin Heidelberg; 1999:261-265.
16. Friedman RJ, Hawthorne KB, Genez BM (1992) The use of computerized tomography in the measurement of glenoid version. J Bone Joint Surg Am 74:1032-1037
17. Garret J, Harly E, Le Huec J-C, Brunner U, Rotini R, Godenèche A (2019) Pyrolytic carbon humeral head in hemi-shoulder arthroplasty: preliminary results at 2-year follow-up. JSES Open Access 3:37-42
18. Gerber C, Costouros JG, Sukthankar A, Fucentese SF (2009) Static posterior humeral head subluxation and total shoulder arthroplasty. Journal of Shoulder and Elbow Surgery 18:505-510
19. Grothe T, Postler A, Nowotny J, Lützner J, Günther KP, Klemm HT (2019) Endoprothetik der großen Gelenke. Trauma und Berufskrankheit 21:127-143
20. Hamada K, Fukuda H, Mikasa M, Kobayashi Y (1990) Roentgenographic findings in massive rotator cuff tears. A long-term observation. Clinical orthopaedics and related research 92-96
21. Hannoun A, Ouenzerfi G, Brizuela L, Mebarek S, Bougault C, Hassler M, et al. (2019) Pyrocarbon versus cobalt-chromium in the context of spherical interposition implants: an in vitro study on cultured chondrocytes. Eur Cell Mater 37:1-15
22. Harjula JNE, Paloneva J, Haapakoski J, Kukkonen J, Äärimaa V (2018) Increasing incidence of primary shoulder arthroplasty in Finland - a nationwide registry study. BMC Musculoskelet Disord 19:245

23. Hartwell MJ, Harold RE, Sweeney PT, Seitz AL, Marra G, Saltzman MD (2021) Imbalance in Axial-plane Rotator Cuff Fatty Infiltration in Posteriorly Worn Glenoids in Primary Glenohumeral Osteoarthritis: An MRI-based Study. Clin Orthop Relat Res 479:2471-2479
24. Hopkins CM, Azar FM, Mulligan RP, Hollins AM, Smith RA, Throckmorton TW (2021) Computed Tomography and Magnetic Resonance Imaging are Similarly Reliable in the Assessment of Glenohumeral Arthritis and Glenoid Version. Arch Bone Jt Surg 9:64-69
25. Iannotti JP, Jun B-J, Patterson TE, Ricchetti ET (2017) Quantitative Measurement of Osseous Pathology in Advanced Glenohumeral Osteoarthritis. JBJS 99:1460-1468
26. Iannotti JP, McCarron J, Raymond CJ, Ricchetti ET, Abboud JA, Brems JJ, et al. (2010) Agreement study of radiographic classification of rotator cuff tear arthropathy. J Shoulder Elbow Surg 19:1243-1249
27. Iannotti JP, Norris TR (2003) Influence of preoperative factors on outcome of shoulder arthroplasty for glenohumeral osteoarthritis. J Bone Joint Surg Am 85:251-258
28. Iannotti JP, Norris TR (2003) Influence of Preoperative Factors on Outcome of Shoulder Arthroplasty for Glenohumeral Osteoarthritis. JBJS 85:251-258
29. Jacxsens M, Van Tongel A, Henninger HB, De Coninck B, Mueller AM, De Wilde L (2016) A three-dimensional comparative study on the scapulohumeral relationship in normal and osteoarthritic shoulders. J Shoulder Elbow Surg 25:1607-1615
30. Johnson MH, Paxton ES, Green A (2015) Shoulder arthroplasty options in young (<50 years old) patients: review of current concepts. J Shoulder Elbow Surg 24:317-325
31. Jost PW, Dines JS, Griffith MH, Angel M, Altchek DW, Dines DM (2011) Total shoulder arthroplasty utilizing mini-stem humeral components: technique and short-term results. Hss j 7:213-217
32. Kappe T, Cakir B, Reichel H, Elsharkawi M (2011) Reliability of radiologic classification for cuff tear arthropathy. J Shoulder Elbow Surg 20:543-547
33. Kim JH, Min YK (2018) Normal Range of Humeral Head Positioning on the Glenoid on Magnetic Resonance Imaging: Validation through Comparison of Computed Tomography and Magnetic Resonance Imaging. Clin Shoulder Elb 21:186-191
34. Kircher J, Ohly B, Albers S, Kirchner F, Hudek R, Magosch P (2022) Versorgungsrealität in Deutschland: ein Auszug aus dem Schulterendoprothesenregister der Deutschen Vereinigung für Schulter- und Ellenbogenchirurgie e.V. (DVSE). Obere Extremität 17:92-98
35. Klawitter JJ, Patton J, More R, Peter N, Podnos E, Ross M (2020) In vitro comparison of wear characteristics of PyroCarbon and metal on bone: Shoulder hemiarthroplasty. Shoulder Elbow 12:11-22
36. Kleim BD, Garving C, Brunner UH (2020) Cementless curved short stem shoulder prostheses with a proximal porous coating: ingrowth properties at 2-5 years of radiological follow-up with clinical correlation. J Shoulder Elbow Surg 29:2299-2307
37. Kleim BD, Garving C, Brunner UH (2020) RSA, TSA and PyC hemi-prostheses: comparing indications and clinical outcomes using a second-generation modular short-stem shoulder prosthesis. Archives of Orthopaedic and Trauma Surgery;10.1007/s00402-020-03529-w
38. Kleim BD, Hinz M, Geyer S, Scheiderer B, Imhoff AB, Siebenlist S (2022) A 3-Dimensional Classification for Degenerative Glenohumeral Arthritis Based on Humeroscapular Alignment. Orthop J Sports Med 10:23259671221110512
39. Kleim BD, Lappen S, Kadantsev P, Degenhardt H, Fritsch L, Siebenlist S, et al. (2023) Validation of a novel 3-dimensional classification for degenerative arthritis of the shoulder. Arch Orthop Trauma Surg;10.1007/s00402-023-04890-2
40. Kleim BD, Zolotar A, Hinz M, Nadjar R, Siebenlist S, Brunner UH (2023) Pyrocarbon hemiprostheses show little glenoid erosion and good clinical function at 5.5 years of follow up. J Shoulder Elbow Surg;10.1016/j.jse.2023.05.027
41. Knowles NK, Keener JD, Ferreira LM, Athwal GS (2015) Quantification of the position, orientation, and surface area of bone loss in type B2 glenoids. J Shoulder Elbow Surg 24:503-510
42. Kocsis G, Thyagarajan DS, Fairbairn KJ, Wallace WA (2016) A new classification of glenoid bone loss to help plan the implantation of a glenoid component before revision arthroplasty of the shoulder. Bone Joint J 98-b:374-380
43. Krukenberg A, Imiolczyk JP, Moroder P, Scheibel M (2018) [Shoulder Arthroplasty]. Z Orthop Unfall 156:227-238
44. Kumar R, Arora A, Lakkireddy M, Srirambhatla A, Maley DK, Eppakayala S, et al. (2022) Achieving adequacy of shoulder Grashey’s view on X-ray: A small step to improve patient care. Clinical Radiology 77:e11-e12
45. Luedke C, Kissenberth MJ, Tolan SJ, Hawkins RJ, Tokish JM (2018) Outcomes of Anatomic Total Shoulder Arthroplasty with B2 Glenoids: A Systematic Review. JBJS Reviews 6:

46. Marsh H, Rodríguez-Reinoso F. CHAPTER 9 - Production and Reference Material. In: Marsh H, Rodríguez-Reinoso F, eds. *Activated Carbon*;https://doi.org/10.1016/B978-008044463-5/50023-6. Oxford: Elsevier Science Ltd; 2006:454-508.
47. Matsen FAI, Carofino BC, Green A, Hasan SS, Hsu JE, Lazarus MD, et al. (2021) Shoulder Hemiarthroplasty with Nonprosthetic Glenoid Arthroplasty: The Ream-and-Run Procedure. JBJS Reviews 9:e20.00243
48. Maurer A, Fucentese SF, Pfirrmann CW, Wirth SH, Djahangiri A, Jost B, et al. (2012) Assessment of glenoid inclination on routine clinical radiographs and computed tomography examinations of the shoulder. J Shoulder Elbow Surg 21:1096-1103
49. McBride AP, Ross M, Hoy G, Duke P, Page R, Peng Y, et al. (2021) Mid-term outcomes of pyrocarbon humeral resurfacing hemiarthroplasty compared to metal humeral resurfacing and metal stemmed hemiarthroplasty for osteoarthritis in young patients: Analysis from the Australian Orthopaedic Association National Joint Replacement Registry. J Shoulder Elbow Surg;10.1016/j.jse.2021.08.017
50. Morwood MP, Johnston PS, Garrigues GE (2017) Proximal ingrowth coating decreases risk of loosening following uncemented shoulder arthroplasty using mini-stem humeral components and lesser tuberosity osteotomy. J Shoulder Elbow Surg 26:1246-1252
51. Nagels J, Stokdijk M, Rozing PM (2003) Stress shielding and bone resorption in shoulder arthroplasty. J Shoulder Elbow Surg 12:35-39
52. Neyton L, Kirsch J, Collotte P, Collin P, Gossing L, Chelli M, et al. (2019) Mid- to long-term follow-up of shoulder arthroplasty for primary glenohumeral osteoarthritis in patients aged 60 or under. Journal of Shoulder and Elbow Surgery 28:
53. Oh HK, Lim TK (2018) Short Humeral Stems in Shoulder Arthroplasty. Clin Shoulder Elb 21:105-110
54. Otto A, Scheiderer B, Murphy M, Savino A, Mehl J, Kia C, et al. (2021) Biconcave Glenoids Show Three Differently Orientated Posterior Erosion Patterns. Journal of Shoulder and Elbow Surgery;https://doi.org/10.1016/j.jse.2021.04.028
55. Parsons IMt, Millett PJ, Warner JJ (2004) Glenoid wear after shoulder hemiarthroplasty: quantitative radiographic analysis. Clin Orthop Relat Res;10.1097/01.blo.0000119249.61696.f1120-125
56. Raiss P, Schnetzke M, Wittmann T, Kilian CM, Edwards TB, Denard PJ, et al. (2019) Postoperative radiographic findings of an uncemented convertible short stem for anatomic and reverse shoulder arthroplasty. J Shoulder Elbow Surg 28:715-723
57. Razfar N, Reeves JM, Langohr DG, Willing R, Athwal GS, Johnson JA (2016) Comparison of proximal humeral bone stresses between stemless, short stem, and standard stem length: a finite element analysis. J Shoulder Elbow Surg 25:1076-1083
58. Reuther F, Irlenbusch U, Kääb MJ, Kohut G (2022) Conversion of Hemiarthroplasty to Reverse Shoulder Arthroplasty with Humeral Stem Retention. J Clin Med 11:
59. Ricchetti ET, Khazzam MS, Denard PJ, Dines DM, Bradley Edwards T, Entezari V, et al. (2021) Reliability of the modified Walch classification for advanced glenohumeral osteoarthritis using 3-dimensional computed tomography analysis: a study of the ASES B2 Glenoid Multicenter Research Group. J Shoulder Elbow Surg 30:736-746
60. Salkeld SL, Patron LP, Lien JC, Cook SD, Jones DG (2016) Biological and functional evaluation of a novel pyrolytic carbon implant for the treatment of focal osteochondral defects in the medial femoral condyle: assessment in a canine model. Journal of orthopaedic surgery and research 11:155-155
61. Schnetzke M, Coda S, Raiss P, Walch G, Loew M (2016) Radiologic bone adaptations on a cementless short-stem shoulder prosthesis. J Shoulder Elbow Surg 25:650-657
62. Schoch B, Schleck C, Cofield RH, Sperling JW (2015) Shoulder arthroplasty in patients younger than 50 years: minimum 20-year follow-up. J Shoulder Elbow Surg 24:705-710
63. Shu B, Ou X, Hu L (2023) Influential articles on shoulder arthroplasty: bibliometric analysis and visualized study. J Shoulder Elbow Surg 32:677-684
64. Shukla DR, McLaughlin RJ, Lee J, Cofield RH, Sperling JW, Sánchez-Sotelo J (2019) Intraobserver and interobserver reliability of the modified Walch classification using radiographs and computed tomography. J Shoulder Elbow Surg 28:625-630
65. Siebert MJ, Chalian M, Sharifi A, Pezeshk P, Xi Y, Lawson P, et al. (2020) Correction to: Qualitative and quantitative analysis of glenoid bone stock and glenoid version: inter-reader analysis and correlation with rotator cuff tendinopathy and atrophy in patients with shoulder osteoarthritis. Skeletal Radiol;10.1007/s00256-020-03386-z
66. Sperling JW, Cofield RH, Rowland CM (2004) Minimum fifteen-year follow-up of Neer hemiarthroplasty and total shoulder arthroplasty in patients aged fifty years or younger. J Shoulder Elbow Surg 13:604-613

67. Sumner DR, Galante JO (1992) Determinants of stress shielding: design versus materials versus interface. Clin Orthop Relat Res 202-212
68. Tan MT, Read JW, Bokor DJ (2018) Does proximal porous coating in short-stem humeral arthroplasty reduce stress shielding? Shoulder & Elbow 11:56-66
69. Terrier A, Ston J, Larrea X, Farron A (2014) Measurements of three-dimensional glenoid erosion when planning the prosthetic replacement of osteoarthritic shoulders. Bone Joint J 96-b:513-518
70. Verhaegen F, Meynen A, Matthews H, Claes P, Debeer P, Scheys L (2021) Determination of pre-arthropathy scapular anatomy with a statistical shape model: part I—rotator cuff tear arthropathy. Journal of Shoulder and Elbow Surgery 30:1095-1106
71. Visotsky JL, Basamania C, Seebauer L, Rockwood CA, Jensen KL (2004) Cuff Tear Arthropathy: Pathogenesis, Classification, and Algorithm for Treatment. JBJS 86:35-40
72. Wagner ER, Farley KX, Higgins I, Wilson JM, Daly CA, Gottschalk MB (2020) The incidence of shoulder arthroplasty: rise and future projections compared with hip and knee arthroplasty. J Shoulder Elbow Surg 29:2601-2609
73. Walch G, Badet R, Boulahia A, Khoury A (1999) Morphologic study of the Glenoid in primary glenohumeral osteoarthritis. The Journal of Arthroplasty 14:756-760
74. Walch G, Moraga C, Young A, Castellanos-Rosas J (2012) Results of anatomic nonconstrained prosthesis in primary osteoarthritis with biconcave glenoid. J Shoulder Elbow Surg 21:1526-1533
75. Walker KE, Simcock XC, Jun BJ, Iannotti JP, Ricchetti ET (2018) Progression of Glenoid Morphology in Glenohumeral Osteoarthritis. JBJS 100:49-56
76. Werner BS, Stehle J, Abdelkawi A, Plumhoff P, Hudek R, Gohlke F (2017) Progressive glenoid bone loss caused by erosion in humeral head resurfacing. Orthopade 46:1028-1033
77. Youderian AR, Ricchetti ET, Drews M, Iannotti JP (2014) Determination of humeral head size in anatomic shoulder replacement for glenohumeral osteoarthritis. J Shoulder Elbow Surg 23:955-963

Publikationsliste

1) Baker P, Muthumayandi K, Gerrand C, **Kleim B**, Bettinson K, Deehan D. Influence of body mass index (BMI) on functional improvements at 3 years following total knee replacement: a retrospective cohort study. PLoS One. 2013;8(3):e59079. doi: 10.1371/journal.pone.0059079. Epub 2013 Mar 19. PMID: 23527090.

2) Malviya A, Wilson G, **Kleim B**, Kurtz SM, Deehan D. Factors influencing return to work after hip and knee replacement. Occup Med (Lond). 2014 Sep;64(6):402-9. doi: 10.1093/occmed/kqu082. PMID: 25146049.

3) **Kleim BD**, Malviya A, Rushton S, Bardgett M, Deehan DJ. Understanding the patient-reported factors determining time taken to return to work after hip and knee arthroplasty. Knee Surg Sports Traumatol Arthrosc. 2015 Dec;23(12):3646-52. PMID: 25193567.

4) Bardgett M, Lally J, Malviya A, **Kleim B**, Deehan D. Patient reported factors influencing return to work after joint replacement. Occup Med (Lond). 2015. doi: 10.1093/occmed/kqv187. First published online: December 13, 2015.

5) **Kleim BD**, Garving C, Brunner UH. RSA, TSA and PyC-Hemiprostheses: Comparing indications and clinical outcomes using a second-generation modular short stem shoulder prosthesis. AOTS 2020. DOI: 10.1007/s00402-020-03529-w. PMID: 33025070.

6) **Kleim BD**, Garving C, Brunner UH. Cementless curved short stem shoulder prostheses with a proximal porous coating: ingrowth properties at 2-5 years of radiological follow-up with clinical correlation. JSES Nov 2020. 29(11):2299-2307. PMID: 32666922.

7) **Kleim BD**, Siebenlist S, Scheiderer B, Imhoff AB. Irreparable Rotatorenmanschettenruptur – inverse Prothese und Alternativverfahren. Der Unfallchirurg 2020. DOI 10.1007/s00113-020-00922-3. PMID: 33245367.

8) Maximilian Hinz, **Benjamin D Kleim**, Felix Mayr, Andreas B Imhoff, Sebastian Siebenlist. Acute rupture of the pectoralis major muscle at the musculotendinous junction: Case

report of a rare injury and literature review. Unfallchirurg 2021. doi: 10.1007/s00113-021-00997-6. PMID: 33876275.

9) Maximilian Hinz, **Benjamin D Kleim**, Daniel P. Berthold, Stephanie Geyer, Andreas B. Imhoff, Julian Mehl. Brazilian Jiu Jitsu: frequent injuries, injury mechanisms, risk factors & return to sport - a cross-sectional survey on 1140 athletes. OJSM 2021. PMID: 34988235.

10) Hinz M, Geyer S, Winden F, Braunsperger A, Kreuzpointner F, **Kleim BD**, Imhoff AB, Mehl J. Mid-Term Outcome and Strength Assessment after Proximal Rectus femoris Refixation in Athletes. Archives of Orthopaedic and Trauma Surgery. PMID: 34664130.

11) Geyer S, Winden F, Braunsperger A, Kreuzpointner F, **Kleim BD**, Lappen S, Imhoff AB, Mehl J, Hinz M. Mid-Term Outcome and Strength Assessment after Quadriceps Tendon Refixation in Athletes. European Journal of Orthopaedic Surgery & Traumatology. (accepted)

12) **Kleim BD,** Hinz M, Geyer S, Scheiderer B, Imhoff AB, Siebenlist S. A 3-Dimensional Classification for Degenerative Glenohumeral Arthritis Based on Humeroscapular Alignment. Orthopaedic Journal of Sports Medicine. August 2022. doi:10.1177/23259671221110512.

13) José Fernando Sánchez Carbonel, Maximilian Hinz, Christian Lozano, **Benjamin Daniel Kleim**, Andreas B Imhoff, Sebastian Siebenlist. Pectoralis major and pectoralis minor transfer for irreparable subscapularis tendon tears Oper Orthop Traumatol. 2022 Feb;34(1):45-54. doi: 10.1007/s00064-021-00760-5. Epub 2022 Feb 3.

14) Sebastian Lappen, Stephanie Geyer, Pavel Kadantsev, Maximilian Hinz, **Benjamin Kleim**, Hannes Degenhardt, Andreas B Imhoff, Sebastian Siebenlist. All-suture anchors for distal biceps tendon repair: a preliminary outcome study. Arch Orthop Trauma Surg. 2022 Nov 22. doi: 10.1007/s00402-022-04690-0.

15) **Kleim BD,** Carbonel JFS, Hinz M, Rupp MC, Scheiderer B, Imhoff AB, Siebenlist S. A shallow morphology of the intertubercular groove is associated with medial and bilateral but not lateral pulley lesions. Knee Surg Sports Traumatol Arthrosc. 2023 Feb 23. doi: 10.1007/s00167-023-07350-x. Epub ahead of print. PMID: 36820903.

16) **Kleim BD**, Lappen S, Kadantsev P, Degenhardt H, Fritsch L, Siebenlist S, Hinz M. Validation of a novel 3-dimensional classification for degenerative arthritis of the shoulder. Archives of orthopaedic and trauma surgery. 2023. PMID: 37308783. DOI: 10.1007/s00402-023-04890-2.

17) **Kleim BD**, Zolotar A, Hinz M, Nadjar R, Siebenlist S, Brunner UH. Pyrocarbon hemiprostheses show little glenoid erosion and good clinical function at 5.5 years of follow-up. Journal of shoulder and elbow surgery. 2024. PMID: 37385424. DOI: 10.1016/j.jse.2023.05.027.

Danksagung

An dieser Stelle möchte ich mich recht herzlich bei all Denen bedanken, die mich bisher in meiner klinischen und wissenschaftlichen Karriere betreut und unterstützt haben. Ein besonderes Dankeschön geht hierbei an Prof. Dr. Sebastian Siebenlist, der meine Forschungsprojekte seit meinem Anfang in der Sportorthopädie am Klinikum rechts der Isar begleitet und unterstützt hat und mich immer wieder dazu gebracht hat meine Ziele höher zu setzen und meine Arbeit mit bestmöglicher Qualität zu erbringen. Ich freue mich diese wissenschaftliche Zusammenarbeit auch in der Zukunft fortführen zu dürfen. Ebenso ein besonderes Dankeschön an seinen Vorgänger, Prof. Dr. Andreas Imhoff, der mich in die außerordentlich energetische und motivierte Kultur der Abteilung aufgenommen hat. Sie haben mich ermutigt meine wissenschaftlichen Ideen zu verwirklichen und mich auch klinisch gelehrt und geprägt.

Zudem ein riesiges Dankeschön an das gesamte Team der Sportorthopädie, für all das was ich bei euch und mit euch lernen durfte. Danke an Dr. med. univ. Maximilian Hinz, Dr. med. Yannick Ehmann, Dr. Pavel Kadantsev, Dr. med. Sebastian Lappen, PD Dr. med. Stefanie Geyer, PD Dr. Bastian Scheiderer, Dr. med. Hannes Degenhardt, Dr. med. univ. Lorenz Fritsch, Dr. med. univ. Romed Vieder und Dr. med. Marco Rupp, für die tolle Zusammenarbeit bei den Projekten.

Außerdem habe ich meinem Fachmentorat, bestehend aus Prof. Dr. Peter Bieberthaler und Prof. Dr. Stefan Buchmann, für die Betreuung meiner Forschung und Habilitation zu danken.

Meinem Doktorvater Prof. Dr. med. U. Brunner und seiner Abteilung im Krankenhaus Agatharied, möchte ich für die fortbestehende Zusammenarbeit und wissenschaftliche Kollaboration danken. Meinem ersten wissenschaftlichen Mentor Prof. David Deehan aus der University of Newcastle upon Tyne in England, der mich mit seinem Team zur Erlangung des MRes (Masters of Research of medical Sciences) betreut und instruiert hat, gilt ebenfalls ein andauerndes Dankeschön.

Ein ewiges Dankeschön meinen lieben Eltern für die ununterbrochene Unterstützung und das unzerbrechliche Glauben an mich bei all meinen Vorhaben. Letztlich möchte ich mich bei meiner lieben Frau Sarah und beiden kleinen Söhnen Frederick und Hugo bedanken, für die Geduld und das Verstehen für meine oft in unser Privatleben einschneidende Arbeit, und dafür das ihr mir zu jeder Zeit den Rücken stärkt.

Abdruck der für die Habilitation relevanten Publikationen

(Accepted manuscript, DOI: 10.1016/j.jse.2020.02.025)

Cementless curved short stem shoulder prostheses with a proximal porous coating: ingrowth properties at 2-5 years of radiological follow-up with clinical correlation

Benjamin D. Kleim, MBBS, MRes, Christina Garving, MD,
Ulrich H. Brunner, MD, PhD*

Trauma and Orthopaedic Surgery, Krankenhaus Agatharied, Hausham, Bavaria, Germany

Abstract

Background

Little is known about the way the newest generation of stems integrate into the proximal humerus and their effect on the surrounding bone. Factors which may influence ingrowth have not been investigated.

Methods

A consecutive cohort study examining 74 anatomical, reverse or pyrocarbon hemi-prostheses, using a curved modular short stem with a proximal porous coating 2-5 years postoperatively (mean 35 months). X-rays were reviewed by 2 examiners independently. Bone loss was scored with one point per zone with partial and 2 points per zone with complete resorption (10 zones). The Constant score was used for clinical correlation. Multiple linear regression was employed to investigate correlations between variables.

Results

No subsidence or shift of the stems occurred. 2 of 74 patients showed 1 zone of periprosthetic lucency of 1mm. The filling ratio averaged 0.54 (range 0.36-0.75). 30 patients (40.5%)

displayed bony resorption, first seen at 16.6 months (range 3-40), commonly in zones 1 and 5. 22 patients had ≥1 zone with partial resorption and 8 (10.8%) developed full thickness resorption after 32 (range 10-49) months.

One new finding was that female sex and older age accounted for 51% of the variation of the filling ratio. A high filling ratio, especially when >0.55, correlated with bone resorption ($p<0.001$). Age, sex and prosthesis type did not directly predict bone resorption. Bony sclerosis correlated with a high filling ratio ($p=0.019$) and thereby indirectly with resorption. A direct correlation between sclerosis and resorption was narrowly insignificant ($p=0.058$) once correcting for filling ratio. RSA had a higher filling ratio than TSA patients ($p<0.001$), resulting indirectly in more bone resorption. The preoperative diagnosis did not significantly correlate with filling ratio ($p=0.59$) or the resorption score ($p=0.69$). A varus or valgus alignment did not predict resorption ($p=0.21$) or the formation of sclerotic lines ($p=0.93$). Bone loss did not correlate with clinical results.

Conclusions

These short stems are firmly anchored 2-5 years postoperatively. However, significant bone loss, linked to a high filling ratio (>0.55), is observed proximally around these stems. The development of sclerotic lines around the stem indicates oversizing. Other factors were not found to have a significant effect on stem ingrowth. The implantation of stems with a large filling ratio is more common in older females and in patients receiving RSA. Autologous impaction bone grafting could downsize the required stem. If adequate hold is not afforded by a suitably small stem cementation is advisable.

Level of evidence: 3

Key words: shoulder prosthesis, short stem, resorption, remodelling, radiological, pyrocarbon.

Introduction

Uncemented short stems with a proximal porous coating are becoming widely used in anatomical, reverse and hemi shoulder arthroplasties [9, 11]. Previous short stem prostheses, without the proximal porous coating, have been found to have high rates of aseptic loosening [3]. The clinical results that can be achieved using this latest implant type have been shown to be at least comparable to standard shafts [16, 20]. However, the way this newest generation of stems integrate into the bone and their effect on the surrounding bone stock is yet to be examined in detail.

Stress shielding is a reduction of bone density resulting from decreased mechanical stimulation of bone surrounding an implant (Wolf's law). It is a problem which was first described in hip prostheses, but has since been found after shoulder arthroplasty [7, 17]. Shortening the humeral component of a shoulder prosthesis brings about a more natural stress distribution [6], so could ameliorate stress shielding caused by the implant. This is important as bone resorption could affect the long-term clinical function of the prostheses, increase the likelihood of periprosthetic fracture and make revision surgery more difficult.

The filling ratio of the prosthesis in the proximal humerus has been shown to be an important predictor of bone resorption in previous studies [16, 17, 18, 20]. The filling ratio gives an indication of the size of the prosthesis relative to the patient's bone structure. Larger prostheses are stiffer than thinner ones. The stiffness dictates how much force is conducted to the distal end of the implant. Stiff shafts conduct a greater proportion of load forces to the distal tip of the prosthesis, shielding the metaphysis. Conversely, thin shafts are more flexible and convey more load to the proximal bone, avoiding stress shielding.

Recently other authors have begun to describe the radiological properties of this newest range of short stem prostheses, with a proximal porous coating [16, 18, 20, 22]. Of these, Schnetzke and Raiss both found, mirroring the findings of the first generation of short stem prostheses, that a high filling ratio was linked to increased bone remodelling. However their analysis did not consider the interaction of different variables such as age, sex, diagnosis and all prosthesis types (RSA, TSA or hemiprostheses) on the remodelling processes observed. Nor did they differentiate between anabolic and catabolic developments (sclerosis vs resorption), the relationship and significance of these are still to be uncovered. Tan et. al. showed a trend to similar levels of stress shielding, but with more medial calcar resorption in the absence of the proximal porous coating when compared to prostheses with the coating [22]. However, this was a comparison study with small numbers and the findings were not statistically significant. A clear recommendation of how to avoid bone loss due to remodelling when implanting these novel short stem shoulder prostheses has not been made.

The aim of this study was therefore to describe the radiological ingrowth properties of short stem shoulder prostheses with a proximal porous coating. Furthermore, we set out to explain the remodelling processes observed, investigate their interactions with other factors and correlate these with the clinical outcome.

Materials and Methods

Patient population and study design

We conducted a consecutive cohort study of 74 out of 103 patients who were operated with a second-generation modular short stem shoulder prosthesis with a proximal porous coating between May 2013 and June 2015 at Agatharied hospital. Implanted were anatomical (TSA), reverse (RSA) or hemi-prostheses with a pyrocarbon head (PyC) (Aequalis Ascend Flex, Wright medical, Bloomington, USA). All 103 patients were invited for follow-up examinations. Our department had clinical follow-up data for 76 and x-ray images with adequate quality and projection for 74 of these 103 patients 2-5 years postoperatively (mean 35, range 23-60 months). 9 patients had complications leading to revision or rendering them incomparable to the rest of the cohort, the others were lost to follow-up. Reasons for this were old age, inability to travel, refusal of follow-up and death unrelated to the prosthesis. This paper reports on the radiological findings of this cohort using the x-ray images taken at follow-up examinations, investigates interacting factors and correlates these with the clinical outcome.

Prostheses and operative technique

Titanium short stem uncemented modular prostheses with a proximal porous coating (Aequalis Ascend Flex™, Wright medical, Bloomington, USA) were implanted in three forms: Hemi-arthroplasty using a pyrocarbon head (PyC), anatomic total shoulder prosthesis (TSA) and reversed shoulder prosthesis (RSA). Cementless, this stem achieves metaphyseal fixation through bony ingrowth after a press-fit implantation. The oval shaped stem takes the path of least resistance during implantation, which helps to guide this into the natural retrotorsion of the humeral head. The glenoid retroversion was calculated relative to the Friedman line [10], the inclination according to the Maurer angle [15] using the preoperative x-rays and CT.

The operative technique uses the deltopectoral approach. In all cases the subscapularis was taken down in the “peel-off“ technique. The humeral head is resected in a manner depending on the type of prosthesis (see below). The proximal humerus was sequentially prepared using a sounder to define the width of the medullary canal and a compactor to check for the definitive implant size. All stems in this series were uncemented. The subscapularis tendon was repaired in all cases transosseously in double row technique.

RSA

For reversed prostheses a cut was made at 132.5° of inclination, using a guide, aiming for a final inclination of 145° when including the 12.5° of the inlay. The height of the resection should place the highest point of the tray at the level of the tip of the greater tuberosity. The glenoid baseplate was implanted with the inferior border flush to the inferior glenoid with 0-10° of inclination and a retroversion of <10°. If the retroversion was >10° this was corrected with the use of autologous wedge-shaped cancellous bone grafting (wedged BIO-RSA) under the base plate (4 cases). Additionally, in 2 cases with extreme glenoid wear, BIO-RSA was employed to lateralize the long peg base plate. All other RSA patients received the standard base plate with 25 mm or 29 mm diameter, depending on the native glenoid size. The size of the metaglene was 36 for females and 42 for males and this was implanted with an inferior overlap of at least 5mm. The humeral trial with the tray in position 6 and the required inlay was then reduced into the joint. The surgeon checked for deltoid tension, stability, range of motion and impingement. Finally the definitive humeral stem with the reversed head components, assembled on a back table, were implanted.

TSA

For the anatomical prostheses a free-hand resection along the anatomical neck, after removal of osteophytes, was undertaken. The natural inclination was then matched using a prosthesis with 127.5, 132.5 or 137.5° of inclination. Minimal reaming of the glenoid, according to the radius of the curvature of the glenoid, was undertaken and a cemented keeled glenoid was implanted. The humeral trial with the required head was then reduced into the joint and examined as described for RSA above. Finally, the definitive humeral stem with the anatomical head component, assembled on a back table, were implanted.

PyC

The technique for preparation and implantation of the humeral component mirrored that described for TSA. The joint capsule was mobilized and the labrum preserved. In some cases with Walch B1 and B2 glenoids these were treated with minimal reaming (so as to spare as much glenoid bone as possible) and then perforation of any remaining areas of sclerosis with a 1.2 mm Kirschner-wire. The size and rotation of the head was then chosen to maximize coverage of the resected surface whilst avoiding overlap. After trialling, the final stem was implanted and the Pyrocarbon head was mounted in vivo in the optimum rotation with the spring impactor.

Radiological assessment

Two experienced examiners (CG and BK) independently scruitinised the patients‘ x-rays in 3 planes on a diagnostic monitor in the manor described by Denard et. al. [7]. Where intra observer differences occurred, the cases were discussed and a consensus reached. The location of adaptations found was described in terms of the 10 Zones, as pictured in **figure 1**. The filling ratio was calculated by taking an average of the bone vs prosthesis diameter measured at 4 sites: Proximally and distally in both the AP and axillary views as shown in **figure 2**. In order to better differentiate and quantify bone resorption a novel scoring system

was employed: It was categorised into partial (osteopenia) and complete (full thickness) resorption and scored with one point for every zone with partial and 2 points for every zone with complete resorption.

Clinical evaluation

Patients were examined in our follow-up clinic at regular intervals by experienced examiners. The Constant score [4] was calculated pre- and postoperatively and used as a quantitative marker for the clinical outcome. Delta values (postoperative - preoperative) were used to allow for a more reliable comparison between subjects.

Statistics

Statistical models using multiple linear regression and hierarchical multiple linear regression were constructed to investigate correlations between the variables. This was performed using the SPSS V25.0 (IBM) software.

Results

The Demographics of the cohort of 74 patients which were analysed for this study are shown in **table 1**.

Implantation properties

55 stems were centered, 14 in valgus and 5 in varus alignment (illustrated in **figure 3**). The filling ratio, as described above, averaged at 0.54 (range 0.36-0.75). No subsidence or shift of the prosthesis was observed in any patients.

Bony adaptations

The bony adaptations which were found are summarised in **Table 2**. An example of reactive bony sclerosis (also called condensation lines) is shown in **figure 4**. 10 of these patients had sclerosis in zone 3, 4 cases in zone 2 and 3 patients in zone 4. 4 patients also had sclerotic reactions in the proximal zones: 3 patients in zone 1 and 1 patient in zone 6. These were accompanied by scleroses in the central distal zone in 3 cases and in zone 2 (lateral distal) in one case. All cases with sclerosis in the proximal zones had prostheses which were centred in alignment. Of those with sclerosis in zone 3 all but one were centred in alignment. Reactive sclerosis in zone 2 was present in cases with centered or varus alignment, never with valgus. 2 patients who developed bony scleroses had a valgus alignment, in both cases scleroses were observed only in zone 4.

Cortical thinning was observed in 30 patients (40.5%). Of these, 22 patients had at least one zone with partial resorption and 8 (10.8%) additionally had one or more zones with full thickness resorption. Partial resorption in zones 1 and 5 were the most common, with 15 and 17 cases respectively. Two patients had partial resorptions in zone 10, one patient in zone 7 and one patient in zone 2. These were first seen radiologically at an average of 16.6 months (range 3-40). The average resorption score, as described above, was 0.84 (range 0-6).

Full thickness resorption was present in two patients in zone 1, three patients in zone 2 (proximal part), two patients in zone 5 and one patient in zone 6. An example of this is shown in **figure 5**. The transition from partial to complete resorption was first seen on average after 32 (range 10-49) months. It can be observed that progressive osteopenia takes place with loss of bone density and cortical thickness. Following this, the bone collapses all the way down to the prosthesis, as shown in **figure 6.**

Statistical correlations

The outcomes of the linear regression analysis are displayed in **Table 3**. There was a strong correlation between a high filling ratio and more bone resorption ($p<0.001$), especially when the filling ratio exceeded 0.55 (see **figure 7**). Age and sex predict 51% of the variation in filling ratio ($p<0.001$). A higher bone resorption score did not significantly correlate with the constant score gained ($p=0.17$). The diagnosis leading to surgery did not significantly correlate with filling ratio ($p=0.59$) or the resorption score ($p=0.69$). The prosthesis type had no significant relationship with the resorption score ($p=0.47$). The presence of a varus or valgus alignment vs a centred one did not correlate with the development of condensation lines ($p=0.93$). A varus or valgus alignment was also not predictive of increased bony resorption ($p=0.42$). A higher filling ratio correlated significantly with the development of reactive bony sclerosis ($p=0.019$), explaining 8.1% of the variation in sclerosis.

In a hierarchical multiple linear regression model, when accounting for the effect of filling ratio first, age ($p=0.22$) and sex ($p=0.95$) do not have any significant direct association with bone resorption. The presence of a reactive bony sclerosis seemed to be a significant predictor of bone resorption ($p=0.003$) when tested independently, however when correcting for its collinearity with filling ratio, sclerosis added little variation to the model (3%) and was an insignificant factor ($p=0.058$). A comparison of the remodelling processes between RSA and

TSA showed more resorption in the RSA group, as well as a higher filling ratio in RSA patients. Once correcting for the effect of filling ratio there was no significant difference in resorption score between RSA and TSA ($p=0.70$). A specific comparison of resorption in zone 1 in RSA vs TSA patients, which could be different due to absence of the rotator cuff in many RSA patients, did not show a significant difference ($p=0.081$).

Discussion

Larger prostheses carry more forces from the shoulder joint to the proximal diaphysis, shielding the metaphysis and thereby causing bone remodelling. This effect may also be fortified by the loss of intraosseous blood supply [14]. Our finding that patients with a filling ratio under 0.55 had few problems with bony remodelling largely fits with the study by Raiss et al. who described an average filling ratio of 0.57 in patients with low levels of bony adaptations [18]. In contrast to the method proposed by Denard [7], Raiss measured the filling ratio using the endosteal bone diameter (a smaller distance, making the ratio compared to the stem larger) and only in the AP projection (where the shaft is thicker). This will be the reason why the average diameter of low remodelling patients was on the upper end of our safe cut-off for patients with little resorption. Also, in addition to describing what filling ratio patients with low remodelling have, we have assessed how large the filling ratio is allowed to be without risking a lot of bony resorption using this stem. The shape of the stem has been found to influence stress shielding and bone remodelling [1, 21, 24], therefore the critical filling ratio may vary when using other short stem prostheses. The pattern of bony resorption is that the proximal medial and lateral zones (1 and 5) are most commonly affected. The proximal area of zone 2 is then involved in the collapse of bone down to the stem, often creating an hour glass like formation.

In our cohort 17 of 74 patients (23%) displayed medial calcar osteopaenia, which is considerably less than the 83% reported by Schnetzke et al. in 2016 for the previous model of this prosthesis [19]. This may be a result of the proximal porous coating, which allows more transfer of load to the metaphyseal bone than the previous stem did.

Another adaptation that has previously been described is that of sclerosis of the cancellous bone surrounding the shaft, often around the distal tip, also called “condensation lines” [18, 20].

A new finding is the appearance of these scleroses at the proximal end of the stem, possibly due to the proximal porous coating, which gives this prosthesis hold in the proximal metaphysis. The formation of sclerosis, we have been able to show, seems not to be directly linked to bony resorption. Instead it mainly correlates indirectly, as it also occurs in patients with a higher filling ratio more commonly. A slight correlation may be present however, given the marginal p-value of 0.058, responsible for 3% of variation in resorption.

The alignment of the prosthesis in the proximal humerus (varus, valgus or centred) does not influence the formation of sclerosis. It does however dictate where sclerosis may occur, as it impacts upon the areas where loads and forces are transferred to and carried by the bone. When bony sclerosis occurs in centred prostheses it is found centrally at the tip of the stem with occasional additional scleroses in the proximal zones- axial load bearing. Patients with sclerotic reactions in zone 2 (lateral to the tip of the stem) have either a centred or varus alignment, never valgus. Finally, a valgus alignment seems to direct a sclerotic reaction medially of the tip of the stem.

Most of the adaptations observed appear in the AP radiograph and therefore occur medial or lateral to the shaft. This may be due to the shape of the shaft, which is thickest and least flexible at this point and could also be influenced by the direction of the forces which are applied during the movement of the shoulder. Despite the proximal porous coating, it seems that when prostheses are large and anchor at the distal tip, forces are not passed on to the proximal metaphysis, resulting in stress shielding and bone resorption here. If the shape of the prosthesis was revised to be thinner at the tip and have a more flexible stem, more force may be shared with the proximal bone.

Female sex and older age were described by a previous study to influence bony remodelling [18], however in our analysis we were able to explain that this relationship is only an indirect one. Age and sex influence the relative size of prostheses implanted, most likely due to poorer bone quality and it is only through this that older patients and those of female sex had more bony resorption.

In our cohort there was no direct relationship between the type of prosthesis implanted and bone remodelling. As TSA and RSA have polyethylene components and PyC does not, it seems that the remodelling processes seen cannot be explained by polyethylene wear, as has been suggested in other settings [1, 2]. Periprosthetic osteolysis is commonly caused by an inflammatory reaction to polyethylene wear particles. Only 2 patients (2.7%) were found to have one zone each of lucency of 1mm in our cohort. This is at a stark contrast with the results achieved using previous models of short stem shoulder prostheses, which have shown rates of lucent lines of 71% [3]. The low rate of lucent zones in this most recent stem type, when compared to previous models, may be in part a result of the proximal porous coating which integrates into the bone or fills with fibrous tissue [24] and may act as a barrier to polyethylene debris matter, as this migrates best along surfaces without a porous coating [1, 24]. Nevertheless, RSA patients did show more resorption than TSA, mediated through a higher filling ratio in this subgroup. Interestingly the preoperative diagnosis did not show a relationship with the filling ratio. This is probably because TSA patients all had primary OA and there were also a lot of primary OA patients in the RSA group. However, the OA patients who were treated with RSA are more likely to have high grade disease with posterior subluxation and therefore a rotator cuff insufficiency. It may be that these and the CTA patients, which are the other big diagnosis group to receive RSA, have a comparatively low cancellous bone density resulting in a larger filling ratio. The increased sheer forces the stems of RSA patients are likely to be

subjected to do not seem to affect the remodelling process significantly, perhaps just replacing the effect of forces from the rotator cuff.

Revision operations in patients with a lot of bone resorption will be challenging. Therefore, as ease of revision is one of the main arguments for the implantation of uncemented prostheses, it must be considered that these are not a good option for patients where the implantation of a small prosthesis does not afford good hold. Preoperatively, this can more likely be expected when operating older female patients, or when planning RSA, according to our findings. A maximum size of prosthesis which can be implanted whilst avoiding over-filling should be calculated. Intraoperatively, it may be necessary to adapt the surgical technique to the bone quality and its resulting hold after impaction, as ascertained using the twist test. If the largest calculated prosthesis which can be implanted without exceeding a filling ratio of 0.55 does not find satisfactory hold in the proximal humerus there are two alternative options. The transfer of autologous cancellous bone graft from the resected humeral head to the humeral metaphysis in order to increase bone stock has been found to be successful at ensuring fixation [12, 13, 23]. This may enable the implantation of an adequately small prosthesis with sufficient stability. If this is not possible, the implantation of a cementless prosthesis should be abandoned. Cemented prostheses cause a more even distribution of forces to the surrounding bone and allow for the implantation of thinner, less stiff prostheses, as a result of which they cause significantly less stress shielding [1, 5, 8, 17, 21]. Cementation may therefore be the alternative option to revert to if adequate fixation cannot be achieved with a small stem.

Limitations

The inherently retrospective design of this type of study makes direct comparisons between male/female, old/young and different prostheses as well as diagnoses difficult. As is commonly the case in studies of shoulder surgery, a larger cohort size would have increased

the reliability of our findings further. 29 of the cohort of 103 patients were not able to be analysed for this study, largely due to lack of follow-up data. This reduces the reliability of our findings, as we cannot be sure that the 74 patients analysed fully represent the entire cohort. As the range of development of resorption was 3-40 for partial and 10-49 for full thickness resorption, it is likely that some patients at the lower end of the range of follow-up would have developed further bone resorption in time. The absence of a clinical correlation with bone remodelling is a finding which mirrors what has been described by other authors [18, 20]. However, as there is only short- to mid-term data available on this thus far, it may be that a correlation is found in long-term studies in the future.

A problem with retrospectively analysed x-ray images is the ubiquitous slight differences in projection. Although only patients with x-rays of adequate quality and projection, where all 10 zones could be reliably analysed, were included, slight rotational differences could have led to decreased accuracy of the results. Having said this, our scoring system for bone resorption is relatively coarse, so does not require perfect images to lead to reproduceable results. Also, these are the kind of images which clinicians encounter regularly, making our method transferable to everyday clinical practice. Nonetheless, it may be that a method which accurately measures bone density and volume could uncover relationships between resorption and other factors more sensitively. As the area between zones 1 and 2 is a common site for bone loss, the previously described and used zones are not ideal in describing the adaptations around these prostheses.

Conclusions

Cementless short stem shoulder prostheses with a proximal porous coating are firmly embedded 2-5 years postoperatively, seemingly with improvements in comparison to previous models of this stem. Our findings suggest that the proximal porous coating, which is new to this model of short stem prosthesis, may have the following benefits: Reduced proximal bone resorption, increased fixation in the proximal metaphysis as suggested by the appearance of sclerosis here in some cases and decreased periprosthetic osteolysis.

Overall, large shafts appear to anchor distally, often causing a sclerotic hyperdensity of cancellous bone here. The area where this occurs is directed by the stem alignment. The proximal metaphysis is then shielded from physical stresses, causing resorption. The implantation of a prosthesis with a high filling ratio, in this stem over 0.55, carries the risk of high levels of bone loss. Bony sclerosis is also caused by overfilling of the proximal humerus, but resorption and sclerosis seem not to be directly associated with each other significantly. Formation of sclerosis can be seen as a marker of overfilling in the follow up clinic, which is also likely to lead to resorption. Resorption becomes evident after around 16.6 months in the proximal humeral metaphysis in a substantial proportion of patients. In around 1 in 10 patients in our cohort osteopenia progressed, around two and a half years postoperatively, to full thickness bone resorption in the proximal zones and proximal part of zone 2.

Preoperative diagnosis did not correlate with filling ratio or remodelling in our cohort. Age, sex and prosthesis type are not independent predictors of Bone resorption. However, the filling ratio is influenced by the age and sex of the patient and is also higher in RSA patients. Older and female patients, as well as those receiving RSA, are thereby indirectly at increased risk of periprosthetic bone remodelling.

There is no clinical correlation with bone resorption at this stage. However, there could be a higher risk of periprosthetic fracture in the future and the decreased bone stock will present problems when performing revision operations.

Autologous bone grafting from the resected humeral head to decrease the prosthesis size needed should be considered. Alternatively, cemented implants exhibit little stress shielding and therefore reduce the risk of bone resorption. We therefore propose that it is advisable to revert to the use of cemented prostheses when adequate fixation cannot be achieved with a press-fit implant of a safe size.

Further work

We suggest that large studies with long-term follow up to investigate the clinical and radiological properties of these prostheses are required in the future. Survival rates and contributing factors should be investigated. Furthermore, results after revision surgery are of interest.

References

1. Bauer TW, Schils J. The pathology of total joint arthroplasty.II. Mechanisms of implant failure. Skeletal Radiol 1999;28:483-497. 10.1007/s002560050552
2. Boileau P. Complications and revision of reverse total shoulder arthroplasty. Orthopaedics & Traumatology: Surgery & Research 2016;102:S33-S43. https://doi.org/10.1016/j.otsr.2015.06.031
3. Casagrande DJ, Parks DL, Torngren T, Schrumpf MA, Harmsen SM, Norris TR et al. Radiographic evaluation of short-stem press-fit total shoulder arthroplasty: short-term follow-up. J Shoulder Elbow Surg 2016;25:1163-1169. 10.1016/j.jse.2015.11.067
4. Constant CR, Murley AH. A clinical method of functional assessment of the shoulder. Clin Orthop Relat Res 1987:160-164.
5. Corten K, Bourne RB, Charron KD, Au K, Rorabeck CH. Comparison of total hip arthroplasty performed with and without cement: a randomized trial. A concise follow-up, at twenty years, of previous reports. J Bone Joint Surg Am 2011;93:1335-1338. 10.2106/jbjs.J.00448
6. Denard PJ, Noyes MP, Walker JB, Shishani Y, Gobezie R, Romeo AA et al. Proximal stress shielding is decreased with a short stem compared with a traditional-length stem in total shoulder arthroplasty. J Shoulder Elbow Surg 2018;27:53-58. 10.1016/j.jse.2017.06.042
7. Denard PJ, Raiss P, Gobezie R, Edwards TB, Lederman E. Stress shielding of the humerus in press-fit anatomic shoulder arthroplasty: review and recommendations for evaluation. J Shoulder Elbow Surg 2018;27:1139-1147. 10.1016/j.jse.2017.12.020
8. Digas G, Karrholm J, Thanner J. Different loss of BMD using uncemented press-fit and whole polyethylene cups fixed with cement: repeated DXA studies in 96 hips randomized to 3 types of fixation. Acta Orthop 2006;77:218-226. 10.1080/17453670610045948
9. Dillon MT, Ake CF, Burke MF, Singh A, Yian EH, Paxton EW et al. The Kaiser Permanente shoulder arthroplasty registry: results from 6,336 primary shoulder arthroplasties. Acta Orthop 2015;86:286-292. 10.3109/17453674.2015.1024565
10. Friedman RJ, Hawthorne KB, Genez BM. The use of computerized tomography in the measurement of glenoid version. J Bone Joint Surg Am 1992;74:1032-1037.
11. Kim SH, Wise BL, Zhang Y, Szabo RM. Increasing incidence of shoulder arthroplasty in the United States. J Bone Joint Surg Am 2011;93:2249-2254. 10.2106/jbjs.J.01994
12. Levy O. Reverse Shoulder Arthroplasty: Biomechanics, Clinical Techniques, and current technologies: Springer; 2016.
13. Lucas RM, Hsu JE, Gee AO, Neradilek MB, Matsen FA, III. Impaction autografting: bone-preserving, secure fixation of a standard humeral component. Journal of Shoulder and Elbow Surgery 2016;25:1787-1794. 10.1016/j.jse.2016.03.008
14. Marenzana M, Arnett TR. The Key Role of the Blood Supply to Bone. Bone Res 2013;1:203-215. 10.4248/br201303001
15. Maurer A, Fucentese SF, Pfirrmann CW, Wirth SH, Djahangiri A, Jost B et al. Assessment of glenoid inclination on routine clinical radiographs and computed tomography examinations of the shoulder. J Shoulder Elbow Surg 2012;21:1096-1103. 10.1016/j.jse.2011.07.010
16. Morwood MP, Johnston PS, Garrigues GE. Proximal ingrowth coating decreases risk of loosening following uncemented shoulder arthroplasty using mini-stem humeral components and lesser tuberosity osteotomy. J Shoulder Elbow Surg 2017;26:1246-1252. 10.1016/j.jse.2016.11.041
17. Nagels J, Stokdijk M, Rozing PM. Stress shielding and bone resorption in shoulder arthroplasty. J Shoulder Elbow Surg 2003;12:35-39. 10.1067/mse.2003.22
18. Raiss P, Schnetzke M, Wittmann T, Kilian CM, Edwards TB, Denard PJ et al. Postoperative radiographic findings of an uncemented convertible short stem for anatomic and

reverse shoulder arthroplasty. J Shoulder Elbow Surg 2019;28:715-723. 10.1016/j.jse.2018.08.037
19. Schnetzke M, Coda S, Raiss P, Walch G, Loew M. Radiologic bone adaptations on a cementless short-stem shoulder prosthesis. J Shoulder Elbow Surg 2016;25:650-657. 10.1016/j.jse.2015.08.044
20. Schnetzke M, Rick S, Raiss P, Walch G, Loew M. Mid-term results of anatomical total shoulder arthroplasty for primary osteoarthritis using a short-stemmed cementless humeral component. Bone Joint J 2018;100-b:603-609. 10.1302/0301-620x.100b5.Bjj-2017-1102.R2
21. Sumner DR, Galante JO. Determinants of stress shielding: design versus materials versus interface. Clin Orthop Relat Res 1992:202-212.
22. Tan MT, Read JW, Bokor DJ. Does proximal porous coating in short-stem humeral arthroplasty reduce stress shielding? Shoulder & Elbow 2018;11:56-66. 10.1177/1758573218773533
23. Wirth MA, Lim MS, Southworth C, Loredo R, Kaar TK, Rockwood CA, Jr. Compaction bone-grafting in prosthetic shoulder arthroplasty. J Bone Joint Surg Am 2007;89:49-57. 10.2106/jbjs.E.01069
24. Yao Z, Lin T-H, Pajarinen J, Sato T, Goodman S. Chapter 12 - Host Response to Orthopedic Implants (Metals and Plastics). In: Badylak SF, editor. Host Response to Biomaterials. Oxford: Academic Press; 2015. p. 315-373. (ISBN No. 978-0-12-800196-7)

Legends

Figures

1. The 10 Zones around the proximal humerus in the AP and axillary views.
2. Method of determining the filling ratio in 2 x-ray planes.
3. Examples of varus and valgus alignment of the implanted short stem prostheses.
4. Example of bony sclerosis around the tip of a large prosthesis 2 years postoperatively in a 67 y/o female patient.
5. Example of full thickness bone loss in zone one and the proximal part of zone 2, as well as partial resorption in zone 5 in a 70 y/o female patient.
6. Transition from good bone stock postoperatively, to osteopaenia after 24 Months and eventually collapse of the bone down to the prosthesis after 37 months in a 69 y/o female patient.
7. Scatter plot depicting the strong correlation between filling ratio and bony resorption.

Tables

1. Patient population demographics
2. Results of the correlation analysis, showing the effect of independent variables on dependent variables. The extent to which the independent variable influences the variability in the dependent variable is shown as %, the significance in terms of a p-value.
3. Types of bony adaptations observed and number of cases in which these occurred.

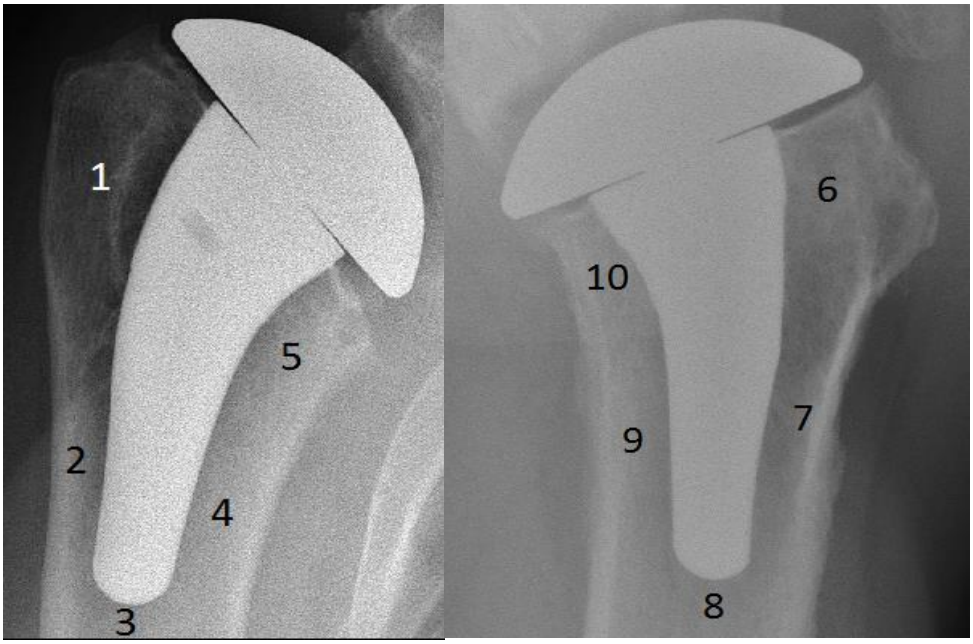

Figure 1: The 10 zones around the proximal humerus, in the AP (left) and axillary (right) views, categorising the site of bone remodelling. In the axillary view the count starts from the proximal ventral zone.

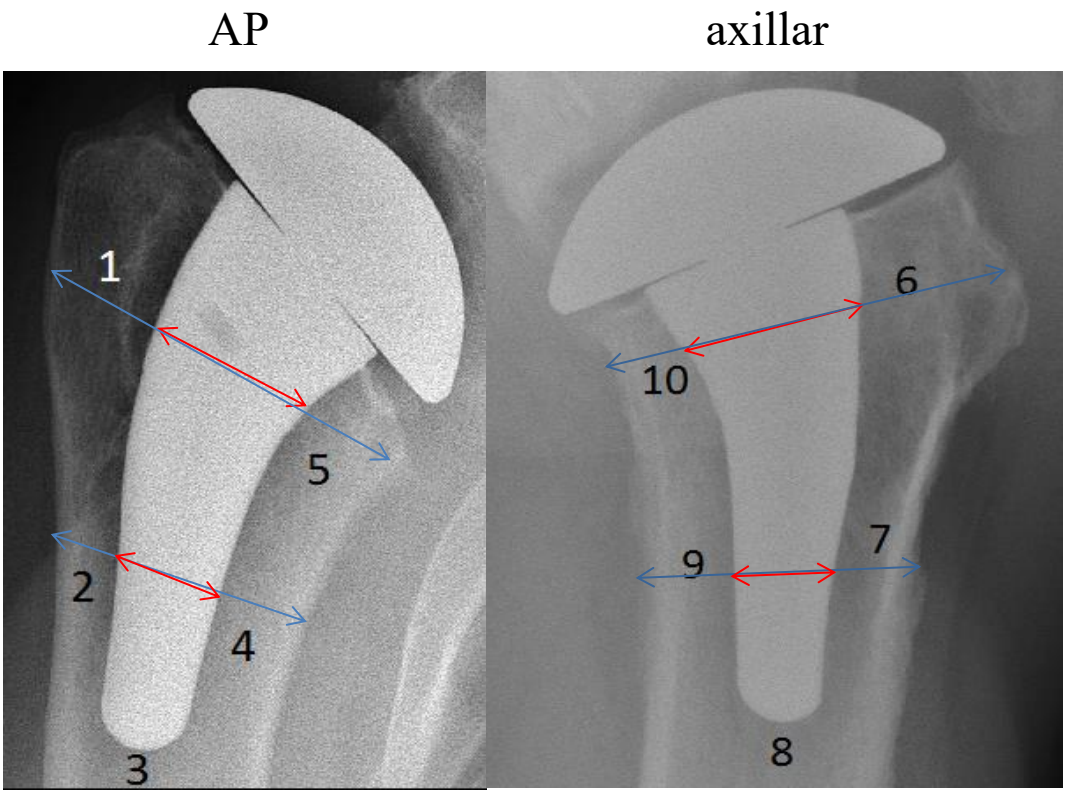

Figure 2: The method of determining the filling ratio in 2 x-ray planes. The mean average of the 4 ratios (red/blue) is taken.

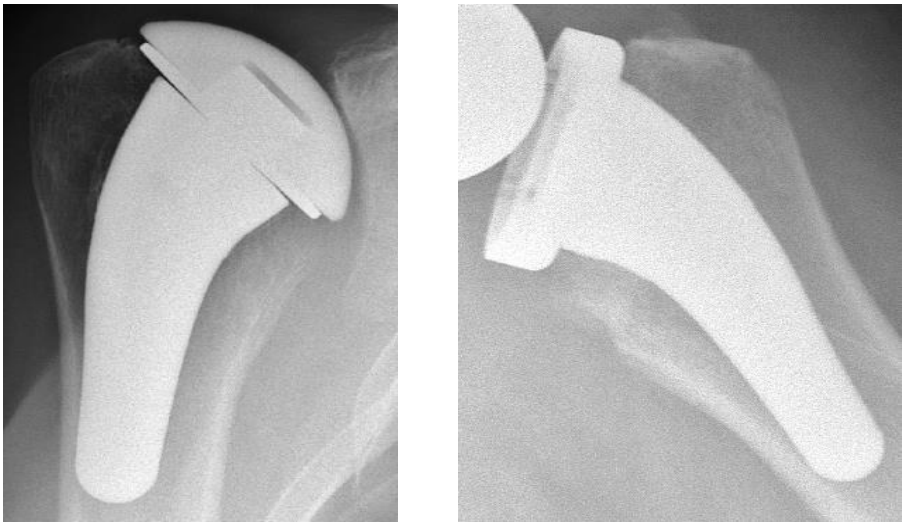

Figure 3: Examples of varus (left) and valgus (right) alignment of the implanted short stem prostheses.

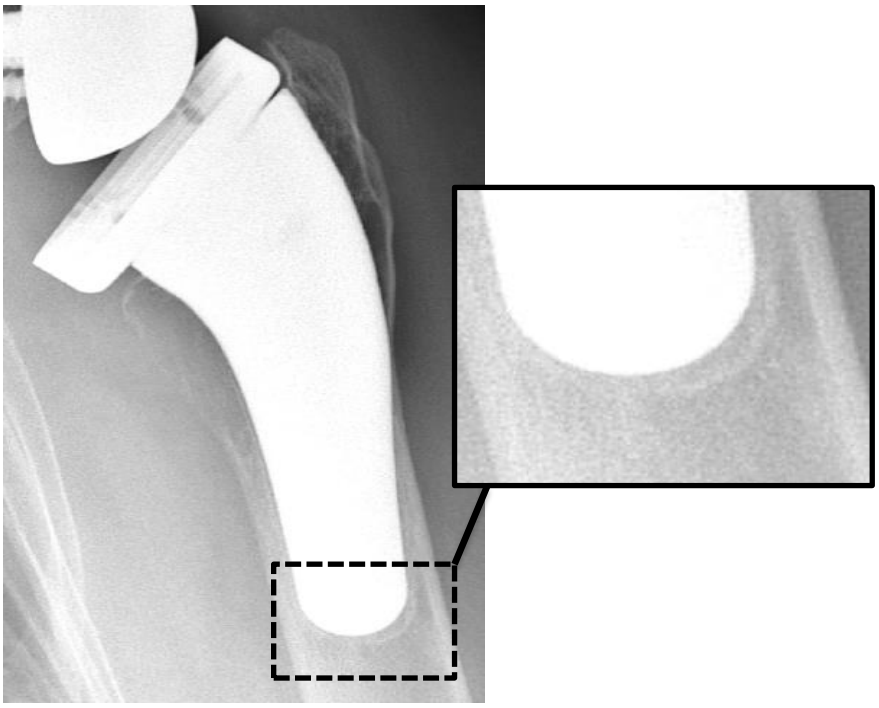

Figure 4: Example of bony sclerosis around the tip of a large prosthesis 2 years postoperatively in a 67 y/o female patient.

Figure 5: Example of full thickness bone loss in zone one and the proximal part of zone 2, as well as partial resorption in zone 5 in a 70 y/o female patient.

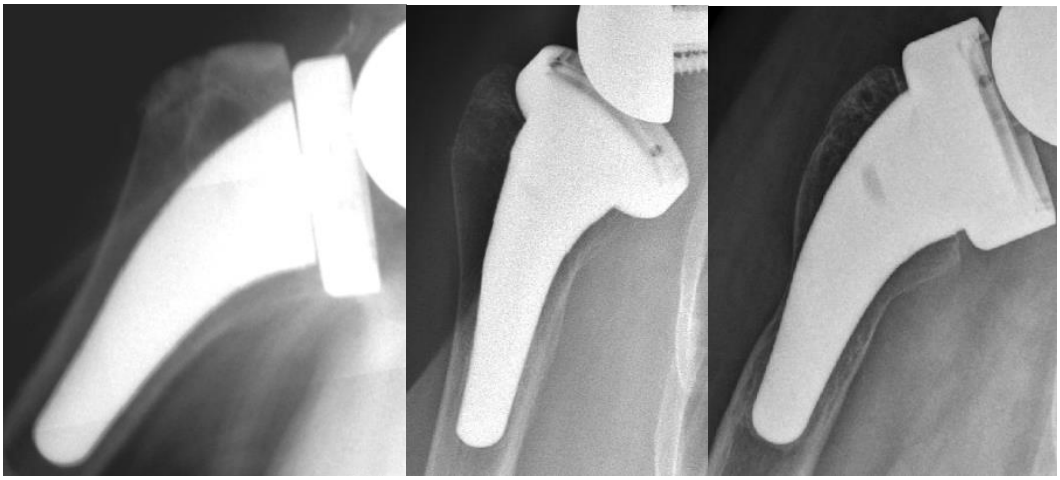

Figure 6: Transition from good bone stock postoperatively (left), to osteopaenia after 24 Months (middle) and eventually collapse of the bone down to the prosthesis after 37 months (right) in a 69 y/o female patient.

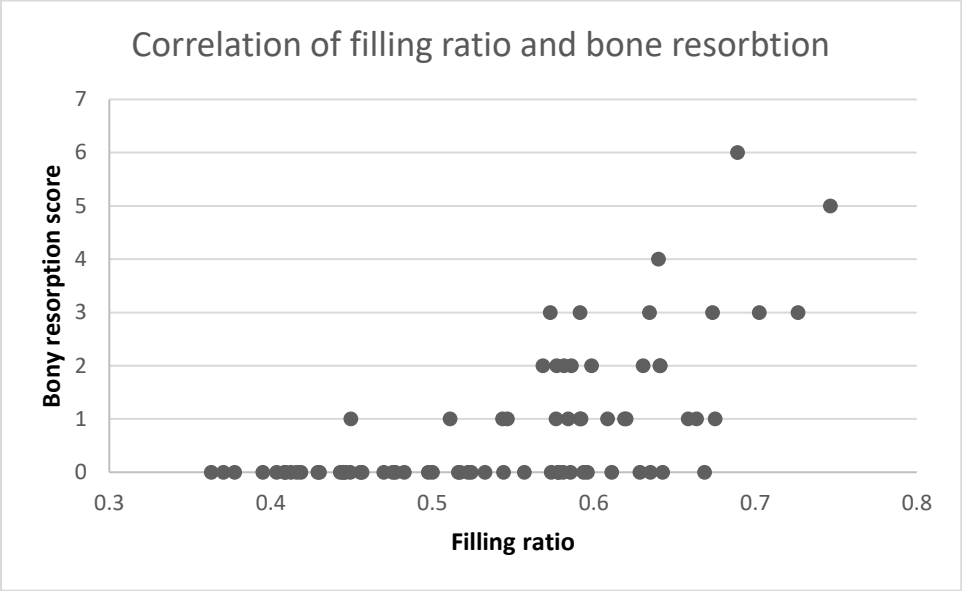

Figure 7: Scatter plot depicting the strong correlation between filling ratio and bony resorption. Noticeable is that at a filling ratio of <0.55 little resorption occurs.

Table 1: Patient population demographics

	Number	Age (years)	Sex	Diagnoses	Follow-up (months)
TSA	21	71.1 (range 62-84)	14 female	21 primary osteoarthritis	34 (range 23-52)
RSA	32	74.1 (65-84)	26 Female	7 primary osteoarthritis, 24 cuff tear arthropathy, 1 irreparable rotator cuff tear	39 (range 23-60)
PyC	21	58.3 (22-84)	4 Female	14 primary osteoarthritis, 1 fracture sequelae, 3 avascular necrosis, 3 arthritis resulting from instability	29 (range 23-48)

Table 2: Types of bony adaptations observed and number of cases in which these occurred.

Bony adaptation	**Number of cases**
Periprosthetic lucency	2 (each 1 mm in zone 1)
Reactive bony sclerosis	14
Partial thickness resorption	30
Full thickness resorption	8

Table 3: Shows the effect of independent variables on dependent variables. The extent to which the independent variable influences the variability in the dependent variable is shown as %, the significance in terms of a p-value. Age and sex were tested in combination as they are colinear in our cohort (men were younger).

Correlation	**variability influenced**	**p-value**
Filling ratio with bone resorption score	39%	<0.001
Age and sex with filling ratio	51%	<0.001
Age and sex with bone resorption score	18%	0.00067
Bone resorption score with constant score	2.6%	0.17
Diagnosis with filling ratio	0.39%	0.59
Diagnosis bone resorption score	0.22%	0.69
Filling ratio with reactive sclerosis	8.1%	0.019
Varus/valgus alignment with reactive sclerosis	0.0016%	0.93
Varus/valgus alignment with bone resorption score	0.89%	0.42
Prosthesis type with bone resorption	0.71%	0.47
Reactive sclerosis with bone resorption score	11%	0.003
RSA vs TSA on resorption score	9.8%	0.021
RSA vs TSA on filling ratio	36%	<0.001
RSA vs TSA on resorption score in zone 1	5.7%	0.081
When correcting for the effect of filling ratio first:		
Age and sex with bone resorption score	1.3%	0.22 and 0.95 respectively
Reactive sclerosis with bone resorption score	3.0%	0.058
RSA vs TSA on resorption score	0.19%	0.70

Archives of Orthopaedic and Trauma Surgery
https://doi.org/10.1007/s00402-020-03529-w

ORTHOPAEDIC SURGERY

RSA, TSA and PyC hemi-prostheses: comparing indications and clinical outcomes using a second-generation modular short-stem shoulder prosthesis

Benjamin D. Kleim[1,2] · Christina Garving[1] · Ulrich H. Brunner[1]

Received: 27 January 2020 / Accepted: 14 July 2020

Abstract

Introduction The goal of this study was to provide an insight into the clinical results after modular short-stem shoulder arthroplasty for various indications.

Materials and methods A consecutive cohort study of 76 patients followed up for 23–55 (mean 31.4) months. 23 anatomical (TSA), 32 reverse (RSA) and 21 hemi-prostheses with a pyrocarbon head (PyC), using a modular short stem with proximal porous coating were implanted. Range of motion, pain and Constant score (CS) were recorded. Comparisons of pre- vs postoperative outcomes, between prosthesis types and indications, were made.

Results All prosthesis types brought about a significant improvement ($p < 0.05$) in all measured outcomes. TSA had a significantly higher increase in the CS than PyC and RSA ($p = 0.002$ and 0.003, respectively). TSA produced superior gains in all ROM compared with RSA ($p < 0.02$). RSA brought about significantly smaller improvements in internal rotation than TSA and PyC ($p = 0.0001$ and 0.008, respectively). TSA had greater pain relief than PyC ($p = 0.02$). TSA with Walch A glenoids seemed to improve more than type B in the CS. PyC patients with Walch B glenoids improved more than Walch A ($p = 0.03$). When implanted due to Osteoarthritis (OA), PyC had a comparable final outcome to TSA ($p = 0.95$), although the preoperatively worse TSA patients had a greater improvement in the CS ($p = 0.026$). The outcome of RSA did not differ between indications, but Walch A glenoids tended to improve more.

Conclusions Using a second-generation short-stem shoulder prostheses, TSA achieves the best clinical improvements overall, especially for OA with a Walch A glenoid. Despite refixation of the subscapularis tendon in all cases, RSA has inferior internal rotation than TSA and PyC, suggesting a mechanical limitation. OA, a Walch B glenoid and arthritis caused by instability seem to be ideal indications when considering PyC.

Keywords Short stem · Shoulder arthroplasty · Pyrocarbon · Clinical · Hemiarthroplasty · Modular

Introduction

Shoulder arthroplasty is an increasingly common therapy for osteoarthritis, rheumatoid arthritis, cuff tear arthropathy, osteonecrosis as well as intra-articular fractures of the proximal humerus [1, 2].

Uncemented modular short-stemmed prostheses are still a relatively novel design type in shoulder prostheses and early results have been very positive with good function and low complication rates [3, 4]. A benefit is that one stem can be used in different configurations, as part of a hemi-prosthesis, RSA or anatomical TSA.

Hemi-prostheses are often considered for young patients with predominantly humeral disease, to avoid the complications of a glenoid replacement, subsequent bone loss and difficult revision surgery. However, a major problem when replacing only the humeral joint surface, traditionally with a cobalt-chrome head, is progressive glenoid wear and pain [5, 6]. Consequently, it has been found that TSA has a better outcome and more pain relief than hemiarthroplasty [7]. Pyrocarbon is a novel material thought to have

✉ Benjamin D. Kleim
Drkleim@doctors.org.uk

[1] Teaching Hospital of the Ludwig-Maximilians-University Munich, Munich, Germany

[2] Present Address: Department of Sports Orthopaedic Surgery, Klinikum rechts der Isar, Technical University Munich, Ismaningerstr 22, 81675 Munich, Germany

Published online: 06 October 2020

biomechanical properties similar to cartilage and is therefore being used in hemi-prostheses in a hope to ameliorate this problem [8]. Clinical results achieved with this new material are yet scarce and to our knowledge no data exist where these are compared to total shoulder replacement.

A recent comparison of elderly patients receiving RSA or TSA for glenohumeral arthritis with an intact rotator cuff was unable to find a significant difference in outcomes [9]. However, other studies have shown TSA to be superior in external rotation [10] and in internal rotation when compared in patients who had contralateral implantation of both RSA and TSA [11].

For cuff tear arthropathy there is a consensus that joint replacement should be performed with RSA. However, for primary osteoarthritis a TSA, RSA or hemi-prosthesis may be used. The choice of which type to implant is based on the patient age, function and disease morphology. The morphology of glenoid wear, as described by Walch and later modified by Bercik [12], has been shown to impact on the outcomes after shoulder arthroplasty. Outcomes of hemi-prostheses were found to be adversely affected by eccentric posterior wear [13]. This trend has also been described for outcomes after TSA, although these still had better results than hemi-prostheses in patients with Walch B2 glenoids [14]. For this reason a trend has emerged to opt for RSA in cases with excessive posterior glenoid wear [15].

The aim of this study was to investigate and compare the clinical outcomes of this second-generation short-stem modular shoulder prosthesis, when used in its different forms (TSA, RSA and PyC) and for different indications.

Materials and methods

Patient population and study design

In this single-centre cohort study, all 103 patients who consecutively underwent shoulder arthroplasty, using a curved titanium short-stem uncemented modular prostheses with a proximal porous coating (Aequalis Ascend Flex™, Wright Medical, Bloomington, USA), between May 2013 and June 2015 at Agatharied hospital, were invited for follow-up at regular intervals. All the operations were carried out by one of two senior surgeons.

Preoperatively the glenoid retroversion was calculated relative to the Friedman line [16], the inclination according to the Maurer angle [17] using X-rays and CT. The prostheses were implanted in three forms: Hemiarthroplasty using a pyrocarbon head (PyC), anatomic total shoulder prosthesis (TSA) and reversed shoulder prosthesis (RSA). Patients were offered prosthesis types best suited to their pathology: Patients with primary osteoarthritis, intact rotator cuffs, a glenoid retroversion of $< 10°$ and a posterior subluxation of the humeral head of $< 80\%$ underwent anatomical TSA; patients with little or no glenoid pathology, an intact rotator cuff and younger age were offered a PyC hemiprosthesis; lastly patients with rotator cuff pathology, glenohumeral subluxation of $> 80\%$ or a glenoid retroversion of 10° or more were treated with RSA. If the retroversion was $> 10°$, this was corrected with the use of autologous wedge-shaped cancellous bone grafting (wedged BIO-RSA) under the base plate (4 cases). Furthermore, in 2 cases with extreme glenoid wear, BIO-RSA was employed to lateralize the base plate. The subscapularis tendon was repaired in all cases transosseously in double-row technique.

10 Patients were excluded from this study: 1 with a hemiprosthesis with a titanium head (in place of the pyrocarbon due to nickel allergy) and 9 with complications as outlined in the results below, leaving a potential study group of 93. Data from preoperative examinations as well as at most recent follow-up were gathered and analysed. The glenoid morphology was described according to the modified Walch classification [12] from the preoperative CT. We had follow-up data for 76 of the eligible 93 patients (82%). Patients were lost to follow-up for reasons, such as old age and frailty, death (unrelated to the operation or prosthesis), missing data or refusal of follow-up examinations.

Clinical evaluation

Preoperatively and during follow-up appointments clinical outcomes, such as range of movement (ROM) and pain on the visual analogue scale (VAS), as well as the validated Constant Score (CS) [18], were recorded. This and further patient information including the demographics, diagnosis and operations were gathered from the patient records. To quantify internal rotation, this was scored as shown in Table 1.

Statistics

The statistics software SPSS V25.0 (IBM) was used. To assess the significance of changes in pre- and post-operative outcomes, the paired *t* test was calculated; to compare the delta values (difference between pre- and postoperative)

Table 1 Scoring system for internal rotation

Internal rotation score	Level reached with the back of the hand
0	Thigh
1	Gluteal
2	Iliosacral joint
3	Lumbar spine
4	Thoracic spine
5	Scapula

Table 2 Patient demographics and preoperative diagnoses

	Total	TSA	RSA	PyC
Number	76	23	32	21
Age	68.5 (22–84)	70.0 (58–84)	74.1 (65–84)	58.3 (22–84)
Sex	45 female	15 female	26 female	4 female
Follow-up (months)	31.4 (23–55)	31.6 (23–51)	34.3 (23–55)	26.7 (23–38)
Primary osteoarthritis	44	23	6	14
Cuff tear arthropathy	24	0	25	0
Irreparable rotator cuff tear	1	0	1	0
Fracture sequelae	1	0	0	1
Avascular necrosis	3	0	0	3
Arthritis resulting from instability	3	0	0	3

Table 3 Preoperative glenoid morphology according to the modified Walch classification [18]

Glenoid type (Walch)	Total	TSA	RSA	PyC Hemi
A1	14	0	9	5
A2	28	13	11	4
B1	19	6	7	6
B2	11	4	2	5
B3	0	0	0	0
C	0	0	0	0
D	4	0	3	1

between implant types, the *t* test was employed. In each case the significance threshold was set at $p < 0.05$.

Results

Patient demographics

The patient demographics and diagnoses leading to surgery of the study group of 76 patients are shown in Table 2. With the exception of the PyC subgroup, the cohort was made up of more women than men. The PyC contingent was younger and male dominated. The average age was the highest in the RSA subgroup.

Table 3 shows the glenoid morphologies of the patients prior to surgery. TSA patients had mostly A2 glenoids, but also B1 and B2 wear patterns. RSA also had predominantly A type glenoids, but also B and D morphologies. The PyC subgroup contained patients with mixed glenoid types.

Pre- vs postoperative clinical outcomes

The clinical outcomes pre- vs postoperative are displayed in Table 4. All patient groups improved significantly ($p < 0.05$) in all outcomes measured. TSA patients had, on average, the lowest preoperative and the highest postoperative CS. The PyC patients had the highest preoperative CS. All patient groups benefited from pain reduction, reducing from VAS 6.6 pre-change to preoperatively down to 1.0 postoperatively. Abduction increased from 88° to 129°, forward flexion from 93° to 137°. Internal rotation increased from reaching the gluteal area before, to placing the back of the hand on the lumbar spine after the operation. On average, patients also benefited from more external rotation, 21° preoperatively and 40° postoperatively.

Comparison between implant types

To reduce the confounding effect of the demographical differences in the subgroups, delta values (difference between

Table 4 Pre- and postoperative outcomes for the measured variables for the cohort and subgroups

Outcome	Total pre-OP	Total post-OP	TSA pre-OP	TSA post-OP	RSA pre-OP	RSA post-OP	PyC pre-OP	PyC post-OP
CS	38.2	78.3	34.5	84.0	36.9	72.9	44.2	80.3
Pain VAS	6.6	1.0	6.7	0.37	6.8	1.1	6.4	1.5
Abduction°	88.2	129.4	84.3	138.3	88.1	121.7	92.6	131.4
Flexion°	92.5	137.1	87.6	144.3	91.4	128.0	99.5	143.1
Internal rotation (score)	1.4	2.6	1.0	3.1	1.7	2.3	1.2	2.7
External rotation°	21.1	39.6	6.1	40.0	19.8	36.3	17.6	44.3

All comparisons between pre- and postoperative values were statistically significant ($p < 0.05$)

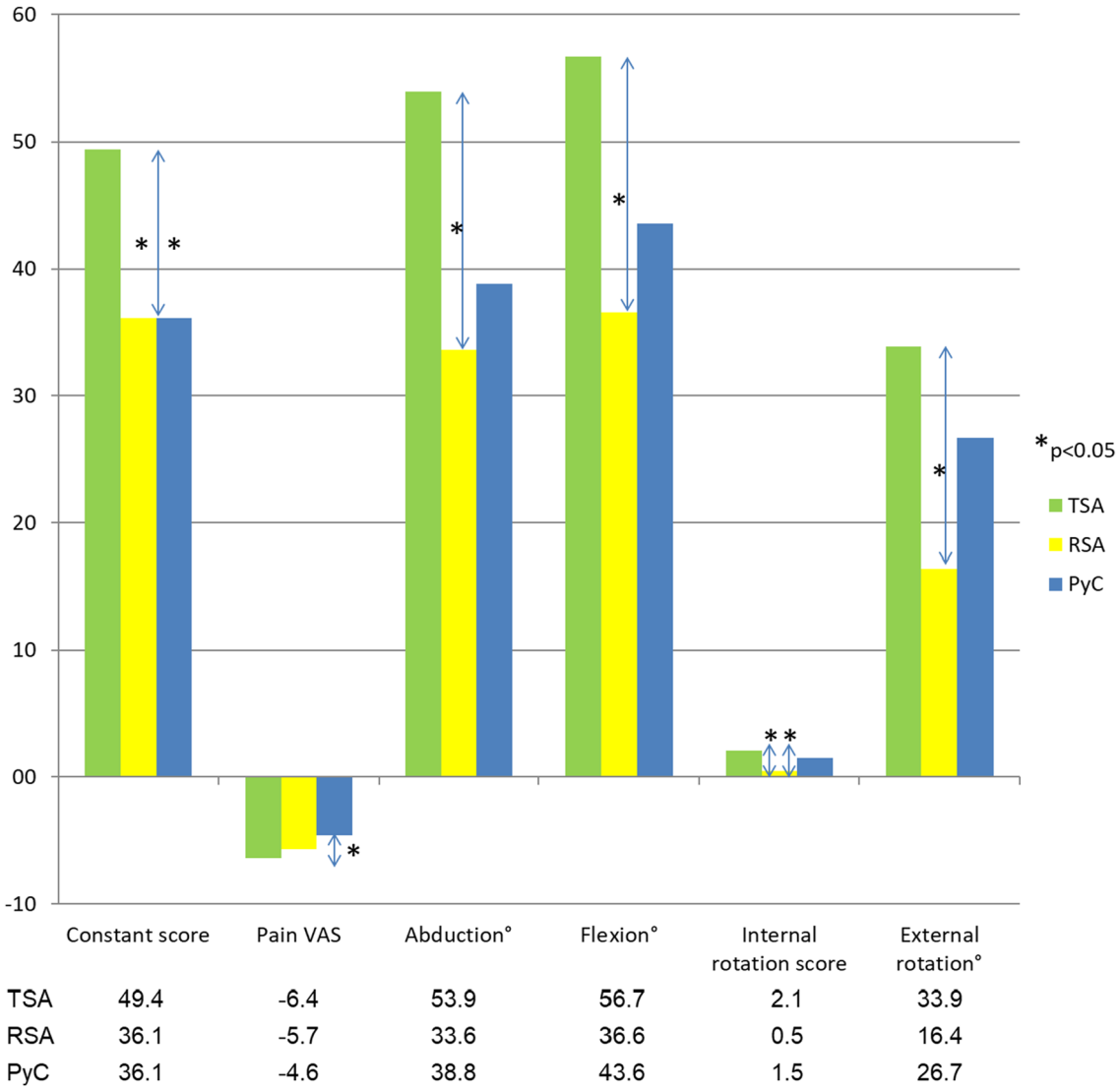

Fig. 1 Delta (postoperative minus preoperative) values for the measured outcomes compared between the implant types. Statistically significant ($p < 0.05$) differences are identified with a *

pre- and postoperative) were compared between prosthesis types (Fig. 1).

Notably, anatomical total shoulder replacements had a significantly higher increase in the CS than the other two types. They also brought about more pain alleviation than the pyrocarbon hemiarthroplasties. In abduction and flexion the RSA had less improvement than the TSA. Both the TSA and the PyC gained more internal rotation than the RSA. Additionally, the TSA had larger improvements in external rotation than the RSA. All other comparisons between the implants were not statistically significant. Nevertheless, the trend emerged that TSA was superior to the other two in all aspects and PyC bettered the RSA in everything but pain reduction.

Given that glenoid morphology is an important predictor of outcome, we investigated the performance of the different prostheses when used in patients of varying glenoid types (see Table 5). Interestingly the final outcome of TSA did not differ between A and B glenoids. However, the improvement achieved with TSA seems to be greater in A than in B glenoid patients, although this was not statistically significant ($p = 0.085$). Conversely, using PyC, patients with B glenoids improved significantly more than those with A glenoids ($p = 0.034$), again achieving the same final outcome. The one patient with a D glenoid in PyC had a poor preoperative function and improved less than A and B patients. When comparing the result with PyC vs TSA in arthritis with B type glenoids, little

Table 5 Comparison of mean constant score by prosthesis type and glenoid morphology

Glenoid type (modified Walch)	Prosthesis type		
	TSA	RSA	PyC
A			
Preoperative CS	28.9	30.4	52.7
Postoperative CS	83.5	71.5	81.7
Delta CS	53.7	41.1	29.0
B			
Preoperative CS	40.6	47.8	39.5
Postoperative CS	84.5	76.6	82.8
Delta CS	43.9	28.8	43.3
D			
Preoperative CS	–	49.7	18.0
Postoperative CS	–	74.0	39.0
Delta CS	–	24.3	21.0

difference is seen in the outcome or the function gained. In patients with type A glenoids, however, a significantly greater improvement was observed using TSA compared with PyC ($p < 0.0001$). Both subgroups reach a similar postoperative CS.

In the RSA subgroup patients with Walch A glenoids appeared to have the greatest improvement, but this was not significant (A vs B $p = 0.091$; A vs D $p = 0.15$). The postoperative CS was comparable between all three glenoid types.

Table 6 differentiates the results achieved when applying the different prosthesis types for the various diagnoses. The comparison for TSA and PyC hemi-prostheses in osteoarthritic shoulders revealed a significantly greater improvement in the CS of TSA patients ($p = 0.026$), which had a lower preoperative function. However, there is no difference in the final outcome of the PyC and TSA subgroups ($p = 0.95$). When comparing RSA with TSA in osteoarthritis patients, TSA has a significantly greater increase in the CS ($p = 0.011$) and a better postoperative CS ($p = 0.002$). When comparing the results achieved for OA, there was no significant difference in the delta CS using PyC or RSA ($p = 0.43$). Although PyC seemed to have a better final result, this was not statistically significant ($p = 0.058$).

Comparing the results for different indications within the PyC subgroup, this showed no significant differences in the delta scores or postoperative CS between any diagnoses ($p > 0.05$). However, patients operated for OA and arthritis resulting from instability seemed to have a greater benefit and a better postoperative outcome than those with avascular necrosis and fracture sequelae. Although not statistically significant (or measurable using a *t* test), the patient with arthritis resulting from a fracture had the worst postoperative CS and the least improvement compared to the mean values of the other diagnoses.

Table 6 Comparison of mean CS achieved using the different prostheses for the various diagnoses

Diagnosis	Prosthesis type		
	TSA	RSA	PyC
Primary osteoarthritis			
Preoperative CS	34.5	42.5	45.6
Postoperative CS	84.0	74.7	83.8
Delta CS	49.5	32.2	38.2
Cuff tear arthropathy			
Preoperative CS	–	34.8	–
Postoperative CS	–	72.4	–
Delta CS	–	37.6	–
Irreparable rotator cuff tear			
Preoperative CS	–	53	–
Postoperative CS	–	75	–
Delta CS	–	22	–
Fracture sequelae			
Preoperative CS	–	–	50
Postoperative CS	–	–	61.5
Delta CS	–	–	11.5
Avascular necrosis			
Preoperative CS	–	–	41.7
Postoperative CS	–	–	68
Delta CS	–	–	26.3
Arthritis resulting from instability			
Preoperative CS	–	–	38.3
Postoperative CS	–	–	82.3
Delta CS	–	–	44

In the RSA subgroup patients operated for CTA did not improve significantly differently in the CS ($p = 0.53$), nor did they reach a different outcome according to the CS ($p = 0.72$), when compared with patients with OA. The patient with the irreparable rotator cuff tear, although not statistically testable, also appeared to have an outcome comparable to the other RSA patients.

Complications

In the study group of 76 patients, 2 developed stress fractures: 1 of the scapular spine, which was successfully operated with an ORIF; one of the acromion, which was treated conservatively. 2 patients were revised with evacuations of postoperative haematomas. There were 2 cases of postoperative anaemia requiring a blood transfusion (2.7%) and 4 cases had neurological deficits postoperatively which resolved spontaneously in the months following surgery.

Complications leading to exclusion

9 patients had to be excluded as a result of complications which were recorded in the follow-up of the initial patient cohort of 103 shoulder prostheses, as they were no longer deemed comparable to the rest of the cohort: 4 patients were found to have a low-grade infection (3.88%) and had to be revised. 2 of these were RSA patients, one of whom was 88 years old, the other was a psoriasis vulgaris patient under methotrexate therapy. TSA and PyC had one case of infection each; in the case of the PyC this was a patient who had had a previous operation due to a tubercular fracture. 2 of the 4 infections were caused by Cutibacterium acnes (formerly known as Propionibacterium acnes). One patient with a TSA developed a rotator cuff tear and was converted to RSA. There were 2 patients with periprosthetic fractures of the humerus (1.94%), one of whom was treated at another hospital. The other fell and fractured twice, she was treated conservatively the first time, the second time she was operated with a single cerclage with a good outcome. One RSA patient with extremely osteoporotic bone suffered a bony dislocation of the glenoid component, despite the use of a long peg base plate and 4 screws. This was revised, the glenoid component removed and as a salvage operation a modular exchange to place an anatomical head on the existing shaft was performed. 1 patient underwent a cervical spine operation in the months after her shoulder prosthesis and suffered a neurological deficit ipsilaterally, involving the deltoid, as a complication of this. This resulted in recurrent dislocations of the shoulder prosthesis and a stress fracture of the scapula spine of the operated side, leading to exclusion.

Discussion

Key results

This patient cohort showed significant improvements in all measured ROM, pain and the CS compared to preoperative values, using a modular short-stem prosthesis with a proximal porous coating 2–4 years postoperatively. This correlates with previous findings using first-generation short-stemmed shoulder prostheses [3, 4, 19, 20]. The overall very positive clinical outcomes achieved with these shoulder prostheses are also, at least, comparable to those described with the use of standard-stemmed prostheses with diaphyseal anchoring [21, 22].

The modular design of this prosthesis has the advantage of individualized assembly to recreate the anatomy of the proximal Humerus and balance tension of the soft tissues. Eccentric head/tray (depending on anatomical or inverse design) components allow the surgeon to adjust the position of the head/tray by turning it to the ideal position before fixation. In this way ideal coverage without overlap and adjustments of soft tissue tension can be made regardless of the stem position. This is of particular importance in the anatomical prosthesis and may in part have contributed to the successful clinical outcomes.

The hemiprosthesis which was used in this cohort uniformly utilized a novel pyrocarbon head. This material is thought to have a biomechanical profile close to that of cartilage and therefore is hoped to reduce the problem of glenoid wear and pain which complicate traditional hemiarthroplasties [8]. Preliminary results after implantation of these have been encouraging, except in patients with a diagnosis of fracture sequelae (osteonecrosis or secondary osteoarthritis), in a study containing some of the patients from our cohort [23]. Our results equally are encouraging, with improvements in all areas of clinical function. With regard to results in the use for fracture sequelae, we had one patient operated with PyC for this indication, which yielded a poorer result than all other indications, adding weight to the conclusion drawn by Garret et al. [23].

The RSA used in this cohort has a neck shaft angle (NSA) of 145°. This is an intermediate value between the 135° and 155° which inverse prostheses also commonly have. Mechanical studies have shown that a steeper NSA causes earlier impingement in abduction, but reduces glenoid notching and increases joint stability [24]. Computerized models have found a lower NSA (135°) to allow a greater ROM in all motions except abduction [25]. This was also true of internal rotation, although the effect of the lower NSA on internal rotation was negated when the glenosphere had been lateralized. Our cohort demonstrated a successful clinical outcome with this modular tray with a NSA of 145° in terms of the ROM, with no dislocations, suggesting this may be a good compromise between mobility and stability.

The comparison between the different types of this modular prosthesis was interesting, as it showed several differences in their functional characteristics. Overall, though not always statistically significant, the TSA achieved the best outcomes in all measured variables. Kiet et al. have previously described the outcomes of RSA and TSA to be similar, with only better rotation in the TSA group [10]. They, however, did not compare the delta values of the measured parameters. Contradictory to our findings, Flurin et al. described higher outcome scores in TSA but comparatively greater gains in RSA patients [26]. They had implanted the Equinoxe shoulder platform system (Exactech Inc., Florida). Differences in results compared to our study may be due to the implant or differences in the patient cohorts. Trends emerged that patients with PyC heads generally had greater improvements in the ROM than RSA, whilst RSA brought

about more pain relief than PyC. However, the only statistically significant difference between the PyC and the RSA was that PyC had greater improvement in internal rotation. This is mirrored by better internal rotation in TSA compared to RSA patients and is a reproducible finding [10, 27]. As we reconstructed the subscapularis tendon in all prosthesis types, this phenomenon may likely be explained as being a result of a mechanical restriction of the RSAs semi-constrained design.

Comparison between glenoid types

When comparing glenoid types, one important finding was that the final outcome did not differ between TSA patients which had type A or B glenoids. It appears, though, that there may be a greater increase in the CS when operating patients with a centred type A situation. This may be because A glenoids have a purely arthritic problem, which can be solved by replacing the glenoid surface, whereas in the B type situation a soft tissue imbalance complicates the disease. PyC patients with B type glenoids improved more than those with A glenoids, reaching a similar end result. This implies that the presence of a B glenoid does not contraindicate the use of a PyC hemiprosthesis and rather laments that it may be a good indication. It seems that the additional benefit the A types have over B types in TSA is lost in PyC, as the glenoid is not replaced. Strengthening to this is that patients with B glenoids had comparable outcomes when treated with TSA or PyC, whereas type A glenoids improved significantly more when treated with TSA. This does not entirely fit with the findings of Iannotti, who found that both TSA and hemi-prostheses had worse outcomes in a Walch B2 setting, where TSA was still the better choice [14]. This may be because we grouped all B type glenoids together (roughly equal numbers of B1 and B2), whereas they only looked specifically at B2. Also, they used standard cobalt-chrome heads for their hemi-prostheses, so it may be that the new pyrocarbon heads have different clinical properties to these. Perhaps in a type B1 situation with little glenoid wear, the natural glenoid with its labrum is superior to a prosthetic glenoid, giving rise to more clinical improvement when the corresponding arthritic humeral articular surface is replaced. Furthermore, it may be that in a B2 setting with biconcave posterior wear PyC is more effective than standard cobalt-chrome prostheses.

In RSA it appears as if patients with type A glenoids may have the most benefit from the operation. This may be because these are the ones that have cranialized more, rather than posteriorizing and therefore benefit from the distalization of the RSA more. The final outcome appears similar between all glenoid types, including type D, however.

Comparison between Diagnoses

When comparing outcomes between the different types of prostheses in terms of results achieved for osteoarthritis, these mirrored what we found overall when comparing RSA to the other two types. The comparison between TSA and PyC showed a greater improvement in TSA patients with OA, as was the case in the comparison of the entire subgroups for the prostheses. However, the final outcome of the PyC, when only considering OA patients, now matched that of the TSA patients much more closely. In TSA therefore, older patients with worse preoperative function improve more than the on average younger PyC patients. Nevertheless, the function achieved after 2 years when using PyC for OA is equal to that of the TSA.

To allow some insight into what a good indication for the novel PyC hemiprostheses may be, it was interesting to try and compare the results achieved for the various diagnoses. Unfortunately, the group sizes were too small to show any significant differences in this regard. It can be said, though, that there is a trend that OA and arthritis resulting from instability may be the best indications for implanting a PyC hemiarthroplasty.

The improvements and outcomes achieved using RSA seem to be the same irrespective of the preoperative diagnosis. This may be because it has inherent stability due to its semi-constrained design, allows recruitment of the deltoid muscle to substitute rotator cuff function and is limited more by mechanical impingement.

Complications

The infection rate of 3.88% documented in our cohort is comparative to findings of a meta-analysis by Zumstein et al. who found an infection rate of 3.8% in RSA patients [28]. Rates of 1–3.9% have been described for TSA as well [29], whilst it is thought that rates in RSA patients are higher due to haematoma formation in the increased dead space [30]. This is in line with our results. Differences in the reported infection rates are likely to be a result of follow-up and diagnostic differences. Rates of low-grade infections are often likely to be higher than reported as they are difficult to distinguish from aseptic failure [31]. Cutibacterium acnes (formerly Propionibacterium acnes), which made up half of our 4 cases, has been reported to be present in 18–60% of infections [30]. It is found in the deep tissues around the shoulder, more commonly in men, when using the deltopectoral approach and it has been found in the joint fluid of 42% of patients undergoing primary shoulder arthroplasty and more often still in revision surgery [30, 32, 33].

The rate of periprosthetic humeral fractures in our cohort (1.94%) correlates with 1.6–2.4% described in the

literature for standard shaft prostheses [34]. However, we were able to treat a patient with a recurrent periprosthetic fracture successfully with as little as a single cerclage. This may indicate simpler treatment options for periprosthetic fractures around short-stem prostheses, but clearly more data are required to draw any conclusions regarding this. Regarding the two cases of scapula spine and 1 acromion fracture in the potential cohort of 103 patients, it should be noted that these all occurred in RSA patients. This is unlikely to be a coincidence as reverse shoulder prostheses put a lot of stress on the delta muscle which causes tension and can lead to stress fractures of the scapula. This affect may be exacerbated in this model due to the additional lateralization and distalization brought about by the onlay design of the modular tray.

Limitations and generalizability

The main limitation of this study is the retrospective design and tailored patient selection for the different subgroups, leading to selection bias. The resulting differences in diagnostic indications for arthroplasty and patient demographics in the subgroups limit the extent to which interventions can be reliably compared. Furthermore, the sample size, although when compared with other similar studies in the literature is large, may have inhibited the emergence of further statistical significances in the comparison between the prosthesis's subtypes. The follow-up rate of 82%, which for a mid-term cohort study is satisfactory, could to some extent jeopardize the generalizability of the study. Furthermore, whilst using a single-centre study design increases reliability in a scientific method, it also reduces the extent to which results can be extrapolated to other settings. This must be taken into account when interpreting results. The treatment of this cohort took place before we adopted the use of 3-dimensional planning, so it is not known if and how much correction of version and/or inclination was achieved. Another limitation is that although the subscapularis tendon was repaired in all cases, we did not carry out any controls of the success of this repair.

Conclusions

This study provides an insight into the clinical properties of the different forms in which modular short-stem shoulder prostheses can be implanted and their results for various indications.

When implanted for the diagnoses for which each were conceptualized, it can be said that TSA patients can expect the greatest clinical improvement postoperatively compared to RSA and PyC. PyC patients seem to have bigger improvements in ROM than RSA patients but may subjectively have less pain reduction. Interestingly, despite refixation of the subscapularis tendon in all prosthesis types, RSA had less improvements in internal rotation than the other two prosthesis types, which suggests a mechanical restriction of RSA.

When comparing the clinical success of these prostheses when used for different glenoid types according to the modified Walch classification, we can surmise that TSA has the same outcome regardless of A or B glenoid type, but possibly with more improvement for type A glenoids. Novel PyC hemiprostheses are a good indication for patients with type A and type B glenoids, with equal clinical outcomes and a greater improvement in B glenoids. In fact, type B glenoids were treated just as successfully with PyC as with TSA.

If OA is the indication for arthroplasty, TSA and PyC achieve a comparable clinical result 2–4 years postoperatively, although the preoperatively worse TSA patients have more improvement. It can be said that if glenoid replacement is to be avoided, for example due to young age, that OA patients or those with arthritis resulting from instability and especially in the presence of a type B glenoid seem to be good candidates for treatment with PyC.

The diagnosis for which RSA is implanted does not seem to greatly affect the outcome, but those with a Walch A glenoid may improve more.

Acknowledgements The authors would like to thank Dr. med. Rudolf Nadjar (Krankenhaus Agatharied) for the inclusion of his patients in the study.

Funding No funding was sought or received to undertake or publish this study. Open Access funding provided by Projekt DEAL.

Compliance with ethical standards

Conflict of interest B. D. Kleim: None. C. Garving: None. U. H. Brunner: Consultant for Wright Medical, has given paid presentations for Wright Medical.

Ethical approval Ethical approval was sought and granted by the ethics commission of the medical faculty of the Ludwig-Maximilians-University Munich (Reference number: 667-15) in advance of study commencement.

References

1. Dillon MT, Ake CF, Burke MF, Singh A, Yian EH, Paxton EW, Navarro RA (2015) The Kaiser Permanente shoulder arthroplasty registry: results from 6,336 primary shoulder arthroplasties. Acta Orthop 86(3):286–292. https://doi.org/10.3109/17453674.2015.1024565
2. Kim SH, Wise BL, Zhang Y, Szabo RM (2011) Increasing incidence of shoulder arthroplasty in the United States. J Bone Joint Surg Am 93(24):2249–2254. https://doi.org/10.2106/jbjs.J.01994
3. Bell S, Coghlan J (2014) Short stem shoulder replacement. Int J Shoulder Surg 8(3):72–75. https://doi.org/10.4103/0973-6042.140113
4. Schnetzke M, Coda S, Walch G, Loew M (2015) Clinical and radiological results of a cementless short stem shoulder prosthesis at minimum follow-up of two years. Int Orthop 39(7):1351–1357. https://doi.org/10.1007/s00264-015-2770-2
5. Johnson MH, Paxton ES, Green A (2015) Shoulder arthroplasty options in young (< 50 years old) patients: review of current concepts. J Shoulder Elbow Surg 24(2):317–325. https://doi.org/10.1016/j.jse.2014.09.029
6. Schoch B, Schleck C, Cofield RH, Sperling JW (2015) Shoulder arthroplasty in patients younger than 50 years: minimum 20-year follow-up. J Shoulder Elbow Surg 24(5):705–710. https://doi.org/10.1016/j.jse.2014.07.016
7. Bryant D, Litchfield R, Sandow M, Gartsman GM, Guyatt G, Kirkley A (2005) A comparison of pain, strength, range of motion, and functional outcomes after hemiarthroplasty and total shoulder arthroplasty in patients with osteoarthritis of the shoulder. A systematic review and meta-analysis. J Bone Joint Surg Am 87(9):1947–1956. https://doi.org/10.2106/jbjs.d.02854
8. Salkeld SL, Patron LP, Lien JC, Cook SD, Jones DG (2016) Biological and functional evaluation of a novel pyrolytic carbon implant for the treatment of focal osteochondral defects in the medial femoral condyle: assessment in a canine model. J Orthop Surg Res 11(1):155. https://doi.org/10.1186/s13018-016-0488-5
9. Wright MA, Keener JD, Chamberlain AM (2020) Comparison of clinical outcomes after anatomic total shoulder arthroplasty and reverse shoulder arthroplasty in patients 70 years and older with glenohumeral osteoarthritis and an intact rotator cuff. J Am Acad Orthop Surg 28(5):e222–e229. https://doi.org/10.5435/jaaos-d-19-00166
10. Kiet TK, Feeley BT, Naimark M, Gajiu T, Hall SL, Chung TT, Ma CB (2015) Outcomes after shoulder replacement: comparison between reverse and anatomic total shoulder arthroplasty. J Shoulder Elbow Surg 24(2):179–185. https://doi.org/10.1016/j.jse.2014.06.039
11. Cox RM, Padegimas EM, Abboud JA, Getz CL, Lazarus MD, Ramsey ML, Williams GR Jr, Horneff JG 3rd (2018) Outcomes of an anatomic total shoulder arthroplasty with a contralateral reverse total shoulder arthroplasty. J Shoulder Elbow Surg 27(6):998–1003. https://doi.org/10.1016/j.jse.2017.12.005
12. Bercik MJ, Kruse K 2nd, Yalizis M, Gauci MO, Chaoui J, Walch G (2016) A modification to the Walch classification of the glenoid in primary glenohumeral osteoarthritis using three-dimensional imaging. J Shoulder Elbow Surg 25(10):1601–1606. https://doi.org/10.1016/j.jse.2016.03.010
13. Levine WN, Djurasovic M, Glasson JM, Pollock RG, Flatow EL, Bigliani LU (1997) Hemiarthroplasty for glenohumeral osteoarthritis: results correlated to degree of glenoid wear. J Shoulder Elbow Surg 6(5):449–454. https://doi.org/10.1016/s1058-2746(97)70052-1
14. Iannotti JP, Norris TR (2003) Influence of preoperative factors on outcome of shoulder arthroplasty for glenohumeral osteoarthritis. JBJS 85(2):251–258
15. Mizuno N, Denard PJ, Raiss P, Walch G (2013) Reverse total shoulder arthroplasty for primary glenohumeral osteoarthritis in patients with a biconcave glenoid. J Bone Joint Surg Am 95(14):1297–1304. https://doi.org/10.2106/jbjs.L.00820
16. Friedman RJ, Hawthorne KB, Genez BM (1992) The use of computerized tomography in the measurement of glenoid version. J Bone Joint Surg Am 74(7):1032–1037
17. Maurer A, Fucentese SF, Pfirrmann CW, Wirth SH, Djahangiri A, Jost B, Gerber C (2012) Assessment of glenoid inclination on routine clinical radiographs and computed tomography examinations of the shoulder. J Shoulder Elbow Surg 21(8):1096–1103. https://doi.org/10.1016/j.jse.2011.07.010
18. Constant CR, Murley AH (1987) A clinical method of functional assessment of the shoulder. Clin Orthop Relat Res 214:160–164
19. Giuseffi SA, Streubel P, Sperling J, Sanchez-Sotelo J (2014) Short-stem uncemented primary reverse shoulder arthroplasty: clinical and radiological outcomes. Bone Joint J 96(4):526–529. https://doi.org/10.1302/0301-620x.96b3.32702
20. Loew M (2013) Short stem shoulder prosthesis: concept and first results. Orthopade 42(7):501–506. https://doi.org/10.1007/s00132-012-2021-9
21. Iriberri I, Candrian C, Freehill MT, Raiss P, Boileau P, Walch G (2015) Anatomic shoulder replacement for primary osteoarthritis in patients over 80 years: outcome is as good as in younger patients. Acta Orthop 86(3):298–302. https://doi.org/10.3109/17453674.2015.1006036
22. Boileau PWD, Hatzidakis AM, Hovorka I (2006) Neer Award 2005: the Grammont reverse shoulder prosthesis: results in cuff tear arthritis, fracture sequelae, and revision arthroplasty. J Shoulder Elbow Surg 15(5):527–540. https://doi.org/10.1016/j.jse.2006.01.003
23. Garret J, Harly E, Le Huec JC, Brunner U, Rotini R, Godeneche A (2019) Pyrolytic carbon humeral head in hemi-shoulder arthroplasty: preliminary results at 2-year follow-up. JSES Open Access 3(1):37–42. https://doi.org/10.1016/j.jses.2018.09.002
24. Oh JH, Shin SJ, McGarry MH, Scott JH, Heckmann N, Lee TQ (2014) Biomechanical effects of humeral neck-shaft angle and subscapularis integrity in reverse total shoulder arthroplasty. J Shoulder Elbow Surg 23(8):1091–1098. https://doi.org/10.1016/j.jse.2013.11.003
25. Werner BS, Chaoui J, Walch G (2017) The influence of humeral neck shaft angle and glenoid lateralization on range of motion in reverse shoulder arthroplasty. J Shoulder Elbow Surg 26(10):1726–1731. https://doi.org/10.1016/j.jse.2017.03.032
26. Flurin PH, Marczuk Y, Janout M, Wright TW, Zuckerman J, Roche CP (2013) Comparison of outcomes using anatomic and reverse total shoulder arthroplasty. Bull Hosp Jt Dis 71(Suppl 2):101–107
27. Triplet JJ, Everding NG, Levy JC, Moor MA (2015) Functional internal rotation after shoulder arthroplasty: a comparison of anatomic and reverse shoulder arthroplasty. J Shoulder Elbow Surg 24(6):867–874. https://doi.org/10.1016/j.jse.2014.10.002
28. Zumstein MA, Pinedo M, Old J, Boileau P (2011) Problems, complications, reoperations, and revisions in reverse total shoulder arthroplasty: a systematic review. J Shoulder Elbow Surg 20(1):146–157. https://doi.org/10.1016/j.jse.2010.08.001
29. Bohsali KI, Wirth MA, Rockwood CA Jr (2006) Complications of total shoulder arthroplasty. J Bone Joint Surg Am 88(10):2279–2292. https://doi.org/10.2106/jbjs.f.00125
30. Elizabeth M, Pinder JCO, Stephen Bale R, Trail Ian A (2016) Ten questions on prosthetic shoulder infection. Shoulder Elbow 8(3):151–157. https://doi.org/10.1177/1758573216632464
31. Trampuz A, Zimmerli W (2005) Prosthetic joint infections: update in diagnosis and treatment. Swiss Med Wkly 135(17–18):243–251
32. Levy O, Iyer S, Atoun E, Peter N, Hous N, Cash D, Musa F, Narvani AA (2013) Propionibacterium acnes: an underestimated

etiology in the pathogenesis of osteoarthritis? J Shoulder Elbow Surg 22(4):505–511. https://doi.org/10.1016/j.jse.2012.07.007
33. Hudek R, Sommer F, Kerwat M, Abdelkawi AF, Loos F, Gohlke F (2014) Propionibacterium acnes in shoulder surgery: true infection, contamination, or commensal of the deep tissue? J Shoulder Elbow Surg 23(12):1763–1771. https://doi.org/10.1016/j.jse.2014.05.024
34. Greiner S, Stein V, Scheibel M (2011) Periprosthetic humeral fractures after shoulder and elbow arthroplasty. Acta chirurgiae orthopaedicae et traumatologiae Cechoslovaca 78(6):490–500

(Accepted manuscript, DOI: 10.1016/j.jse.2023.05.027)

Pyrocarbon hemiprostheses show little glenoid erosion and good clinical function at 5.5 years of follow-up

BD Kleim, A Zolotar, M Hinz, R Nadjar, S Siebenlist, UH Brunner

Abstract

Background:

The success of traditional shoulder hemiarthroplasty with cobalt-chromium (CoCr) heads is limited by a painful glenoid erosion with problematic bone loss. Hemiprostheses with pyrolytic carbon (PyC) heads have shown reduced glenoid erosion in experimental laboratory studies. Few in vivo data are available.

Methods:

Single-centre consecutive cohort study of 31 of 34 patients (91%) who underwent PyC hemiarthroplasty between 09.2013 and 06.2018. For eleven of these concentric glenoid reaming was additionally performed. The mean follow-up was 5.5 (range 3.5 – 7) years. Standardized x-rays were taken and clinical function (Constant score) and pain on the visual analogue scale (VAS) were recorded. AP x-rays were analysed according to an established method by 2 independent observers: A line parallel to the superior and inferior glenoid rim was translated to the most medial point of the glenoid surface. A further parallel line was placed on the spinoglenoid notch (SGN) and the distance between the two lines was measured. Measurements were scaled using the known diameter of the implanted humeral

head component. To assess eccentric erosion AP and axial images were classified according to Favard and Walch respectively.

Results:

The mean medial glenoid erosion was 1.4 mm over 5.5 years. In the first year there was 0.8 mm of erosion, significantly more than the average erosion per year of 0.3 mm ($p < 0.001$). Mean erosion per year of patients with glenoid reaming was 0.4 mm, without reaming 0.2 mm ($p = 0.09$). An evolution of glenoid morphology was observed in 6 patients, of which 4 had a progression of the erosion grade. Prosthesis survival rate was 100%. The Constant score improved from 45.0 preoperatively to 78.0 2-3 years postoperatively and 78.8 at latest follow-up 5.5 years postoperatively ($p < 0.001$). Pain decreased from VAS 6.7 (3 – 9) preoperatively to 2.2 (0 – 8) at latest follow-up ($p < 0.001$). There was a weak correlation ($r = 0.37$) between erosion and pain improvement ($p = 0.039$) and no correlation between erosion and delta Constant score ($r = 0.06$).

Conclusion:

PyC HA caused little glenoid erosion and a sustained improvement in clinical function in our cohort at mid-term follow-up. PyC demonstrates a biphasic development of glenoid erosion, with a reduced rate after the first year. PyC hemiarthroplasty should therefore be considered as an alternative to total shoulder arthroplasty or CoCr hemiarthroplasty for patients with a high risk of glenoid component complications.

Key words:

Pyrocarbon; shoulder hemiprosthesis; glenoid wear; glenoid erosion; arthritis.

Level of evidence: IV

Introduction

Anatomical total shoulder arthroplasty (TSA) is very successful at treating glenohumeral arthritis in patients with a functional rotator cuff [23, 35]. However, in young patients with glenohumeral arthritis which has failed conservative management, treatment remains challenging. Whilst functional improvements and return to sport are higher after TSA than hemiarthroplasty (HA), TSA carries a high risk of long-term complications resulting from the glenoid component, especially in young patients [9, 28, 31]. TSA can therefore not be recommended ubiquitously, as glenoid component failure leads to loss of bone stock and is associated with higher rates of failure of subsequent revision prostheses [12].

Traditional HA or humeral head resurfacing using cobalt-chromium (Co-Cr) components often leads to painful erosion of the glenoid, resulting in a substantial loss of bone stock and making later revision surgery difficult [20, 32, 36, 37, 39]. Whilst survival rates of these prostheses in young patients have been shown to be good, these are not matched by high patient satisfaction, which decreases in the long term [10].

To fill this treatment gap, hemi-prostheses with a pyrolytic carbon surface (PyC) were developed and have been in use since 2013. Biomechanical cadaver and in vitro laboratory studies have shown reduced glenoid wear and improved biological interplay with chondrocytes and collagen when PyC was compared with CoCr [1, 16, 21, 33].

Short-term clinical studies have shown good functional outcomes, which were comparable to TSA for selected indications [14, 23]. Revision rates have been found to be lower for PyC than traditional HA at mid-term review [6, 30]. Radiological evaluations have shown little glenoid wear at 2 years of follow-up [3, 14, 23].

Aim and hypothesis

The aim of this study was to investigate mid-term radiological outcomes of PyC HA with regard to glenoid wear and bone loss as well as clinical function and subjective pain scores. Our hypothesis was that PyC would cause little glenoid erosion in comparison to data for prostheses with a traditional Co-Cr surface from the literature, whilst exhibiting good clinical function and pain reduction.

Methods

Patient population and study design

We conducted a retrospective consecutive cohort study of all 34 patients that underwent HA with PyC (Aequalis Ascend Flex™, Wright Medical, Bloomington, USA) in the trauma and orthopaedic surgery department of Agatharied hospital between September 2013 and June 2018. Inclusion criteria were implantation of a PyC hemi-prosthesis in the above time-frame. Exclusion criteria were less than a minimum of 3 years of follow-up and x-rays of inadequate projection or quality for reliable measurement (as determined in consensus between two raters, see radiological assessment). One patient who received HA in this time frame was treated with a traditional CoCr head due to a nickel allergy and was therefore not included. Three patients were excluded as they were lost to follow-up before a minimum of 3 years had passed (2 of these had died for reasons unrelated to the surgery and one had developed dementia). The remaining 31 patients (91%) were included in the study.

The operations were performed by one of two senior surgeons (UHB or RN) through a deltopectoral approach with subsequent transosseous double-row repair of the subscapularis tendon. Juxtaglenoidal capsulolabral resection was performed in all cases. The neck-shaft angle (A: 127.5°, B: 132.5° or C: 137.5°) was chosen according to the patients pre-existing anatomy, and determined intraoperatively after resection of the head along the anatomical

neck of the humerus. The size of the humeral head component was determined by placing the resected head onto the humeral head size guide with subsequent trialling of the component and using either a low or high offset head for optimal coverage. In 11 cases where biconcave glenoid wear was present (9 posterior and 2 anterior neoglenoids), this was sparingly reamed to create a concentric concavity. Sclerotic zones were interrupted with Pridie drill holes where present. Indications for surgery were young patients with an intact rotator cuff, patients with little glenoid pathology, or patients where TSA was not possible due to high risk of glenoid complications due to advanced posterior subluxation and wear (B2 or B3 glenoids on CT according to the modified Walch classification [4]).

All patients were invited for clinical and radiological follow-up in our outpatient clinic at regular intervals.

Patient demographics

The age of the 31 patients included in the investigation ranged from 22 to 87 years (mean 59). The mean age of patients for whom reaming was performed was 50 years (range 22 – 64), patients without reaming 62 years (range 45 – 84). Eleven patients were female. The follow-up period was minimum 3.5 years (1 patient) and up to 7 years (8 patients) with a mean of 5.5 years. None of the patients required revision operations or conversion to total shoulder arthroplasty in the follow-up period (prosthesis survival rate 100%). Indications leading to PyC HA are shown in table III.

Clinicical assessment

Preoperatively and at each follow-up visit the range of movement (ROM) was determined with a goniometer. Internal rotation was quantified according to a previously published method [23] (table I). The subjective pain score on the visual analogue scale (VAS) was determined. The Constant score was determined according to the method described by

Constant and Murley [7]. The minimal clinically important difference in Constant score of between 5.7 and 9.4 points was taken as described previously [8].

Radiological assessment

True AP, lateral and axillary view x-rays were taken preoperatively, 2 days postoperatively (without axial view) and at the subsequent follow-up appointments annually (if patients presented), according to a standardized in-house protocol. These were independently analyzed by 2 specialist trauma and orthopaedic surgeons with experience in shoulder surgery (BDK and AZ). Glenoid wear was quantified on the true AP x-rays according to a standardized technique which has been described in the literature [24, 39] (Fig. 1). A true AP view, as described by Grashey, was used and the quality of the images was assessed for adequacy according to free projection of the joint space (where present), projection of the glenoid rim, as well as projection of the scapula body and the spinoglenoid notch [26]. Measured values were scaled in relation to the known diameter of the prosthetic head component taken from the operative reports.

To evaluate evolution of glenoid morphology, possibly resulting in eccentric bone loss, this was assessed according to the modified Walch classification in the axillary view and according to the Favard classification in the AP x-ray [4, 11] (see table II). This was done in complete consensus between the two observers. For 21 of the patients x-ray follow-up 3 months postoperatively was carried out at our institution, others had interim follow-up with the referring specialist nearer home. For patients where glenoid reaming had been performed, when available (8 of 11 patients), these 3-month axial images were considered as a baseline for assessing the anteroposterior subluxation using the Walch classification. Additionally, the acromiohumeral interval (AHI), between the apex of the humeral head and the acromion, was measured and scaled as above.

Statistics

The mean average of the values measured by the 2 observers was taken for analysis and is shown rounded to one decimal place ± standard deviation (SD). Statistical analysis was performed using SPSS V27.0 (IBM) statistics software. Normal distribution was confirmed using the Shapiro-Wilk test. Student's t-test and the paired t-test were employed to investigate significance between values from different groups or at different timepoints respectively. Pearson's correlation coefficient was calculated to determine the strength of possible linear relationships between outcomes. The interrater correlation coefficient (ICC) was calculated to ascertain the reliability of the measurements. As we included all available patients in the cohort a power analysis was not carried out.

Results

Glenoid erosion

The ICC of measurements showed a high reliability (0.94 – 0.97).

The mean distance between the deepest point of the glenoid and the SGN was 17.1 mm (range 9.6 – 27.5 mm) 2 days postoperatively and 15.8 mm (range 8.7 – 24.3 mm) at latest follow-up. The mean medial bone loss was 1.4 mm (SD ± 1.20) at an average of 5.5 years of follow-up. The development of erosion over time is shown in Fig. 2 and illustrated by a case in Fig. 3. Measurements of medial glenoid bone loss are shown in Table IV. Bone loss in the first year was significantly higher than the average bone loss per year ($p < 0.001$).

Considering patients without glenoid reaming, the youngest ten patients (aged 45 – 60 years at time of surgery) had a mean bone loss of 0.2 mm per year, the oldest ten (aged 61 to 84 years) of 0.3 mm per year ($p = 0.38$). Pearson's correlation showed no significant correlation between patient age and erosion per year ($r = 0.10$, $p = 0.68$).

Evolution of glenoid morphology and acromiohumeral interval

Preoperative glenoid morphology and cases of evolution of this according to the Favard and modified Walch classifications are shown in table V [4, 11]. Disregarding the iatrogenic changes in glenoid morphology caused by reaming, 6 patients had an evolution of morphology which can be described by the modified Walch classification and 3 progressed in the Favard classification.

The preoperative AHI was mean 14.5 mm (SD ± 4.10) and at latest follow-up this had declined to 9.8 mm (SD ± 2.96), $p < 0.001$. Correspondingly the mean delta value for AHI was -4.7 mm (SD ± 2.80).

Clinical outcome

The mean active forward flexion increased from 99° preoperatively (SD ± 30.3) to 140° (SD ± 19.6), abduction from 93° (SD ± 29.0) to 127° (SD ± 19.8), external rotation from 16° (SD ± 17.9) to 38° (SD ± 13.3), internal rotation score from 1.3 (SD ± 1.1) to 2.8 (SD ± 0.80) (from gluteal to lumbar region reached) at final follow-up. Increases were statistically significant in each instance ($p < 0.001$).

The Constant score improved significantly by 2-3 years postoperatively (23 patients with 2-year and 8 patients with 3-year follow-up) and this result was sustained at final follow-up (Fig. 4). A Subgroup analysis for clinical outcome according to the Constant score for different indications is presented in Table III. The minimal clinically important difference (5.7 – 9.4 points) was surpassed in each instance [8]. Patients with Walch type B OA had a significantly greater improvement ($p = 0.036$) in the Constant score than type A, whilst achieving an equally good final outcome.

Preoperatively pain on the VAS was mean 6.7 (SD ± 1.64) and postoperatively this had reduced to 2.2 (SD ± 2.25), $p < 0.001$. The mean delta value for pain pre- vs postoperatively

was -4.5 (SD ± 2.09). 23 of 31 patients (74%) had a VAS of 3 or less at latest follow-up, of these 10 reported no pain at all (VAS 0).

There was a weak correlation between higher glenoid bone loss and more pain reduction, r = 0.37, p = 0.039, as depicted in Fig. 5. There was no correlation between glenoid erosion and the change in Constant score r = 0.06.

Patients with a diagnosis of post-traumatic arthritis or with avascular necrosis of the humeral head had more residual pain than those with other diagnoses (mean VAS 4.6 vs 1.5, p < 0.001).

Glenoid reaming

The comparison between the 11 patients with and 20 without glenoid reaming regarding subsequent glenoid erosion showed a mean erosion per year of 0.4 mm for the reaming group and 0.2 mm without reaming (p = 0.09). In the first year the mean bone loss for the reaming group was 1.0 mm (SD ± 0.56) vs 0.6 mm (SD ± 0.68) for those without reaming (p = 0.13).

Iatrogenic changes in glenoid morphology after concentric glenoid reaming are shown in table V. Fig. 6 shows an example where lasting realignment of the glenohumeral joint occurred after concentric reaming.

Patients who had undergone glenoid reaming seemed to report more pain reduction (delta VAS -5.2, SD ± 1.8) compared to those without reaming (delta VAS -4.2, SD ± 2.2), but this difference was not statistically significant (p = 0.19). The improvement in the Constant scores of patients with OA which underwent reaming (biconcave Walch types B and D) vs those with OA who were not reamed was not significantly different (p = 0.51) (table III).

Discussion

Key results

In this cohort of PyC hemiarthroplasty patients, medial glenoid erosion was 0.3 mm per year. We observed a biphasic development of erosion, where most of this occurred in the first year after which erosion slowed significantly. This suggests a consolidation or remodeling process which seems to occur in the first year after implantation. The mean bone loss of 1.4 mm over an average of 5.5 years represents comparatively little bone loss overall [15, 25, 39]. Furthermore, our analysis of glenoid evolution showed morphological progression of erosion in only 4 patients (13%), discounting changes attributed to glenoid reaming. Additionally, 2 patients displayed a change of glenohumeral alignment.

Glenoid reaming was not significantly associated with more erosion in our cohort. Concentric reaming of the glenoid did however result in re-centering of the glenohumeral joint in 3 patients with a B2 glenoid and one with a biconcave D glenoid (4/11, 36%). Having said this, 3 patients which were not reamed (3/20, 15%) and had posterior alignment preoperatively had also recentered at latest follow-up. This may be in part due to resection of the contracted capsule and possibly also weakening the subscapularis during the deltopectoral approach, perhaps rebalancing the force couple.

The clinical result after PyC HA showed a statistically and clinically significant improvement, which was sustained at latest follow-up 5.5 years postoperatively. No revision operations were required by latest follow-up. We therefore accept our hypothesis. Our results suggest that PyC HA is a good treatment alternative to TSA, to avoid complications of the glenoid component in patients who are at increased risk of these.

Limitations

Although invited, not all patients presented at each follow-up timepoint, making comparisons between timepoints difficult. Additionally, the length of follow-up investigation available varied between 3.5 and 7 years. We were able to ameliorate this problem somewhat by expressing erosion in relation to years of follow-up.

It can be argued that x-ray images offer limited accuracy for both bone erosion and morphology (the modified Walch classification was described with CT images). However, CT images were not available and it would be ethically difficult to justify CTs for a cohort of patients with little discomfort. MRI on the other hand would produce poor images given the proximity to the metal prostheses. Whilst the linear medial migration of the joint surface or prosthesis on x-ray has been shown to correlate with volumetric wear in hip arthroplasty, this is difficult to predict and will vary when erosion is eccentric [19].

To include as large a cohort as possible, patients from a broad age spectrum with a wide range of diagnoses were included in this study. The study may however not have been adequately powered to detect significant differences between subgroups.

Interpretation

Our results can be put into context when compared to the study by Werner et al. which we based the method of our radiological analysis on [39]. This study investigated glenoid erosion after humeral head resurfacing with CoCr implants. The cohort was of a similar size (38 patients), with a similar sex distribution (21 men, 14 women) and age range (20 – 72 years) as ours. The length of follow-up, with a mean of 5.5 years, also matches that of our study. They found a mean of 5.5 mm of medial erosion (range 1.1 – 12.2 mm) at 5.5 years of follow-up, with continuous progression. A high rate of glenoid erosion of 1 mm per year for

CoCr implants is supported by others in the literature [15, 25]. Our cohort of PyC implants showed comparatively little medial glenoid erosion.

The comparison with the data of Werner et al., is however not only a comparison between CoCr and PyC, but also between HA and resurfacing. This may have further influence as it has been postulated that both the increased offset and decreased radius of surface replacement prostheses compared to HA leads to more erosion [27, 38]. Further previously described risk factors for erosion include valgus alignment, glenoid cysts and fatty degeneration of the rotator cuff [17].

A study investigating mid-term results after PyC interposition shoulder arthroplasty (PISA) had found problematic, chiefly humeral, erosion and lysis of the tubercula leading to pain and revision surgery in 10% of their cohort [2]. However, a follow-on multicenter study including patients from this group more recently published by Garret et al. revised these findings to some extent [13]. Garret described little erosion of the joint surfaces overall with good clinical function after PISA, especially for patients with posttraumatic osteonecrosis with intact tubercula [13]. Their recommendation for PISA was however limited for other diagnoses due to the risk of tubercular lysis [13]. Radiological ingrowth of this PyC HA using a modular short stem was shown to be good in a recent study by our group and was no different to ingrowth after TSA or RSA [22].

Concentric glenoid reaming, also called “ream-and-run” or “nonprosthetic glenoid arthroplasty”, has been shown to be successful in restoring joint congruence with good clinical function, which was even comparable to that of total shoulder replacement [5, 29, 34, 37]. Whilst there was a trend to a slightly higher initial erosion rate with better pain reduction and improvement in the Constant score in patients with reaming compared with patients without, these differences were not significant in our cohort.

The clinical improvements seen after PyC HA in our cohort are comparable to those of previously published short-term results [6, 14]. We were able to add that the improvements achieved were maintained at mid-term follow-up. Patients of each preoperative diagnosis had a significant improvement in their function, which surpassed the MCID for the Constant score in each instance [8]. A detailed subgroup analysis for indications was not possible due to small subgroup sizes. However, it can be said that patients with OA and Walch type B glenoids had a greater improvement in the Constant score than those with OA and type A. The type B patients had worse function preoperatively. The final outcome between the two subgroups was comparable. The use of shoulder HA in patients with type B alignment is controversial in the literature [5, 18, 23, 29, 34].

The prosthesis survival was 100% in our cohort, whilst others have described survival rates of 92% after 2-3 years [6]. This difference may be due to patient selection, surgical technique or because our sample size was relatively small for a survival analysis. A large register study has shown that the survival of PyC HA is better than traditional CoCr HA, which is supported by our findings [30].

The finding of a weak correlation between more erosion and better pain reduction in our PyC cohort is not in line with what is known for CoCr prostheses in the literature, where painful erosion has frequently been reported [20, 32, 36, 37, 39]. This suggests that with the very small amount of bone loss found, erosion is not the problem causing pain in PyC HA. Instead, other causes of pain such as rotator cuff insufficiency or post-traumatic states remain in some cases. Furthermore, although insignificant in our analysis, patients with glenoid reaming seem to have slightly more initial bone loss and slightly better pain reduction, which may have some influence on this relationship.

The biphasic development of glenoid erosion found in the present study suggests some initial adaptation or consolidation of the glenoid bone, following which the smooth PyC surface causes little wear. This is an interesting finding which, given that previous in vivo studies suggested an interplay with chondrocytes and collagen matrix formation, deserves further research [16, 33].

Generalizability

As patients from a diverse age range with a range of diagnoses were included in this study, the results can be applied to a correspondingly diverse patient population. As the cohort size is still small in absolute terms though, caution should be taken, especially when considering subgroup analyses. Long term results and results after revision of PyC HA are not yet available, limiting the confidence with which recommendations can be made.

Conclusion

PyC HA caused little glenoid erosion and a sustained improvement in clinical function in our cohort at mid-term follow-up. PyC demonstrates a biphasic development of glenoid erosion, with a reduced rate after the first year. PyC hemiarthroplasty should therefore be considered as an alternative to total shoulder arthroplasty or CoCr hemiarthroplasty for patients with a high risk of glenoid component complications.

References

1. Ajdari N, Tempelaere C, Masouleh MI, Abel R, Delfosse D, Emery R et al. Hemiarthroplasties: the choice of prosthetic material causes different levels of damage in the articular cartilage. Journal of Shoulder and Elbow Surgery 2020;29:1019-1029. https://doi.org/10.1016/j.jse.2019.09.041
2. Barret H, Gauci MO, Langlais T, van der Meijden O, Tran L, Boileau P. Pyrocarbon interposition shoulder arthroplasty in young arthritic patients: a prospective observational study. J Shoulder Elbow Surg 2020;29:e1-e10. 10.1016/j.jse.2019.05.044
3. Barret H, Mathieu E, Mansat P, Bonnevialle N. Pyrocarbon hemiarthroplasty of the shoulder: indications and pitfalls. Seminars in Arthroplasty: JSES 2021. https://doi.org/10.1053/j.sart.2021.04.006
4. Bercik MJ, Kruse K, 2nd, Yalizis M, Gauci MO, Chaoui J, Walch G. A modification to the Walch classification of the glenoid in primary glenohumeral osteoarthritis using three-dimensional imaging. J Shoulder Elbow Surg 2016;25:1601-1606. 10.1016/j.jse.2016.03.010
5. Clinton J, Franta AK, Lenters TR, Mounce D, Matsen FA, 3rd. Nonprosthetic glenoid arthroplasty with humeral hemiarthroplasty and total shoulder arthroplasty yield similar self-assessed outcomes in the management of comparable patients with glenohumeral arthritis. J Shoulder Elbow Surg 2007;16:534-538. 10.1016/j.jse.2006.11.003
6. Cointat C, Raynier JL, Vasseur H, Lareyre F, Raffort J, Gauci MO et al. Short-term outcomes and survival of pyrocarbon hemiarthroplasty in the young arthritic shoulder. J Shoulder Elbow Surg 2022;31:113-122. 10.1016/j.jse.2021.06.002
7. Constant CR, Murley AH. A clinical method of functional assessment of the shoulder. Clin Orthop Relat Res 1987:160-164.
8. Dabija DI, Jain NB. Minimal Clinically Important Difference of Shoulder Outcome Measures and Diagnoses: A Systematic Review. Am J Phys Med Rehabil 2019;98:671-676. 10.1097/phm.0000000000001169
9. Denard PJ, Raiss P, Sowa B, Walch G. Mid- to long-term follow-up of total shoulder arthroplasty using a keeled glenoid in young adults with primary glenohumeral arthritis. J Shoulder Elbow Surg 2013;22:894-900. 10.1016/j.jse.2012.09.016
10. Eichinger JK, Miller LR, Hartshorn T, Li X, Warner JJ, Higgins LD. Evaluation of satisfaction and durability after hemiarthroplasty and total shoulder arthroplasty in a cohort of patients aged 50 years or younger: an analysis of discordance of patient satisfaction and implant survival. J Shoulder Elbow Surg 2016;25:772-780. 10.1016/j.jse.2015.09.028
11. Favard L, Lautmann S, Clement P. Osteoarthritis with Massive Rotator Cuff-Tear: The Limitation of its Current Definitions. In. Shoulder Arthroplasty. Berlin, Heidelberg: Springer Berlin Heidelberg; 1999. p. 261-265. (ISBN No. 978-3-642-58365-0)
12. Franke KJ, Christmas KN, Simon P, Mighell MA, Frankle MA. The effect of glenoid bone loss and rotator cuff status in failed anatomic shoulder arthroplasty after revision to reverse shoulder arthroplasty. J Shoulder Elbow Surg 2021;30:844-849. 10.1016/j.jse.2020.07.024
13. Garret J, Godenèche A, Boileau P, Molé D, Etzner M, Favard L et al. Midterm results of pyrocarbon interposition shoulder arthroplasty: good outcomes after posttraumatic osteonecrosis without malunion of the tuberosities. JSES International. 10.1016/j.jseint.2022.05.007
14. Garret J, Harly E, Le Huec J-C, Brunner U, Rotini R, Godenèche A. Pyrolytic carbon humeral head in hemi-shoulder arthroplasty: preliminary results at 2-year follow-up. JSES Open Access 2019;3:37-42. https://doi.org/10.1016/j.jses.2018.09.002

15. Geervliet PC, Somford MP, Winia P, van den Bekerom MP. Long-term results of shoulder hemiarthroplasty in patients with rheumatoid arthritis. Orthopedics 2015;38:e38-42. 10.3928/01477447-20150105-58
16. Hannoun A, Ouenzerfi G, Brizuela L, Mebarek S, Bougault C, Hassler M et al. Pyrocarbon versus cobalt-chromium in the context of spherical interposition implants: an in vitro study on cultured chondrocytes. Eur Cell Mater 2019;37:1-15. 10.22203/eCM.v037a01
17. Herschel R, Wieser K, Morrey ME, Ramos CH, Gerber C, Meyer DC. Risk factors for glenoid erosion in patients with shoulder hemiarthroplasty: an analysis of 118 cases. J Shoulder Elbow Surg 2017;26:246-252. 10.1016/j.jse.2016.06.004
18. Iannotti JP, Norris TR. Influence of preoperative factors on outcome of shoulder arthroplasty for glenohumeral osteoarthritis. J Bone Joint Surg Am 2003;85:251-258. 10.2106/00004623-200302000-00011
19. Ilchmann T, Reimold M, Müller-Schauenburg W. Estimation of the wear volume after total hip replacement. A simple access to geometrical concepts. Med Eng Phys 2008;30:373-379. 10.1016/j.medengphy.2007.04.003
20. Johnson MH, Paxton ES, Green A. Shoulder arthroplasty options in young (<50 years old) patients: review of current concepts. J Shoulder Elbow Surg 2015;24:317-325. 10.1016/j.jse.2014.09.029
21. Klawitter JJ, Patton J, More R, Peter N, Podnos E, Ross M. In vitro comparison of wear characteristics of PyroCarbon and metal on bone: Shoulder hemiarthroplasty. Shoulder Elbow 2020;12:11-22. 10.1177/1758573218796837
22. Kleim BD, Garving C, Brunner UH. Cementless curved short stem shoulder prostheses with a proximal porous coating: ingrowth properties at 2-5 years of radiological follow-up with clinical correlation. J Shoulder Elbow Surg 2020;29:2299-2307. 10.1016/j.jse.2020.02.025
23. Kleim BD, Garving C, Brunner UH. RSA, TSA and PyC hemi-prostheses: comparing indications and clinical outcomes using a second-generation modular short-stem shoulder prosthesis. Archives of Orthopaedic and Trauma Surgery 2021;141:1639-1648. 10.1007/s00402-020-03529-w
24. Kocsis G, Thyagarajan DS, Fairbairn KJ, Wallace WA. A new classification of glenoid bone loss to help plan the implantation of a glenoid component before revision arthroplasty of the shoulder. Bone Joint J 2016;98-b:374-380. 10.1302/0301-620x.98b3.36664
25. Krishnan SG, Reineck JR, Nowinski RJ, Harrison D, Burkhead WZ. Humeral Hemiarthroplasty with Biologic Resurfacing of the Glenoid for Glenohumeral Arthritis: Surgical Technique. JBJS 2008;90:9-19. 10.2106/jbjs.G.01220
26. Kumar R, Arora A, Lakkireddy M, Srirambhatla A, Maley DK, Eppakayala S et al. Achieving adequacy of shoulder Grashey’s view on X-ray: A small step to improve patient care. Clinical Radiology 2022;77:e11-e12. 10.1016/j.crad.2022.09.034
27. Lebon J, Delclaux S, Bonnevialle N, Rongières M, Bonnevialle P, Mansat P. Stemmed hemiarthroplasty versus resurfacing in primary shoulder osteoarthritis: A single-center retrospective series of 78 patients. Orthopaedics & Traumatology: Surgery & Research 2014;100:S327-S332. https://doi.org/10.1016/j.otsr.2014.05.012
28. Liu JN, Steinhaus ME, Garcia GH, Chang B, Fields K, Dines DM et al. Return to sport after shoulder arthroplasty: a systematic review and meta-analysis. Knee Surg Sports Traumatol Arthrosc 2018;26:100-112. 10.1007/s00167-017-4547-1
29. Matsen FAI, Carofino BC, Green A, Hasan SS, Hsu JE, Lazarus MD et al. Shoulder Hemiarthroplasty with Nonprosthetic Glenoid Arthroplasty: The Ream-and-Run Procedure. JBJS Reviews 2021;9:e20.00243. 10.2106/jbjs.Rvw.20.00243

30. McBride AP, Ross M, Hoy G, Duke P, Page R, Peng Y et al. Mid-term outcomes of pyrocarbon humeral resurfacing hemiarthroplasty compared to metal humeral resurfacing and metal stemmed hemiarthroplasty for osteoarthritis in young patients: Analysis from the Australian Orthopaedic Association National Joint Replacement Registry. J Shoulder Elbow Surg 2021. 10.1016/j.jse.2021.08.017
31. Neyton L, Kirsch J, Collotte P, Collin P, Gossing L, Chelli M et al. Mid- to long-term follow-up of shoulder arthroplasty for primary glenohumeral osteoarthritis in patients aged 60 or under. Journal of Shoulder and Elbow Surgery 2019;28. 10.1016/j.jse.2019.03.006
32. Parsons IMt, Millett PJ, Warner JJ. Glenoid wear after shoulder hemiarthroplasty: quantitative radiographic analysis. Clin Orthop Relat Res 2004:120-125. 10.1097/01.blo.0000119249.61696.f1
33. Salkeld SL, Patron LP, Lien JC, Cook SD, Jones DG. Biological and functional evaluation of a novel pyrolytic carbon implant for the treatment of focal osteochondral defects in the medial femoral condyle: assessment in a canine model. J Orthop Surg Res 2016;11:155-155. 10.1186/s13018-016-0488-5
34. Saltzman MD, Chamberlain AM, Mercer DM, Warme WJ, Bertelsen AL, Matsen FA, 3rd. Shoulder hemiarthroplasty with concentric glenoid reaming in patients 55 years old or less. J Shoulder Elbow Surg 2011;20:609-615. 10.1016/j.jse.2010.08.027
35. Schnetzke M, Rick S, Raiss P, Walch G, Loew M. Mid-term results of anatomical total shoulder arthroplasty for primary osteoarthritis using a short-stemmed cementless humeral component. The Bone & Joint Journal 2018;100-B:603-609. 10.1302/0301-620X.100B5.BJJ-2017-1102.R2
36. Schoch B, Schleck C, Cofield RH, Sperling JW. Shoulder arthroplasty in patients younger than 50 years: minimum 20-year follow-up. J Shoulder Elbow Surg 2015;24:705-710. 10.1016/j.jse.2014.07.016
37. Sperling JW, Cofield RH, Rowland CM. Minimum fifteen-year follow-up of Neer hemiarthroplasty and total shoulder arthroplasty in patients aged fifty years or younger. J Shoulder Elbow Surg 2004;13:604-613. 10.1016/s1058274604001296
38. Thomas SR, Sforza G, Levy O, Copeland SA. Geometrical analysis of Copeland surface replacement shoulder arthroplasty in relation to normal anatomy. J Shoulder Elbow Surg 2005;14:186-192. 10.1016/j.jse.2004.06.013
39. Werner BS, Stehle J, Abdelkawi A, Plumhoff P, Hudek R, Gohlke F. Progressive glenoid bone loss caused by erosion in humeral head resurfacing. Orthopade 2017;46:1028-1033. 10.1007/s00132-017-3483-6

Legends

Tables

I. Scoring system for internal rotation

II. Descriptions of Favard and modified Walch classifications

III. Preoperative diagnoses and clinical function in Constant score

IV. Glenoid bone loss

V. Preoperative glenoid morphology and evolution of glenoid morphology according to Favard classification and modified Walch classification

Figures

1) Method for quantifying medial glenoid bone loss
2) Graph depicting mean glenoid bone loss for each year of follow-up
3) X-rays of a patient with little glenoid erosion at 7 years follow-up
4) Change in Constant score from preoperatively to short-term and mid-term follow-up
5) Scatter graph of relationship between pain reduction on visual analog scale (VAS) and glenoid wear
6) Axial radiographs showing glenohumeral realignment postoperatively after PyC hemiarthroplasty with concentric glenoid reaming in a patient with preoperative posterior subluxation (Walch B2)

Table I: Scoring system for internal rotation

Internal rotation score	Level reached
0	Thigh
1	Gluteal
2	Iliosacral joint
3	Lumbar spine
4	Thoracic spine
5	Scapula

Table II: Description of the Favard and modefied Walch classifications

Classification	Type/grade	Frequency of subtypes
Modefied Walch [3]	A1	Centred in cross-sectional plane without erosion
	A2	Centred in cross-sectional plane with medial erosion
	B1	Posterior subluxation without erosion
	B2	Posterior subluxation with biconcavity due to neoglenoid
	B3	Posterior subluxation with posterior erosion, neoglenoid takes up the entire glenoid in cross-sectional plane
	C	Dysplastic glenoid with >25° retroversion
	D	Anterior subluxation with/without glenoid anteversion
Favard [8]	E0	Centred in AP x-ray without erosion
	E1	Centred in AP x-ray with medial erosion
	E2	Superior eccentricity with biconcave erosion
	E3	Superior eccentricity with monoconcave erosion
	E4	Inferior eccentricity with biconcave erosion

480 **Table III**: Constant score for different preoperative diagnoses

Diagnosis	**n**	**Preoperative Constant score**	**Constant score at final follow-up**	**Increase in Constant score**
Osteoarthritis	20	47	80	33
- Type A (Walch)	9	52	80	28
- Type B (Walch)	11	40	80	39
▪ With reaming	8	51	87	36
▪ Without reaming	12	45	76	31
Arthritis of instability	3	35	86	51
Avascular necrosis of the humeral head	3	42	64	22
Post-traumatic arthritis	4	45	79	33
Psoriatic arthritis	1	52	78	26

481

482

483 **Table IV**: Glenoid bone loss

Outcome	Measurement (mm)
Mean distance from glenoid surface to SGN	
- 2 days postoperatively	17.1 (± 3.83)
- At latest follow-up	15.7 (± 3.41)
Mean bone loss at latest follow-up	1.4 (± 1.20)
Mean bone loss per year	0.3 (± 0.26)
Mean bone loss after 1 year	0.8 (± 0.66)
Mean bone loss after 2 years	1.1 (± 1.08)

484 Value in brackets is (± standard deviation)

485

Table V: Preoperative glenoid morphology and evolution thereof according to the modified Walch and Favard classifications [3+8]

Modified Walch			
Preoperative glenoid morphology	Frequency	Glenoid evolution	Frequency
A1	7	B2 to B3	1
A2	11	A1 to D (antero-superior)	1
B1	1	B1 to A2 (without reaming)	3
B2	8	A1 to B1	1
B3	2	B2 to A2 **after reaming**	3
C	0	B2 to B1 **after reaming**	1
D	2	D (biconcave) to A2 **after reaming**	1
		A1 to A2 **after reaming**	1
Favard			
Preoperative glenoid morphology	Frequency	Glenoid evolution	Frequency
E0	9	E0 to E1	1
E1	21	E0 to mild E2 after cranialisation	1
E2	1	E1 to E2	1
E3	0	E0 to E1 **after reaming**	2

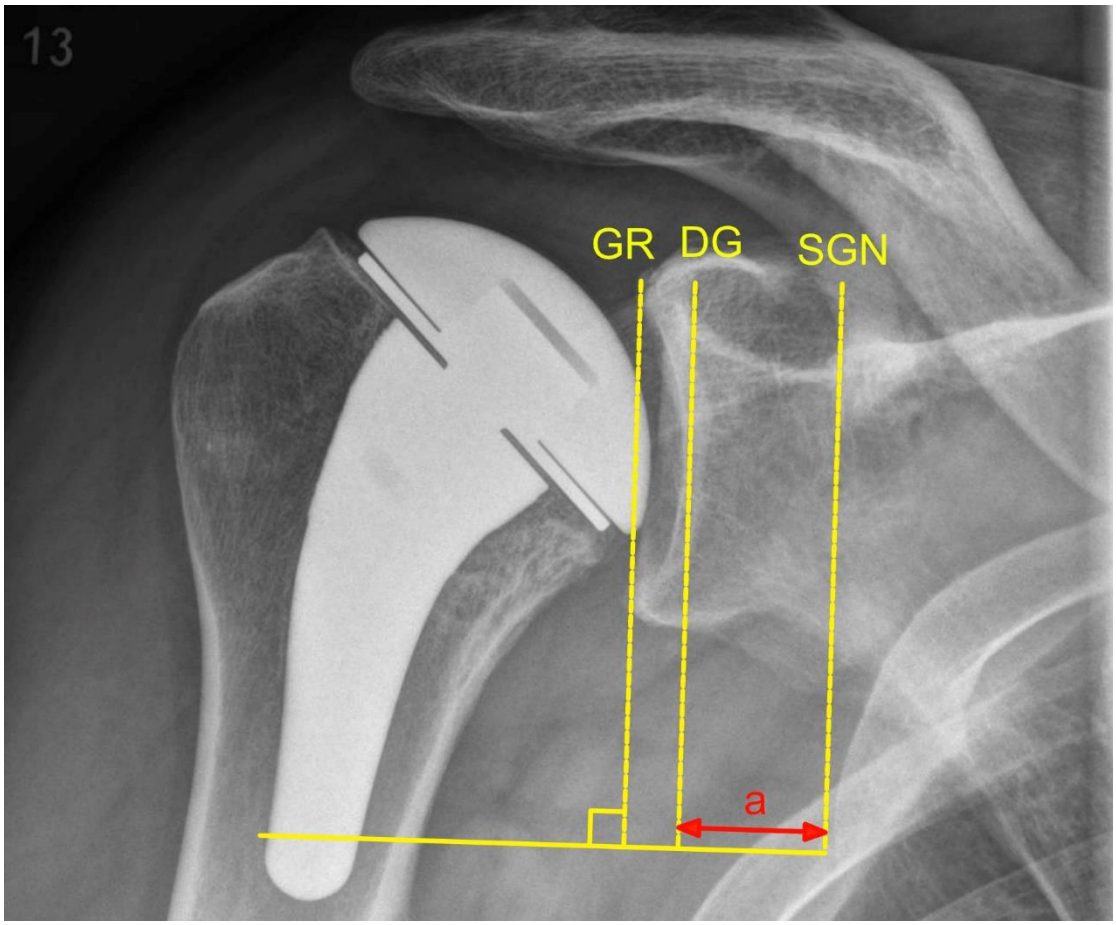

Figure 1: Method for quantifying medial glenoid bone loss. First a line was drawn along the superior and inferior glenoid rim (GR). Then a line parallel to this was placed on the deepest point of the glenoid (DG). Finally, the distance (a) from DG to a parallel line drawn intersecting the spinoglenoid notch (SGN) was measured.

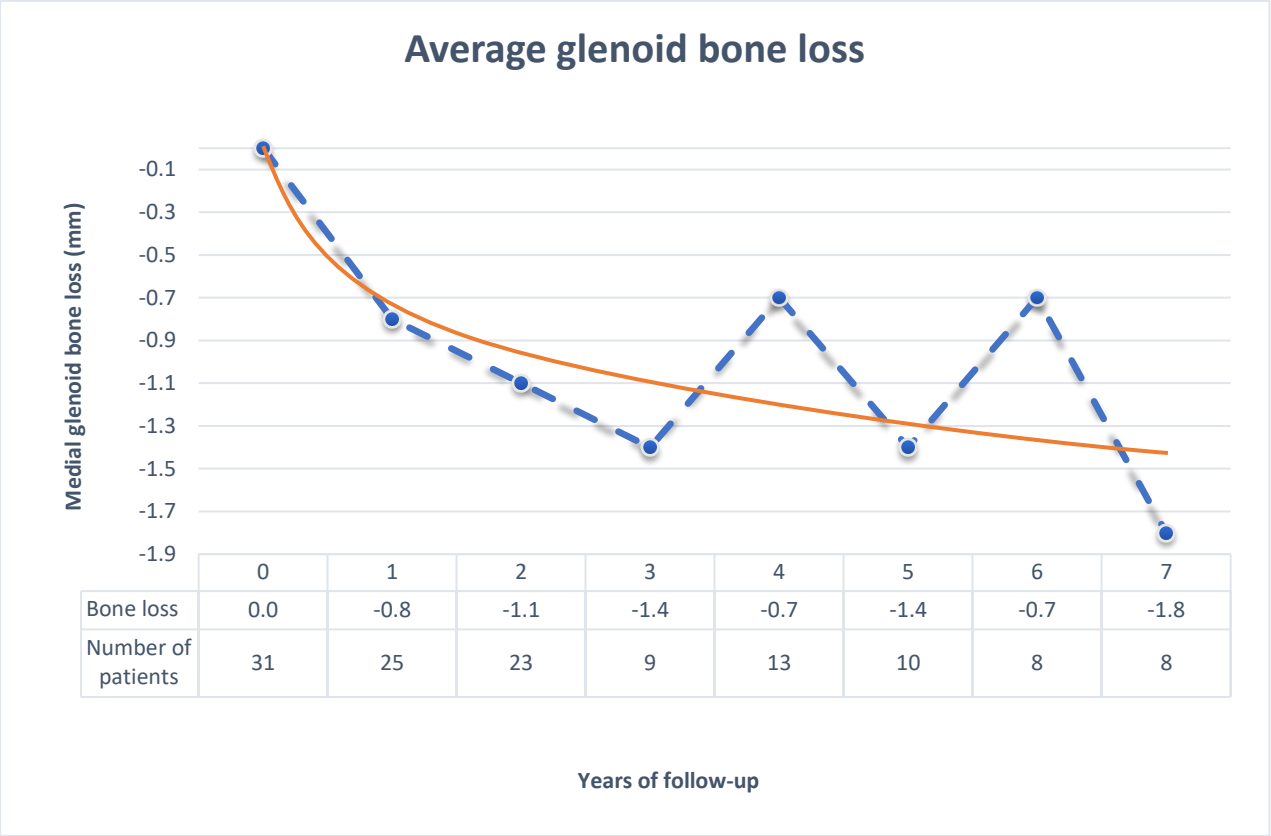

	0	1	2	3	4	5	6	7
Bone loss	0.0	-0.8	-1.1	-1.4	-0.7	-1.4	-0.7	-1.8
Number of patients	31	25	23	9	13	10	8	8

Figure 2: Graph depicting mean glenoid bone loss for the specified number of patients who had x-ray data available for each year of follow-up. The 9 patients with 3-year data and 10 patients with 5-year data were largely the same group, as were the 13 patients with 4-year and 8 patients with 6-year data. The red line represents a line of best fit.

Figure 3: AP and axial images of a 52 year old male patient 3 months after PyC HA (a, c) and 7 years postoperatively (b, d). After 7 years of follow-up there is little glenoid bone loss.

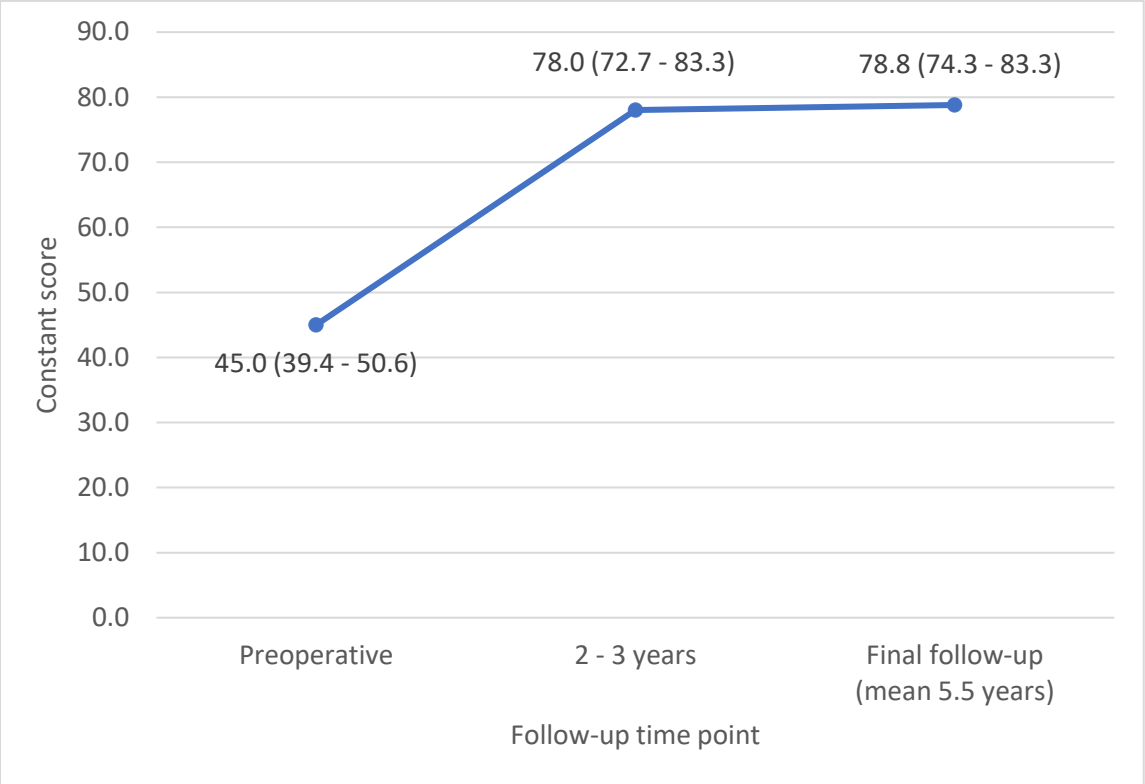

Figure 4: Development of Constant score from preoperative to short-term and mid-term follow-up. The mean and 95% confidence interval are displayed.

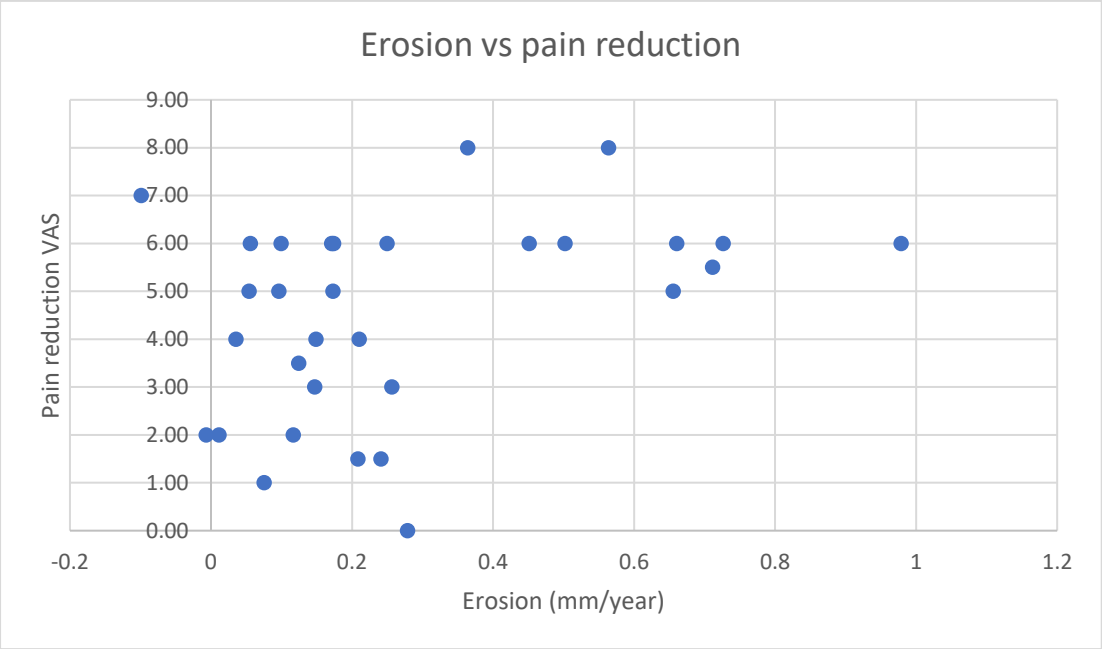

Figure 5: Scatter graph of relationship between pain reduction and glenoid wear. There is a weak correlation suggesting those with more erosion have better pain reduction.

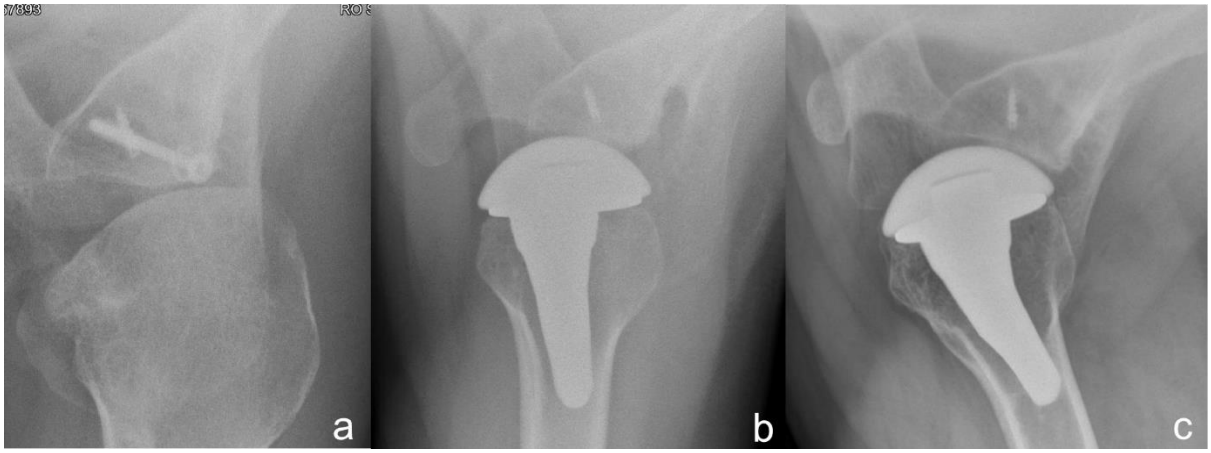

Figure 6: Axial x-rays of a patient with post-traumatic arthritis (glenoid fracture and ORIF) with posterior subluxation and B2 erosion preoperatively (a), 3 months after PyC HA with concentric glenoid reaming (b) and 5.5 years postoperatively (c). Postoperatively the prosthetic head is centrally aligned and it remains centred at latest follow-up. Initially the glenoid joint line is diffuse but later a clear cortex can be defined with slight sclerosis.

A 3-Dimensional Classification for Degenerative Glenohumeral Arthritis Based on Humeroscapular Alignment

Benjamin D. Kleim,*† MBBS, MD, MRes, Maximillian Hinz,† MD, Stephanie Geyer,† MD, Bastian Scheiderer,† MD, PhD, Andreas B. Imhoff,† MD, PhD, and Sebastian Siebenlist,† MD, MHBA, PhD

Investigation performed at the Department of Sports Orthopaedics, Technical University of Munich, Munich, Germany

Background: Seminal classifications of degenerative arthritis of the shoulder (DAS) describe either cuff tear arthropathy in the coronal plane or primary osteoarthritis in the cross-sectional plane. None consider a biplanar eccentricity.

Purpose/Hypothesis: The purpose of this study was to investigate humeroscapular alignment (HSA) of patients with DAS in both the anteroposterior (A-P) and superoinferior (S-I) planes on computed tomography (CT) after 3-dimensional (3D) reconstruction and develop a classification based on biplanar HSA in 9 quadrants. It was hypothesized that biplanar eccentricity would occur frequently.

Study Design: Cross-sectional study; Level of evidence, 3.

Methods: The authors analyzed 130 CT scans of patients who had undergone shoulder arthroplasty. The glenoid center, trigonum, and inferior angle of the scapula were aligned in a single plane using 3D reconstruction software. Subluxation of the HSA was measured as the distance from the center of rotation of the humeral head to the scapular axis (line from trigonum through glenoid center) and was expressed as a percentage of the radius of the humeral head in both the A-P and the S-I directions. HSA was described in terms of A-P alignment first (posterior/central/anterior), then S-I alignment (superior/central/inferior), for a total of 9 different alignment combinations. Additionally, glenoid erosion was graded 1-3.

Results: Subluxation of the HSA was 74.1% posterior to 23.5% anterior in the A-P direction and 17.2% inferior to 68.6% superior in the S-I direction. A central HSA was calculated as between 20% posterior to 5% anterior (A-P) and 5% inferior to 20% superior (S-I), after a graphical analysis. Posterior subluxation >60% of the radius was labeled as extraposterior, and static acetabularization was labeled as extrasuperior. Overall, 21 patients had central-central, 40 centrosuperior, and 1 centroinferior alignment. Of 60 shoulders with posterior subluxation, alignment was posterocentral in 31, posterosuperior in 25, and posteroinferior in 5. There were 3 patients with anterocentral and 4 anterosuperior subluxation; in addition, 4 cases with extraposterior and 17 with extrasuperior subluxation were identified.

Conclusion: There was a high prevalence of biplanar eccentricity in DAS. The 3D classification system using combined HSA and glenoid erosion can be applied to describe DAS comprehensively.

Keywords: classification; alignment; shoulder; arthritis.

The characteristics of glenoid morphology and alignment in degenerative arthritis of the shoulder (DAS) have typically been classified according to primary osteoarthritis (OA) in the cross-sectional plane or cuff tear arthropathy (CTA) in the coronal plane. The widely used modified Walch classification of glenohumeral OA uses cross-sectional computed tomography (CT).[1,21] CTA is categorized using the Hamada classification, which relies on anteroposterior (AP) x-ray images.[8] The Favard classification[4] further classifies the resulting glenoid wear also using AP x-rays (Table 1).

These commonly used seminal classification systems for DAS are based on 2-dimensional descriptions; however, none consider biplanar eccentricity. Several studies have since investigated the glenoid wear patterns in DAS in great detail and have found a combined eccentricity of the erosion sites.[1,5,9,13,17-19,22] Biplanar eccentricity in shoulder arthritis has also been documented in terms of humeroscapular alignment (HSA); Jacxsens et al[11] showed, on average, a posteroinferior alignment in cases classified as

The Orthopaedic Journal of Sports Medicine, 10(8), 23259671221110512
DOI: 10.1177/23259671221110512

TABLE 1
Summary of the Modified Walch,[1] Hamada,[8] and Favard[4] Classifications of OA and CTA[a]

Type/Grade	Description
	Modified Walch classification[1] (cross-sectional CT)
A1	Centered on cross-sectional plane without erosion
A2	Centered on cross-sectional plane with medial erosion
B1	Posterior subluxation without erosion
B2	Posterior subluxation with biconcavity due to neoglenoid
B3	Posterior subluxation with posterior erosion; neoglenoid covers the entire glenoid in cross-sectional plane
C	Dysplastic glenoid with >25° retroversion
D	Anterior subluxation with or without glenoid anteversion
	Hamada classification[8] (A-P radiograph)
1	Centered humeral head with acromiohumeral interval ≥6 mm on A-P radiograph
2	Superior migration of humeral head with acromiohumeral interval ≤5 mm
3	Superior migration of humeral head with acetabularization
4a	Grade 3 plus superior glenoid wear
4b	Grade 3 plus high-grade superior glenoid wear
5	Acetabularization and erosion culminating in necrosis of the humeral head
	Favard classification[4] (A-P radiograph)
E0	Centered on A-P radiograph without erosion
E1	Centered on A-P radiograph with medial erosion
E2	Superior eccentricity with biconcave erosion
E3	Superior eccentricity with monoconcave erosion
E4	Inferior eccentricity with biconcave erosion

[a]A-P, anteroposterior; CT, computed tomography; CTA, cuff tear arthropathy; OA, osteoarthritis.

Walch type B1. However, there are little data regarding HSA in 3 dimensions in DAS.

The purpose of the present study was to investigate HSA in both the anteroposterior (A-P) and the superoinferior (S-I) planes in patients with DAS and to determine whether existing classifications describe the disease comprehensively. We aimed to create a 3-dimensional (3D) CT classification that encompasses alignment in both planes as well as glenoid erosion. We hypothesized that biplanar eccentricity would be found frequently.

METHODS

Study Population

For this descriptive cohort study, we identified patients who had received a primary shoulder prosthesis (total shoulder arthroplasty, reverse shoulder arthroplasty, or hemiprosthesis) between 2009 and 2020 at the Department of Orthopaedic Sports Medicine of the University Hospital Rechts der Isar in Munich using a database search. Operative reports were assessed for a diagnosis of DAS (as type OA or CTA). Shoulders with diagnoses other than CTA or OA or without the availability of CT scans were excluded from the investigation. Of 299 shoulders undergoing primary shoulder replacement, 243 had a diagnosis of DAS. For 135 of these cases preoperative CT scans, performed according to a standardized in-house protocol (slice thickness, 0.9 mm; pitch, 0.39; tube current, 82 mA [range, 50-115 mA]; tube voltage, 120 kV), were available for analysis. All CT scans were taken less than 6 months before surgery. Five CT scans had to be excluded from the analysis: 2 for inadequate exposure of the scapula, 1 for movement artifact, and 2 for extreme erosion, which did not allow for reliable placement of the landmarks for measurement. The remaining CT scans of 130 shoulders were included in the study.

Demographically, the study patients had a mean age of 69.7 years (range, 38-88 years), and 60 (46%) were male. The diagnosis leading to arthroplasty had been documented as OA in 52 cases (40%) and CTA in 78 cases (60%).

*Address correspondence to Benjamin D. Kleim, MBBS, MD, MRes, Department of Sports Orthopaedics, Technical University of Munich, Ismaninger Str 22 81675 Munich, Germany (email: drkleim@doctors.org.uk).
†Department of Sports Orthopaedics, Technical University of Munich, Munich, Germany.
Final revision submitted March 8, 2022; accepted March 23, 2022.
The authors declared that they have no conflicts of interest in the authorship and publication of this contribution. AOSSM checks author disclosures against the Open Payments Database (OPD). AOSSM has not conducted an independent investigation on the OPD and disclaims any liability or responsibility relating thereto.
Ethical approval for this study was obtained from the Technical University of Munich.

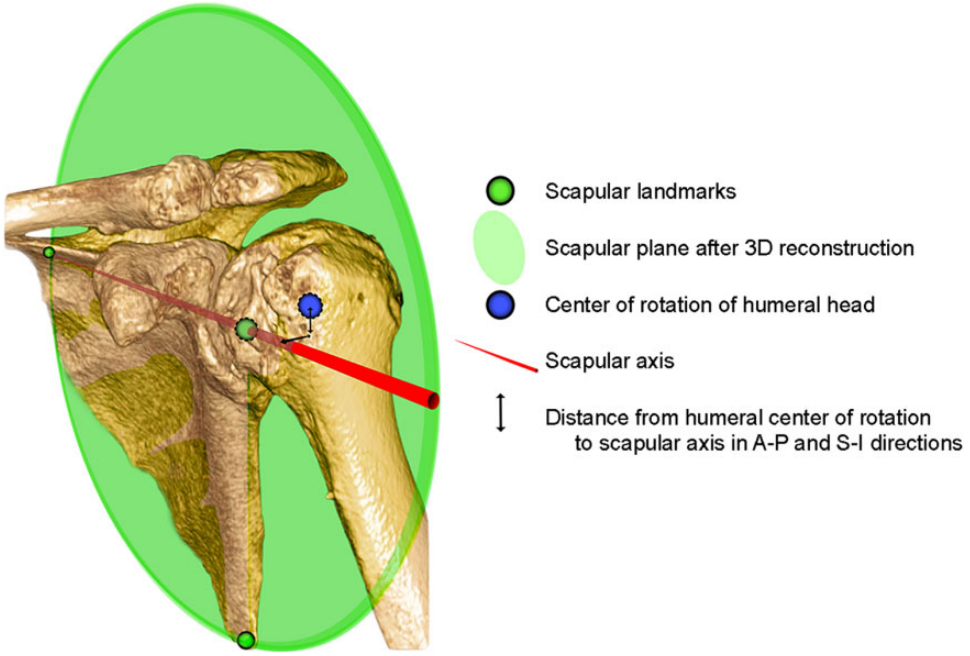

Figure 1. A 3-dimensional (3D) computed tomography reconstruction illustrating the scapular plane using the trigonum, glenoid center, and inferior angle of the scapula as landmarks. The scapular axis is the line passing from the trigonum through the glenoid center in this plane. The eccentricity of the center of rotation of the humeral head was measured as the distance to the scapular axis in both the anteroposterior (A-P) and superoinferior (S-I) directions.

Measurements

The analysis of the CT scans was performed by 2 experienced orthopaedic residents (B.D.K. and M.H.) with an interest in shoulder surgery, using a standardized self-developed protocol that was adapted from methods found in the literature.[6,11,12,25] First, glenoid morphology was described using the existing classifications for shoulder OA (modified Walch,[1] Favard,[4] and Hamada[8]), as has previously been done using CT.[20] This was done in consensus between the 2 observers.

Next, we used clinical 3D medical image viewing software (IDS7 Workstation Version 22.2; Sectra) to align the glenoid center, trigonum, and inferior angle of the scapula in a single plane. This reconstruction has previously been described as the scapular plane.[11,12,18] To ascertain the glenoid center, the midpoint was defined in the cross-sectional and coronal planes, disregarding osteophytes. The scapular axis was defined as a line passing through the scapular trigonum and glenoid center, in corroboration with previous work[11,12,18] (Figure 1). Placing a best-fit circle on the humeral head that followed the articular surface (where intact) and reliably intersected preserved extra-articular landmarks at the borders of the articular surface allowed an accurate determination of the center of rotation and size of the humeral head.[25] The center of rotation of the humeral head was always determined at the widest part of the ellipse of the humeral head in the coronal and cross-sectional views of the scapular plane, respectively, and then translated to the level of the scapular axis. This was particularly relevant to determine the center of rotation accurately in cases with a high degree of subluxation.

The amount of subluxation of the humeral head was then determined by measuring the distance of the center of rotation of the humeral head from the scapular axis in both the A-P and the S-I directions, as has previously been reported[12] (Figure 2). To correct for patient size, this was expressed as a percentage of the radius of the humeral head (similar to the method of describing subluxation in terms of diameter[23]) (Figure 3) in the corresponding plane using the following formula:

$$\%\ \text{subluxation} = \frac{\textit{distance of center of humeral head from scapula axis}}{\textit{radius of the humeral head}} \times 100$$

When calculated for each plane, respectively, this created vector coordinates where (0%, 0%) is the center.

Both observers measured all CT scans independently. Where large differences in measurements (>10%) occurred, the cases were reassessed together until a consensus was reached.

Finally, reconstructed coronal, cross-sectional, and sagittal CT planes were assessed to classify glenoid erosion (the third dimension). This was done according to a grading system which was based on previous studies and adapted for the 3D concept.[1,4] According to our descriptive observations, erosion was categorized into 3 types: grade 1, no significant bony erosion; grade 2, erosion causing a biconcavity if eccentric or a central crater; and grade 3, neoglenoid covering the entire glenoid surface in a single

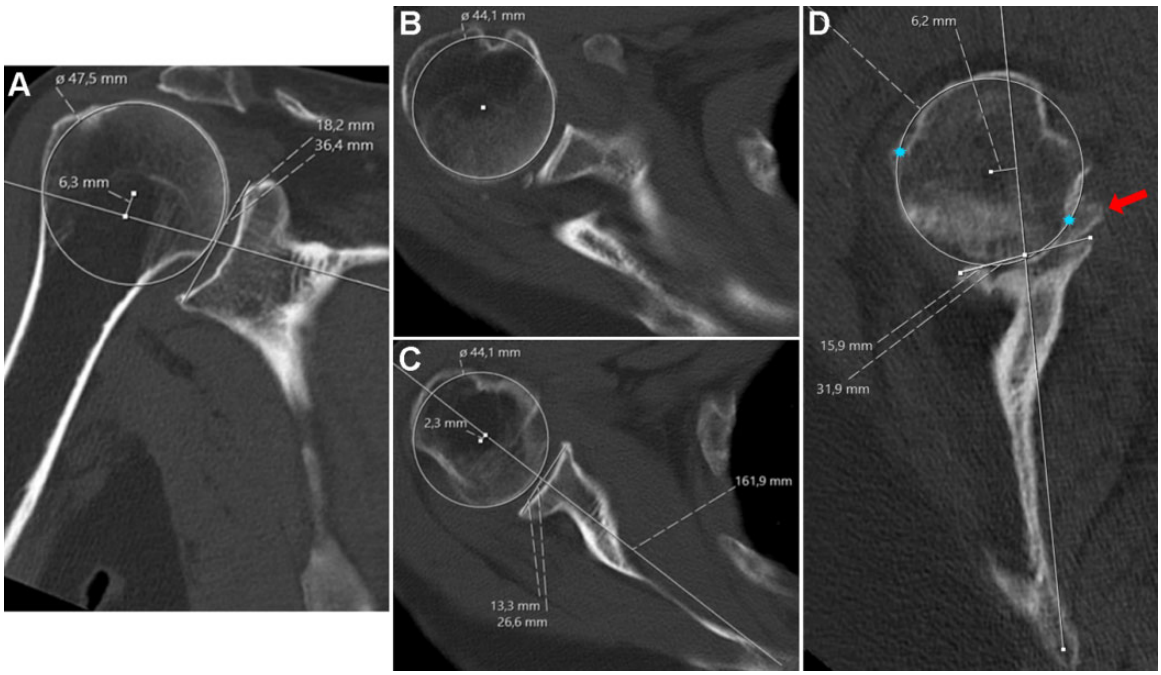

Figure 2. Measurement of humeroscapular alignment on (A) coronal plane and (B and C) cross-sectional plane computed tomography scans, after reconstruction of the scapular plane in 3 dimensions. (B) The center of rotation of the humeral head is determined at the widest part of the head and (C) is then translated down to the level of the scapular axis for measurement of subluxation. (D) Where there is higher-grade erosion with partial humeral head collapse and osteophytes, measurement is more challenging. Osteophytes (red arrow), whether on the humeral or glenoid side, must be disregarded. The center of rotation is determined with the aid of the intact outer margins of the humeral joint surface (blue stars).

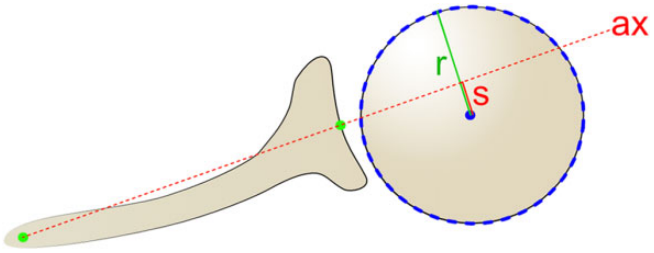

Figure 3. Method for determining the percentage of subluxation, *s*, of the center of rotation of the humeral head from the scapular axis, *ax*, relative to the radius, *r*, using the given formula.

plane (or severe central erosion including the glenoid rim) (Figure 4). All shoulders were graded accordingly, and the grade of erosion was combined with the alignment type to complete the 3D classification.

Statistical Analysis

The statistical analysis was performed using SPSS Version 26.0 (IBM Corp) software. The intraclass correlation coefficient (ICC) was used to measure reproducibility of the measurements between the 2 observers. Normal distribution was confirmed using the Shapiro-Wilk test. The Student *t* test was used to measure the significance of differences in normally distributed data sets, with the significance level set at $P = .05$. Values for measurements were rounded to 1 decimal place, and values for standard deviation as well as the ICC to 3 decimal places. As all available CT scans matching the inclusion criteria were included, a power analysis was not performed.

RESULTS

The results of DAS classification of the 130 shoulders according to the coronal (modified Walch[1]) and cross-sectional (Hamada[8] and Favard[4]) planes frequently suggested a biplanar eccentricity (Table 2), which none of the existing classification systems were able to comprehensively describe.

The mean diameter of the humeral head was 44.4 ± 4.05 mm (range, 36.1-55.8 mm) in the cross-sectional plane and 47.0 ± 4.02 mm (range, 36.5-56.2 mm) in the coronal plane of the reconstructed CT scans. A paired *t* test showed a significant difference between these values ($P < .001$), confirming an elliptical shape of the humeral head. The ICC values indicated a high degree of intrarater reproducibility for all measured variables: humeral head diameter (cross-sectional, 0.988; coronal, 0.981), A-P subluxation (0.901), and S-I subluxation (0.971).

Humeroscapular Alignment

In the A-P plane, the HSA ranged from 74.1% posterior to 23.5% anterior (SD, 19.3%) when expressed relative to the

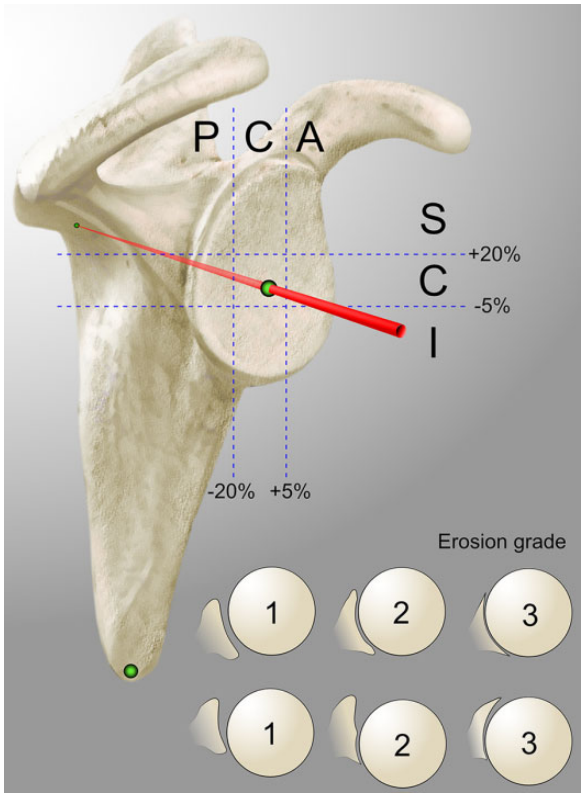

Figure 4. Diagrammatic representation of the 3-dimensional classification for degenerative arthritis of the shoulder. The humeroscapular alignment was described in terms of subluxation of the center of rotation of the humeral head in the anteroposterior direction (posterior [P]/central [C]/anterior [A]) and the superoinferior direction (superior [S]/central [C]/inferior [I]), for a total of 9 different combinations. Erosion was graded from 1 to 3, where 1 = no significant bony erosion, 2 = focal erosion forming a crater or biconcavity of the glenoid (in any location), and 3 = severe glenoid erosion involving the entire glenoid surface in any single plane (central or eccentric).

radius of the humeral head (absolute values, 16.9 mm posterior to 5.2 mm anterior). These values were then plotted graphically in ascending order (Figure 5). With the aid of this graph, as well as the impression gained while performing the measurements, HSA in the A-P plane was classified into 3 types: anterior (>5% anterior subluxation), central (between 5% anterior and 20% posterior subluxation), and posterior (>20% posterior subluxation). A posterior shift of the range for central alignment was supported by both the graphical analysis and our subjective impression and is probably due to the physiological retroversion of the glenoid. A further subtype (referred to as extraposterior) for particularly severe posterior subluxation was defined for those with >60% posterior subluxation, which corresponded to a notable step in the graph (see Figure 5, green arrow).

In the S-I plane, subluxation ranged from 17.2% inferior to 68.6% superior (SD, 17.1%) relative to the radius of the humeral head (absolute values, 4 mm inferior to 16.8 mm superior). These values were also plotted graphically in ascending order (Figure 6) and were classified into 3 types: superior (>20% superior subluxation), central (between 5% inferior and 20% superior subluxation), and inferior (>5% inferior subluxation). A superior shift of the range for central alignment was again supported by both the graphical analysis and our subjective impression and is probably due to the physiological inclination of the glenoid as well as the tension of the deltoid muscle. Additionally, a further subtype for those with extreme superior subluxation (referred to as extrasuperior) was defined for those with static acetabularization. All patients with >50% of superior subluxation (a notable step in the Figure 6 graph) were included in this subtype. Other cases with established acetabularization but <50% subluxation were unable to shift further superiorly because of the bony obstruction, which is why the absolute value of subluxation was not taken as the cutoff for this group.

TABLE 2
DAS Classified According to the Cross-Sectional (Modified Walch[1]) Versus Coronal (Hamada[8] and Favard[4]) Planes (N = 130 Shoulders)[a]

	Modified Walch[1]						
	A1	A2	B1	B2	B3	C	D
Hamada[8]							
1	2	12	4	11	10	0	3
2	11	3	4	4	4	0	1
3	10	2	7	1	1	0	2
4a	4	4	10	1	0	0	3
4b	0	2	2	7	3	0	1
5	0	0	0	0	0	0	1
Favard[4]							
E0	15	0	5	2	0	0	3
E1	9	20	18	12	13	0	5
E2	3	1	4	7	2	0	2
E3	0	1	0	1	2	0	1
E4	0	1	0	2	1	0	0

[a]Data are reported as number of shoulders. DAS, degenerative arthritis of the shoulder.

Using these values to categorize the HSA, the 130 shoulders were classified into the 9 possible combinations, as seen in Table 3. Only 21 shoulders were found to be centered in both planes. Biplanar eccentricity was found in 25 patients with posterosuperior, 5 patients with posteroinferior, and 4 patients with anterosuperior alignment (34/130; 26%).

The mean % A-P and S-I subluxation values for each alignment type can be found in Table 4. There was a significant difference in patients with anterior versus central versus posterior A-P subluxation ($P < .001$; Student's t test), as well as in patients with superior versus central versus inferior S-I subluxation ($P < .001$; Student's t test).

Glenoid Erosion

The frequency of the various glenoid erosion grades according to HSA alignment type is shown in Table 5. Figure 7

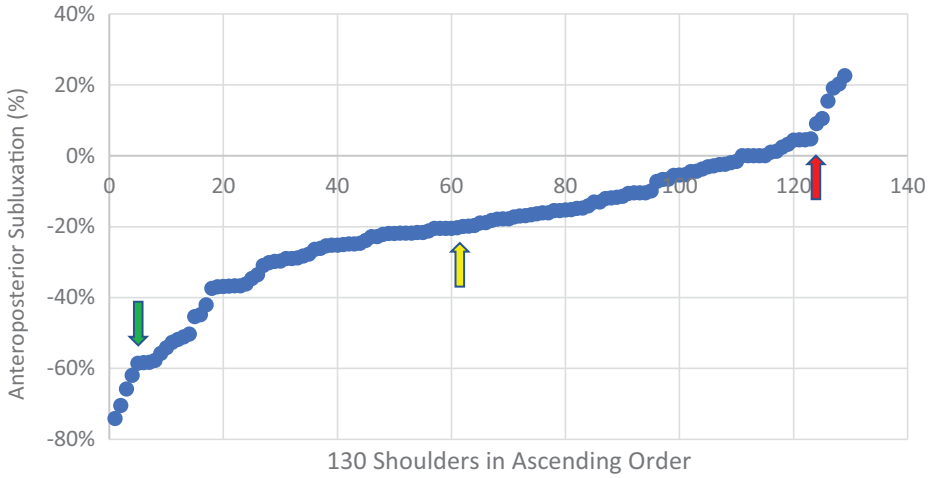

Figure 5. Values for anteroposterior subluxation plotted in ascending order; negative values indicate posterior subluxation. The red arrow marks the step from central to anterior alignment, the green arrow the step from posterior to extraposterior, and the yellow arrow the turning point of increasing posterior subluxation, seen around –20%, which was taken as the defining value between central and posterior alignment.

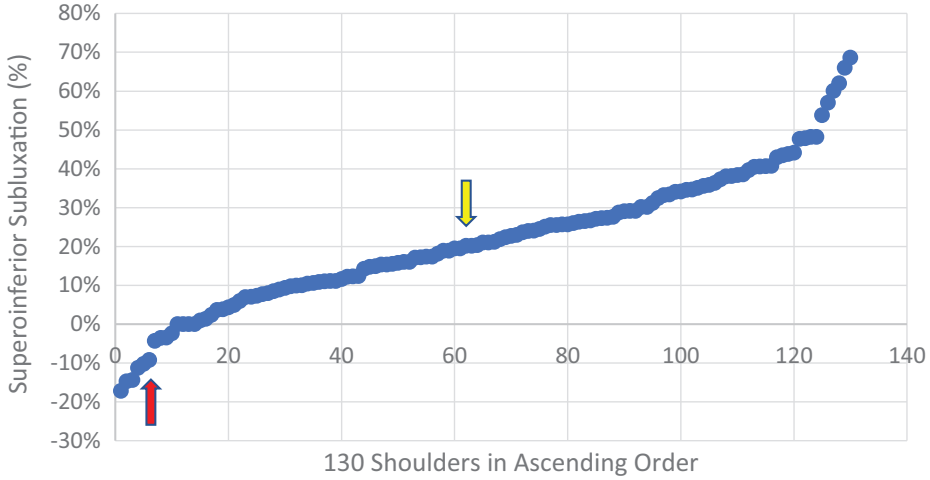

Figure 6. Values for superoinferior subluxation plotted in ascending order; negative values indicate inferior subluxation. The red arrow marks the step from central to inferior alignment, and the yellow arrow identifies the turning point of increasing superior subluxation, seen at around 20%, which was taken as the defining value between central and superior alignment.

TABLE 3
Frequency of Cases According to the Categorization System of HSA[a]

	Posterior	Central	Anterior
Superior	25 (1 XP, 6 XS)	40 (9 XS)	4 (2 XS)
Central	31 (3 XP)	21	3
Inferior	5	1	0

[a]Data in parentheses indicate the number of shoulders additionally defined as having extraposterior (XP) or extrasuperior (XS) alignment. HSA, humeroscapular alignment.

shows examples of grade 2 erosion, and Figure 8 shows an example of grade 3 erosion.

DISCUSSION

The findings of this study can be applied to quantify and categorize alignment of DAS. This will modernize and combine the findings of previous seminal studies that have classified arthritis of the shoulder.[1,4,8,9,21] Much of how previous classifications described glenoid erosion has been incorporated into this classification[1,4,8,21] and adapted for the 3D concept according to our descriptive observations. New to this classification is that the eccentricity is quantified in both the A-P and the S-I planes and combined with the associated glenoid wear in 3 dimensions. This seems to be important, as our study shows that a biplanar eccentricity is common, representing 26% of this cohort. Overall, we accept our hypothesis that biplanar eccentricity is common

TABLE 4
A-P and S-I Subluxation for Each Alignment Type[a]

	Posterior, %	Central, %	Anterior, %
Superior	A-P subluxation: –31.7 ± 12.8 (–20.5 to –70.4) S-I subluxation: 36.1 ± 13.2 (20.2 to 68.6)	A-P subluxation: –9.6 ± 7.70 (–19.8 to 4.8) S-I subluxation: 32.0 ± 9.39 (20.1 to 60.1)	A-P subluxation: 16.8 ± 6.10 (9.1 to 23.5) S-I subluxation: 45.6 ± 13.6 (29.0 to 62.0)
Central	A-P subluxation: –37.4 ± 16.1 (–20.3 to –74.1) S-I subluxation: 7.5 ± 7.12 (–4.3 to 18.8)	A-P subluxation: –7.5 ± 7.88 (–19.9 to 4.5) S-I subluxation: 12.3 ± 5.17 (0.9 to 19.5)	A-P subluxation: 17.7 ± 6.40 (10.5 to 22.6) S-I subluxation: 9.8 ± 5.57 (3.8 to 14.9)
Inferior	A-P subluxation: –37.6 ± 13.7 (–25.1 to –58.3) S-I subluxation: –12.6 ± 3.33 (–9.3 to –17.2)	A-P subluxation: –10.6 S-I subluxation: –14.4	—

[a]Data are reported as mean ± SD (range). Negative values indicate posterior (anteroposterior [A-P] direction) or inferior (superoinferior [S-I] direction) subluxation. The values are ranges of subluxation in each group of the classification, expressed in %. Dashes indicate none.

TABLE 5
Frequency of Cases According to HSA Type and Erosion Grade[a]

	Posterior	Central	Anterior
Superior			
Grade 1	7	20	1
Grade 2	16	15	3
Grade 3	2	5	
Central			
Grade 1	5	4	
Grade 2	11	13	3
Grade 3	15	4	
Inferior			
Grade 1			
Grade 2	3	1	
Grade 3	2		

[a]HSA, humeroscapular alignment. Blank cells indicate no cases.

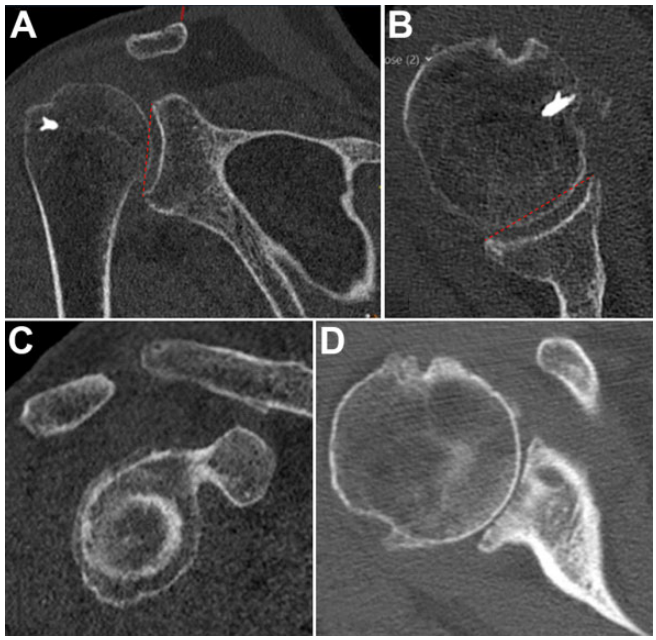

Figure 7. An example of grade 2 central-central erosion shown on computed tomography: (A) coronal, (B) cross-sectional, and (C) sagittal planes. There is medialization of the humeral head, and it bisects a line (dashed red line) drawn between the anterior and posterior and/or superior and inferior glenoid rim, as described previously.[1] (D) An example of grade 2 erosion with a central crater but without involvement of the entire glenoid surface.

and alignment can be categorized into 9 sectors, of which we have found cases in 8. This suggests that to comprehensively describe DAS, a 3D classification such as the one outlined in this work should be used.

Our findings align with a recent study that reported posterior glenoid erosion to be present superiorly, centrally, and inferiorly.[17] Terrier et al[19] also found glenoid erosion to be present in all 3 posterior sectors, as well as anteriorly, but predominantly posterosuperiorly. Jacxsens et al,[11] who assessed HSA in patients with Walch type B1 arthritis and averaged the values between all patients, showed a predominance of the combination of posterior with inferior subluxation of the humeral head. The results from our cohort, in which each patient was assessed individually, are more in line with those of Terrier et al[19] than those of Jacxsens et al.[11] This difference is likely to be in part due to the inclusion of not only OA but both types of DAS (CTA and OA) in our cohort.

In our classification, the grading of glenoid erosion has been adapted from the Walch and Favard systems and modified according to our descriptive observations for the 3D concept.[4,21] In contrast to this, the Lévigne classification of glenoid erosion, which was developed using A-P radiographs of patients with rheumatoid arthritis, categorizes the extent of erosion with reference to the coracoid process.[14] We did not incorporate this into our classification, because while it is useful in describing the depth of erosion on A-P radiographs, it does not describe the localization of erosion and does not transfer well to our 3D CT classification.

The extraposterior alignment type described in this classification (>60% posterior subluxation relative to the radius of the humeral head) corresponds to the cutoff,

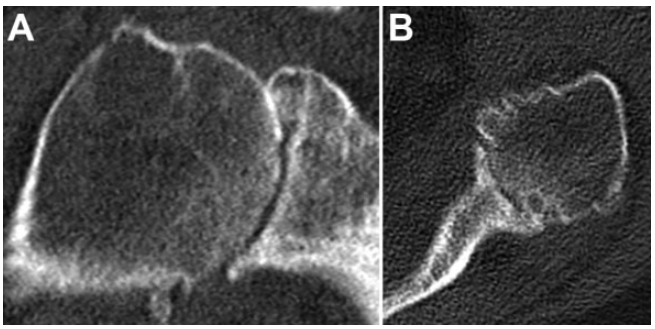

Figure 8. An example of grade 3 central-central erosion shown on computed tomography: (A) coronal and (B) cross-sectional planes. The entire glenoid surface, including the rim, is eroded and the humeral head is embedded.

80% humeral head subluxation relative to the diameter, for implanting an anatomical prosthesis suggested by Walch et al.[23]

Interestingly, not all patients diagnosed with CTA in our cohort had superior subluxation (69 cases with superior alignment, 78 cases of CTA, 8 cases labeled as OA with superior subluxation). It may be that these were cases with early disease (Hamada grade 1), but it is also possible that in some cases the subluxation was greater in the A-P plane after reconstruction. For example, a posterosuperior defect with intact subscapularis may cause little static superior but significant posterior subluxation, still reducing the distance to the acromion that lies posteriorly. This will require further investigation. Of cases with superior subluxation with a diagnosis of OA, 4 had posterosuperior and 4 centrosuperior alignment. This is an important finding and underlines the need to analyze DAS in both planes.

The underlying pathology leading to eccentric glenohumeral arthritis, which is described by our classification, has been investigated to some extent. While direct causality has not been clearly proven, it has been shown that posterior subluxation, preceded by degeneration of the posterior rotator cuff (RC), precedes the development of cartilaginous wear and glenoid erosion in Walch type B cases.[2,24] Increased retroversion/anteversion has also been described as a possible influencing factor.[2,20] Whereas fatty infiltration of the subscapularis muscle leads to arthritis with anterior subluxation,[18] progression of OA can lead to degeneration of all muscles of the RC, culminating in fatty infiltration and dysfunction.[3] Although not yet fully understood, it can be said that to some extent eccentric OA of the glenohumeral joint is, akin to CTA, a disease associated with RC insufficiency. Furthermore, initially centered disease may later become eccentric.[15] As the disease progresses, the RC tendons may degenerate and tear, resulting in a mixed pathology (ie, both OA and CTA). It therefore seems reasonable to describe these diseases in 1 combined classification.

The results of arthroplasty for cases with posterior subluxation are inconsistent.[10,16] Causes for this may include differences in the surgical procedure. However, this may also in part be because the extent of the disease, possibly of a bidirectional nature, is not fully understood by the surgeon preoperatively. Outcomes of cases with biplanar eccentricity may not be comparable to those with unidirectional subluxation, and specific treatment strategies may need to be developed. These may include the use of augmented glenoid components or bone grafting for eccentric erosion. Importantly, cases of OA with superior subluxation may not be suitable for anatomical shoulder replacement and instead require a semiconstrained reverse shoulder arthroplasty. Further studies will be required to determine the clinical significance of this classification.

The 3D reconstruction of the scapular axis has been shown to have a significant effect on measurements of HSA, with which we concur in our own experience.[12] We therefore recommend the use of an image-viewing program that allows a reconstruction of the scapular plane in 3 dimensions when assessing CT scans with this classification. While humeroglenoid alignment is more reproducibly measured than HSA, with and without 3D reconstruction of the scapular plane, this cannot be used to sensitively describe malalignment, as increased/decreased retroversion or inclination will lead to a falsely central measurement of the alignment.[12]

Limitations

One point of criticism that may be made regarding our work is that S-I alignment is usually not assessed in the lying patient on CT scans but rather on the standing radiographs, according to known refence values regarding the acromiohumeral interval.[7] However, we propose that the CT scan with a resting arm, without the interference of gravity, will show an insufficiency of the rotator cuff more sensitively than a standing A-P radiograph. The supine position in CT may also lead to differences in the alignment in the A-P plane when compared with axillary view radiographs taken while standing. Nevertheless, as this is a CT-based classification, all images are taken with the patient lying down, making comparisons fair.

The frequency of high-grade erosion and eccentricity in our cohort may not be representative of patients who undergo joint replacement overall. This is likely to be because, as a university hospital department, we are referred many patients with severe disease. Furthermore, the lack of shoulders with an anteroinferior alignment in our sample does not preclude the existence of these, which may be present in other cohorts. Our study focused purely on patients with OA and CTA. The spectrum of alignment may also differ if the use of the classification is extended to other diagnoses (eg, to patients with arthritis of instability, rheumatoid arthritis, and posttraumatic arthritis).

While the ICC for the measurements showed a high grade of reproducibility, we do not expect clinicians to spend as much time as we did for this in the clinical setting. A validation study to confirm reproducibility of the classification within and between clinicians is required in the future. Three-dimensional reconstruction, however, is paramount, and therefore adequate software and practice, as well as time, will be needed to do this reliably, which may limit the use of this classification. Having said this, 3D

planning software with automated reconstruction protocols is becoming more widely used, which will simplify the application of this classification. The clinical significance of this classification is yet to be determined. However, the present publication presents a method to analyze HSA and erosion in 3 dimensions using a 3D clinical image–viewing software, which gives clinical transferability to much of the knowledge gained by previous authors using complex modeling software.

CONCLUSION

This work has shown a high prevalence of biplanar eccentricity in DAS and has suggested cutoff values for the boundaries of centered HSA in both planes. We therefore suggest the use of a 3D classification, which applies the combined HSA as well as glenoid erosion to comprehensively describe DAS. The clinical significance of a classification like this has yet to be determined.

REFERENCES

1. Bercik MJ, Kruse K II, Yalizis M, et al. A modification to the Walch classification of the glenoid in primary glenohumeral osteoarthritis using three-dimensional imaging. *J Shoulder Elbow Surg*. 2016; 25(10):1601-1606.
2. Domos P, Checchia CS, Walch G. Walch B0 glenoid: pre-osteoarthritic posterior subluxation of the humeral head. *J Shoulder Elbow Surg*. 2018;27(1):181-188.
3. Donohue KW, Ricchetti ET, Ho JC, Iannotti JP. The association between rotator cuff muscle fatty infiltration and glenoid morphology in glenohumeral osteoarthritis. *J Bone Joint Surg Am*. 2018;100(5): 381-387.
4. Favard L, Lautmann S, Clement P. Osteoarthritis with massive rotator cuff-tear: the limitation of its current definitions. In: Walch G, Boileau P, eds. *Shoulder Arthroplasty*. Springer Berlin Heidelberg; 1999: 261-265.
5. Frankle MA, Teramoto A, Luo ZP, Levy JC, Pupello D. Glenoid morphology in reverse shoulder arthroplasty: classification and surgical implications. *J Shoulder Elbow Surg*. 2009;18(6):874-885.
6. Gerber C, Costouros JG, Sukthankar A, Fucentese SF. Static posterior humeral head subluxation and total shoulder arthroplasty. *J Shoulder Elbow Surg*. 2009;18(4):505-510.
7. Goutallier D, Le Guilloux P, Postel JM, et al. Acromio humeral distance less than six millimeter: its meaning in full-thickness rotator cuff tear. *Orthop Traumatol Surg Res*. 2011;97(3):246-251.
8. Hamada K, Fukuda H, Mikasa M, Kobayashi Y. Roentgenographic findings in massive rotator cuff tears. A long-term observation. *Clin Orthop Relat Res*. 1990;(254):92-96.
9. Iannotti JP, Jun BJ, Patterson TE, Ricchetti ET. Quantitative measurement of osseous pathology in advanced glenohumeral osteoarthritis. *J Bone Joint Surg Am*. 2017;99(17):1460-1468.
10. Iannotti JP, Norris TR. Influence of preoperative factors on outcome of shoulder arthroplasty for glenohumeral osteoarthritis. *J Bone Joint Surg Am*. 2003;85(2):251-258.
11. Jacxsens M, Van Tongel A, Henninger HB, et al. A three-dimensional comparative study on the scapulohumeral relationship in normal and osteoarthritic shoulders. *J Shoulder Elbow Surg*. 2016;25(10): 1607-1615.
12. Kim JH, Min YK. Normal range of humeral head positioning on the glenoid on magnetic resonance imaging: validation through comparison of computed tomography and magnetic resonance imaging. *Clin Shoulder Elbow*. 2018;21(4):186-191.
13. Knowles NK, Keener JD, Ferreira LM, Athwal GS. Quantification of the position, orientation, and surface area of bone loss in type B2 glenoids. *J Shoulder Elbow Surg*. 2015;24(4):503-510.
14. Lévigne C, Franceschi JP. Rheumatoid arthritis of the shoulder: radiological presentation and results of arthroplasty. In: Walch G, Boileau P, eds. *Shoulder Arthroplasty*. Springer Berlin Heidelberg; 1999: 221-230.
15. Logli AL, Pareek A, Nguyen NTV, Sanchez-Sotelo J. Natural history of glenoid bone loss in primary glenohumeral osteoarthritis: how does bone loss progress over a decade? *J Shoulder Elbow Surg*. 2021; 30(2):324-330.
16. Luedke C, Kissenberth MJ, Tolan SJ, Hawkins RJ, Tokish JM. Outcomes of anatomic total shoulder arthroplasty with B2 glenoids: a systematic review. *JBJS Rev*. 2018;6(4):e7.
17. Otto A, Scheiderer B, Murphy M, et al. Biconcave glenoids show three differently orientated posterior erosion patterns. *J Shoulder Elbow Surg*. 2021;30(11):2620-2628.
18. Siebert MJ, Chalian M, Sharifi A, et al. Correction to: Qualitative and quantitative analysis of glenoid bone stock and glenoid version: inter-reader analysis and correlation with rotator cuff tendinopathy and atrophy in patients with shoulder osteoarthritis. *Skeletal Radiol*. 2020;49(6):995-1003.
19. Terrier A, Ston J, Larrea X, Farron A. Measurements of three-dimensional glenoid erosion when planning the prosthetic replacement of osteoarthritic shoulders. *Bone Joint J*. 2014;96(4):513-518.
20. Verhaegen F, Meynen A, Matthews H, et al. Determination of pre-arthropathy scapular anatomy with a statistical shape model: part I—rotator cuff tear arthropathy. *J Shoulder Elbow Surg*. 2021;30(5): 1095-1106.
21. Walch G, Badet R, Boulahia A, Khoury A. Morphologic study of the glenoid in primary glenohumeral osteoarthritis. *J Arthroplasty*. 1999; 14(6):756-760.
22. Walch G, Collotte P, Raiss P, Athwal GS, Gauci MO. The characteristics of the Favard E4 glenoid morphology in cuff tear arthropathy: a CT study. *J Clin Med*. 2020;9(11):3704.
23. Walch G, Moraga C, Young A, Castellanos-Rosas J. Results of anatomic nonconstrained prosthesis in primary osteoarthritis with biconcave glenoid. *J Shoulder Elbow Surg*. 2012;21(11):1526-1533.
24. Walker KE, Simcock XC, Jun BJ, Iannotti JP, Ricchetti ET. Progression of glenoid morphology in glenohumeral osteoarthritis. *J Bone Joint Surg Am*. 2018;100(1):49-56.
25. Youderian AR, Ricchetti ET, Drews M, Iannotti JP. Determination of humeral head size in anatomic shoulder replacement for glenohumeral osteoarthritis. *J Shoulder Elbow Surg*. 2014;23(7):955-963.

Archives of Orthopaedic and Trauma Surgery (2023) 143:6159–6166
https://doi.org/10.1007/s00402-023-04890-2

ORTHOPAEDIC SURGERY

Validation of a novel 3-dimensional classification for degenerative arthritis of the shoulder

Benjamin D. Kleim[1] · Sebastian Lappen[1] · Pavel Kadantsev[1] · Hannes Degenhardt[1] · Lorenz Fritsch[1] · Sebastian Siebenlist[1] · Maximilian Hinz[1]

Received: 21 February 2023 / Accepted: 13 April 2023 / Published online: 12 June 2023

Abstract

Introduction A novel three-dimensional classification to comprehensively describe degenerative arthritis of the shoulder (DAS) was recently published by our group. The purpose of the present work was to investigate intra- and interobserver agreement as well as validity for the three-dimensional classification.

Materials and methods Preoperative computed tomography (CT) scans of 100 patients who had undergone shoulder arthroplasty for DAS were randomly selected. Four observers independently classified the CT scans twice, with an interval of 4 weeks, after prior three-dimensional reconstruction of the scapula plane using a clinical image viewing software. Shoulders were classified according to biplanar humeroscapular alignment as posterior, centered or anterior (> 20% posterior, centered, > 5% anterior subluxation of humeral head radius) and superior, centered or inferior (> 5% inferior, centered, > 20% superior subluxation of humeral head radius). Glenoid erosion was graded 1–3. Gold-standard values based on precise measurements from the primary study were used for validity calculations. Observers timed themselves during classification. Cohen's weighted κ was employed for agreement analysis.

Results Intraobserver agreement was substantial ($\kappa = 0.71$). Interobserver agreement was moderate with a mean κ of 0.46. When the additional descriptors extra-posterior and extra-superior were included, agreement did not change substantially ($\kappa = 0.44$). When agreement for biplanar alignment alone was analyzed, κ was 0.55. The validity analysis reached moderate agreement ($\kappa = 0.48$). Observers took on average 2 min and 47 s (range 45 s to 4 min and 1 s) per CT for classification.

Conclusions The three-dimensional classification for DAS is valid. Despite being more comprehensive, the classification shows intra- and interobserver agreement comparable to previously established classifications for DAS. Being quantifiable, this has potential for improvement with automated algorithm-based software analysis in the future. The classification can be applied in under 5 min and thus can be used in clinical practice.

Keywords Classification · Validation · Interobserver · Intraobserver · Reproducibility · Shoulder arthritis · Osteoarthritis · Cuff tear arthropathy

Introduction

Degenerative arthritis of the shoulder (DAS) has traditionally been classified as either primary osteoarthritis (OA) or cuff tear arthropathy (CTA). Anteroposterior subluxation and glenoid morphology in the axial plane for OA is to date commonly described using the modified Walch classification [1, 2]. Superoinferior subluxation and glenoid erosion for CTA has commonly been described in the coronal plane (anteroposterior X-ray) according to the Hamada or Visotsky-Seebauer and Favard classifications, respectively [3–5]. These classifications were originally developed for describing X-ray findings and in the case of the modified Walch classification were later adapted for axial computed tomography (CT).

In recent years, however, several authors described biplanar eccentricity in glenoid erosion patterns [6–10]. OA patients often develop rotator cuff insufficiency as the disease progresses, or the disease may initially be influenced by rotator cuff degeneration [11–13]. Especially in

✉ Benjamin D. Kleim
drkleim@doctors.org.uk

[1] Department of Sports Orthopaedics, Technical University of Munich, Ismaninger Str 22, 81675 Munich, Germany

early disease, axial plane imaging of a lying patient is more sensitive for superior subluxation than standing X-ray [14].

Therefore, a new three-dimensional (3D) classification, which categorizes anteroposterior (A-P) and superoinferior (S-I) alignment with erosion for DAS, was developed and recently published [15].

Whilst this novel classification allows for a more comprehensive description of DAS, it has not yet been validated. The higher number of categories compared to previous classifications may reduce reproducibility [1, 3, 4]. However, alignment is quantifiable in this novel classification, making this less subjective and possibly ameliorating the effect of more categories on reproducibility. Furthermore, the complex nature of the 3D classification and need for CT reconstruction could make it too time consuming for clinical practice, which requires investigation.

The purpose of this study was to validate the 3D classification for patients with DAS. The hypothesis was that validity as well as interobserver reliability would be moderate and, therefore, comparable to values for previous classifications from the literature (Table 1) [16–20].

Materials and methods

Patient population

For this validation study, a previously investigated cohort of patients with DAS who underwent primary shoulder arthroplasty (total shoulder arthroplasty, hemiarthroplasty or reverse shoulder arthroplasty) at the Department of Orthopaedic Sports Medicine of the University Hospital Rechts der Isar in Munich between 2009 and 2020 were identified [15]. 299 shoulder arthroplasty cases were performed in this period for DAS. 135 of these had preoperative CT scans taken according to a standardized in-house protocol (pitch, 0.39; slice thickness, 0.9 mm; tube voltage, 120 kV; tube current, 82 mA [range, 50–115 mA]) available for analysis. CT scans had been taken no more than 6 months prior to surgery. Five of these patients were excluded from analysis: in two cases, the scapula was not adequately exposed, one due to movement artefact and two due to severe erosion, due to which landmarks for measurement could not be reliably placed. Of the remaining 130 CTs, 100 were selected at random.

Demographically the mean patient age was 70 years (range 38–88 years) and 49 were male (49%). 59 patients had a preoperative diagnosis of CTA and 41 of OA, as documented in the operative reports.

CT classification

A clinical image viewing software capable of 3D reconstruction (IDS7 Workstation Version 22.2; Sectra) was used to classify CT images according to the previously described 3D classification for DAS [15]. First, the scapular plane was reconstructed in 3D using two-dimensional orthogonal planes (axial, coronal, and sagittal): The glenoid center, trigonum and inferior angle of the scapula were aligned in one plane (Fig. 1). Following this, anteroposterior alignment was classified as posterior, centered or anterior; superoinferior alignment was classified as superior, centered or inferior and combined with an erosion grade (1–3) (Fig. 2) [15]. Subluxation of the humeral head center from the scapular axis (line passing from

Table 1 Summary of a PubMed search for studies investigating intraobserver and interobserver agreement for the Walch or modified Walch classification published in the last 5 years and Hamada, Visotsky-Seebauer and Favard classifications published in the last 15 years

Study	Classifications investigated	Imaging modality	Intraobserver agreement	Interobserver agreement
Ricchetti et al. 2021 [16]	Modified Walch	CT using 3D image viewer	Moderate to substantial (κ = 0.51–0.61)	Moderate (κ = 0.43)
Hopkins et al. 2021 [18]	Walch	CT and MRI	CT: Substantial (κ = 0.71) MRI: Substantial (κ = 0.71)	CT: Fair (κ = 0.29) MRI: Fair (κ = 0.34)
Shukla et al. 2019 [17]	Modified Walch	X-ray and CT	CT: Substantial (κ = 0.73) X-ray: Substantial (κ = 0.73)	CT: Moderate (κ = 0.52) X-ray: Moderate (κ = 0.55)
Kappe et al. 2011 [19]	Hamada, Visotsky-Seebauer and Favard	X-ray	Hamada: Substantial (κ = 0.75) V-S: Substantial (κ = 0.73) Favard: Substantial (κ = 0.76)	Hamada: Moderate (κ = 0.41) V-S: Moderate (κ = 0.55) Favard: Fair (κ = 0.31)
Iannotti et al. 2010 [20]	Visotsky-Seebauer, Favard and Hamada	X-ray	V-S: Substantial (κ = 0.69) Hamada: Almost perfect (κ = 0.87) Favard: Moderate (κ = 0.59)	V-S: Fair (κ = 0.39) Hamada: Moderate (κ = 0.42) Favard: None to slight (κ = 0.13)

V-S Visotsky-Seebauer; κ kappa; 3D 3-dimensional; *CT* computed tomography; *MRI* magnetic resonance imaging

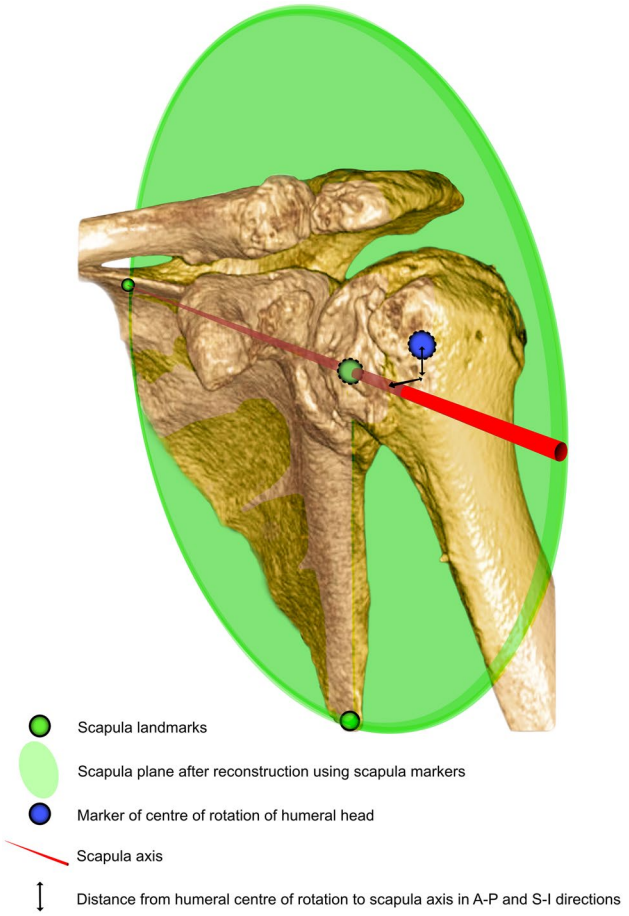

Fig. 1 Illustration of the scapular plane and its landmarks (trigonum, glenoid center, and inferior angle of the scapula) on a three–dimensional reconstruction of a shoulder CT. The scapular axis, in reference to which alignment in the anteroposterior and superoinferior directions was measured, is the red line passing from the trigonum through the glenoid center [15]

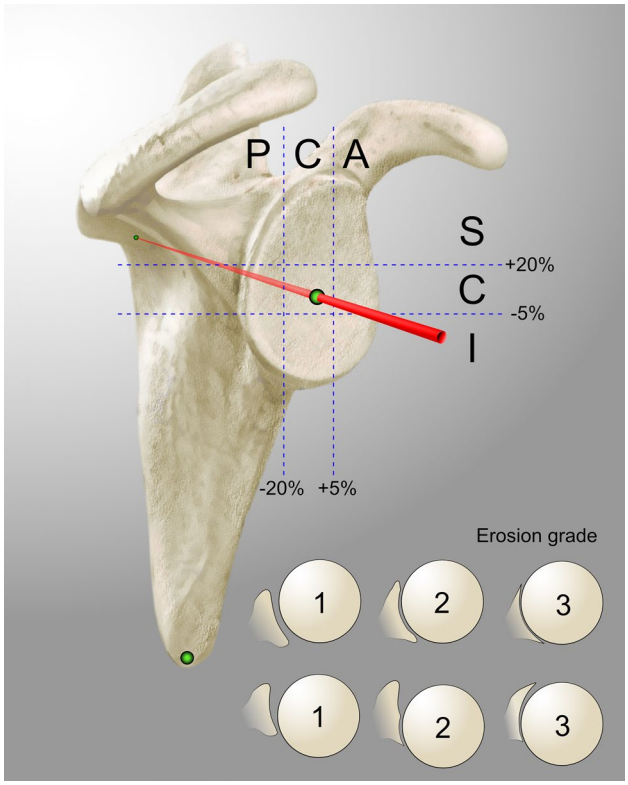

Fig. 2 Schematic illustration of the three–dimensional classification for degenerative arthritis of the shoulder. The humeroscapular alignment was described in terms of alignment of the center of rotation of the humeral head in relation to the scapula axis in the anteroposterior direction (posterior [P]/central [C]/anterior [A]) and the superoinferior direction (superior [S]/central [C]/inferior [I]), for a total of nine different combinations. Erosion was graded from 1 to 3, where 1 = no significant bony erosion, 2 = focal erosion forming a crater or biconcavity of the glenoid (central or eccentric), and 3 = severe glenoid erosion involving the entire glenoid surface in any single plane (central or eccentric) [15]

trigonum scapulae through glenoid center) was assessed relative to the radius of the humeral head (Fig. 3):

$$\%\ \text{of subluxation} = \frac{\text{distance of center of humeral head from scapula axis}}{\text{radius of the humeral head}} \times 100$$

Centered alignment was defined as: Between 20% posterior and 5% anterior subluxation in the anteroposterior direction; between 5% inferior and 20% superior subluxation in the superoinferior direction, as previously described [15]. Additionally, alignment could be described as extra-posterior if posterior subluxation was > 60% of the humeral head *radius* (> 80% of the *diameter*), or extra-superior if static acetabularization was present [15]. Where alignment seemed to be obvious, observers were not required to perform measurements. In borderline cases the scapula axis, humeral circumference with center point, radius and subluxation of the center of the humeral head

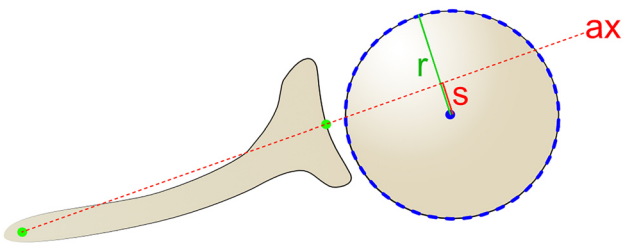

Fig. 3 Method for determining the percentage of subluxation, *s*, of the humeral head center from the scapular axis, ax, relative to the radius of the humeral head, *r* [15]

Fig. 4 Method for measurement of humeroscapular alignment on **A** coronal plane and **B** and **C** cross–sectional plane computed tomography scans, after reconstruction of the scapular plane in three dimensions. (B) The center of rotation of the humeral head is determined at the widest cross–section of the head and (**C**) is then translated down to the level of the scapular axis for measurement of subluxation. (**D**) When higher–grade erosion with partial humeral head collapse and osteophytes are present, measurement is more challenging. Osteophytes (red arrow), whether on the humeral or glenoid side, are disregarded. The center of rotation is determined using the intact outer margins of the humeral joint surface (blue stars) as landmarks [15]

from the scapula axis was determined to quantify the classification (Fig. 4).

After a training seminar of 2 h, four orthopedic residents with experience in shoulder surgery (none of which were involved in measurements for the primary study) independently classified all 100 CT scans. An instructional handout for the 3D reconstruction and classification method, including a schematic representation of the 3D classification (Fig. 2) was provided. Four weeks after the first analysis the same four observers classified the 100 CT scans for a second time. Observers were blinded to the results of their previous attempt. The time needed to apply the new classification was measured for each observer. To simulate time available in clinical practice, observers were instructed to aim to take < 5 min per CT.

The humeroscapular alignment of all 100 shoulder CTs had previously been precisely measured and classified for the primary study by BDK and MH, with almost perfect interobserver agreement for alignment measurements [15]. Erosion was classified in consensus between the two observers. These existing classification values (shown in Table 2) were taken as the gold-standard against which the present values of the Observers were compared for validation.

Table 2 Case distribution of 100 CTs analyzed for the present study according to the 3-dimensional classification, based on measurements from the primary study [15]

	EG	Posterior	Central	Anterior
Superior	1	6	16	–
	2	12	10	3
	3	1	5	–
Central	1	–	4	–
	2	10	10	2
	3	13	3	–
Inferior	1	–	–	–
	2	3	1	–
	3	1	–	–

EG erosion grade

Additionally, 15 shoulders were described as having extra–superior and 4 as extra–posterior alignment

Statistical analysis

Statistical analysis was performed using SPSS Version 29.0 (IBM-SPSS, New York, USA) software. Classification values were recoded and entered as string variables with three ordinal categories. Intraobserver reliability, interobserver reliability and validity (compared to existing gold-standard values) were calculated using Cohen's weighted κ with linear weighting. Mean averages of comparisons of both

attempts from each observer (four comparisons for each individual intraobserver comparison) were calculated for all six individual interobserver comparisons between the four observers. A 95% confidence interval (CI) was determined for each value. Cohen's categorization of agreement (≤ 0 indicating no agreement, 0.01–0.20 none to slight, 0.21–0.40 fair, 0.41– 0.60 moderate, 0.61–0.80 substantial and 0.81–1.00 almost perfect agreement) was taken for interpretation of κ values [21]. Tests were two-sided, with a significance level of 0.05.

Results

The intraobserver reliability of the 3D classification showed substantial agreement with a Cohen's weighted κ of 0.71 (CI 0.63–0.79).

Interobserver agreement was moderate overall, ranging from fair to substantial (Table 3). When assessing agreement for biplanar alignment only (disregarding erosion grade), interobserver agreement improved in each comparison, ranging from moderate to substantial, although differences were not statistically significant (Table 3). Interobserver agreement did not change substantially when the additional descriptors of extra-posterior and extra-superior were included ($\kappa = 0.44$ [CI 0.33–0.55]).

The validity analysis, comparing the observers' classifications to the gold-standard values, showed moderate agreement (Table 4). As observed in the interobserver analysis, when the additional descriptors of extra-posterior and extra-superior were included the agreement for validity did not change substantially ($\kappa = 0.45$ [CI 0.33–0.56]). When analyzing the quantifiable aspect (biplanar alignment) only, κ increased to 0.53 (CI 0.41–0.65).

The mean average for time taken for classification was 2 min and 47 s (range 45 s to 4 min 1 s).

Table 4 Results of the validity analysis showing the mean average of both attempts from each observer with the gold standard values

	Agreement with gold standard
Observer 1	0.49 (0.37–0.61)
Observer 2	0.52 (0.41–0.63)
Observer 3	0.53 (0.41–0.64)
Observer 4	0.37 (0.25–0.48)
Total average	0.48 (0.36–0.59)

Cohen's weighted kappa values are displayed with a 95% confidence interval

Key findings

The most important finding of this study was that interobserver agreement (reproducibility) for the 3D classification for DAS was moderate ($\kappa = 0.46$). Despite being more comprehensive than these, agreement for the 3D classification is at least comparable to that reported for previous monoplanar (two-dimensional) classifications for CTA or OA of the shoulder (Table 1) [16–20]. This is likely to be due to the

Table 3 Interobserver agreement using Cohen's weighted kappa for biplanar alignment with erosion values (upper half) and biplanar alignment only (lower half)

Alignment with erosion	Observer 4 (Attempts 1 and 2)	Observer 3 (Attempts 1 and 2)	Observer 2 (Attempts 1 and 2)
Observer 1 (Attempts 1 and 2)	0.37 (0.26–0.48)	0.67 (0.61–0.73)	0.46 (0.34–0.57)
Observer 2 (Attempts 1 and 2)	0.40 (0.27–0.54)	0.49 (0.38–0.61)	
Observer 3 (Attempts 1 and 2)	0.38 (0.27–0.50)		
Overall mean average	**0.46 (0.36–0.57)**		
Alignment only	Observer 4 (Attempts 1 and 2)	Observer 3 (Attempts 1 and 2)	Observer 2 (Attempts 1 and 2)
Observer 1 (Attempts 1 and 2)	0.41 (0.30–0.54)	0.71 (0.64–0.78)	0.55 (0.42–0.68)
Observer 2 (Attempts 1 and 2)	0.47 (0.34–0.60)	0.61 (0.48–0.73)	
Observer 3 (Attempts 1 and 2)	0.46 (0.33–0.59)		
Overall mean average	**0.55 (0.42–0.65)**		

The mean average agreement for comparisons of both attempts from each observer with both attempts from all other observers is displayed alongside a 95% confidence interval. The overall mean for each analysis is highlighted in bold

quantifiable nature of the alignment aspect of this classification, which allows for clear cut-off values. Furthermore, observers were able to apply the classification in < 5 min, which reflects time available in clinical practice.

Interpretation

The most recently published study to compare intra- and interobserver agreement for the modified Walch classification (modifications by Bercik and Iannotti) is the most comparable to the present study, as it also employed a 3D image viewing software for analysis of CT images [1, 16, 22]. This study also found moderate inter- and moderate to substantial intraobserver agreement, comparable to the results of the present study [16]. The authors did not find an improvement in agreement when considering the alignment groups only (without erosion subgrouping). Although there was a trend to improved agreement when disregarding erosion grading, this was also not statistically significant in the present analysis.

An equally recent study investigating the original Walch classification found substantial intraobserver but only fair interobserver agreement for both CT and MRI images [18]. Shukla et al. found substantial intra- and moderate interobserver agreement of the modified Walch classification on both X-ray and CT [17]. They suggest the use of automated computer-based analysis of CT scans to improve the reproducibility of the modified Walch classification further. Whilst the modifications to the Walch classification have improved interobserver agreement somewhat, it remains a two-dimensional classification with subjective intergroup cut-offs [1, 22]. The presently investigated 3D classification is quantifiable with precise cut-off values and may therefore be better suited to such an automated computer-based software algorithm. Being 3D, it is more aligned with current developments in imaging software, preoperative planning and instrumentation than previous two-dimensional classification systems [23–25]. Modern 3D planning software already comprise algorithms which calculate the anteroposterior subluxation and these merely need to be modified to include superoinferior alignment [24, 26].

Established classification systems for CTA are all based on AP X-ray images and show variable levels of intra- and interobserver agreement [19, 20]. Whilst the Visotsky-Seebauer and Hamada classifications showed substantial to almost perfect intraobserver agreement with moderate interobserver agreement, the Favard classification was found to have moderate intra- and none to slight interobserver agreement [19, 20]. Despite its higher complexity, the presently investigated 3D classification shows comparable intra- and interobserver agreement to those established CTA classifications with better agreement (Visotsky-Seebauer and Hamada). These seminal classifications helped lead to a greater understanding of the disease process, but are now based on outdated technology. To further differentialize diagnosis, treatment and outcomes for DAS for clinical application and in research, use of the 3D classification should be considered.

A validation analysis is new to the present study of the 3D classification for DAS. This can be performed as the alignment of the classification is quantifiable and, therefore, *correct* classification is possible. The erosion subgrouping aspect is, as in the previous classifications subject to interpretation. Statistically significant moderate agreement was found in this validity analysis, rendering it valid for the classification of DAS. Validity agreement was moderate both for alignment alone and for alignment with erosion grade. As agreement for alignment was only moderate when detailed measurements are not performed ubiquitously (simulation of clinical practice), this has potential to be improved using automated software algorithms in the future.

Limitations

The validity analysis of this study depends on gold-standard values, of which only the alignment aspect is quantifiable. Despite being determined by two orthopedic surgeons in consensus the erosion aspect is, as in previous classifications, subject to some interpretation. The analysis, therefore, gives a breakdown of these aspects. As the 3D classification and method to reconstruct the scapular plane was new to the four observers, the training provided may not have been sufficient to get the best results possible. However, this reflects clinical practice as future users of this classification will not receive training beyond reading the published information available. As all observers in the present study were orthopedic residents, a difference in performance for varying levels of expertise could not be investigated.

Generalizability

As a wide variety of classification types were examined in a large sample of patients with DAS by four independent observers, the results of this study can be applied widely to classification of DAS. Availability of an image viewer with the ability of 3D planar reconstruction is, however, a prerequisite for reliable use of this classification.

Conclusion

The 3D classification for DAS is valid. Despite being more comprehensive, the classification shows intra- and interobserver agreement comparable to previously established classifications for DAS. Being quantifiable, this has potential for improvement with automated algorithm-based software

analysis in the future. The classification can be applied in under 5 min and thus can be used in clinical practice.

Funding Open Access funding enabled and organized by Projekt DEAL. No funding was sought or received to undertake this study.

Data availability The datasets generated and analyzed during the current study are not publicly available due to institutional data protection agreements but are available from the corresponding author on reasonable request.

Declarations

Conflict of interest BDK, SL, PK, HD, LF: None. SS is a consultant for Arthrex, Medi, KLSM and MH is on the scientific editorial board of OH and his immediate family hold no relevant shares and receive no royalties from any commercial entity related to the subject of this article. MH: None.

Ethical approval Ethical approval was sought and granted by the ethics commission of the medical faculty of the Technical University of Munich (reference number: 301/20 S) in advance of study commencement.

References

1. Bercik MJ, Kruse K 2nd, Yalizis M, Gauci MO, Chaoui J, Walch G (2016) A modification to the Walch classification of the glenoid in primary glenohumeral osteoarthritis using three-dimensional imaging. J Shoulder Elbow Surg 25(10):1601–1606. https://doi.org/10.1016/j.jse.2016.03.010
2. Walch G, Badet R, Boulahia A, Khoury A (1999) Morphologic study of the Glenoid in primary glenohumeral osteoarthritis. J Arthroplasty 14(6):756–760. https://doi.org/10.1016/S0883-5403(99)90232-2
3. Favard L, Lautmann S, Clement P (1999) Osteoarthritis with Massive Rotator Cuff-Tear: The Limitation of its Current Definitions. In: Walch Gilles, Boileau Pascal (eds) Shoulder Arthroplasty. Springer Berlin Heidelberg, Berlin, Heidelberg, pp 261–265
4. Hamada K, Fukuda H, Mikasa M, Kobayashi Y (1990) Roentgenographic findings in massive rotator cuff tears. A long-term observation. Clin Orthop Relat Res 254:92–96
5. Visotsky JL, Basamania C, Seebauer L, Rockwood CA, Jensen KL (2004) Cuff tear arthropathy: pathogenesis, classification, and algorithm for treatment. J Bone Joint Surg Am 86(2):35–40
6. Terrier A, Ston J, Larrea X, Farron A (2014) Measurements of three-dimensional glenoid erosion when planning the prosthetic replacement of osteoarthritic shoulders. Bone Joint J 96(4):513–518. https://doi.org/10.1302/0301-620x.96b4.32641
7. Otto A, Scheiderer B, Murphy M, Savino A, Mehl J, Kia C, Obopilwe Me E, DiVenere J, Cote MP, Denard PJ, Romeo AA, Mazzocca AD (2021) Biconcave glenoids show three differently orientated posterior erosion patterns. J Shoulder Elbow Surg. https://doi.org/10.1016/j.jse.2021.04.028
8. Knowles NK, Keener JD, Ferreira LM, Athwal GS (2015) Quantification of the position, orientation, and surface area of bone loss in type B2 glenoids. J Shoulder Elbow Surg 24(4):503–510. https://doi.org/10.1016/j.jse.2014.08.021
9. Siebert MJ, Chalian M, Sharifi A, Pezeshk P, Xi Y, Lawson P, Chhabra A (2020) Correction to: qualitative and quantitative analysis of glenoid bone stock and glenoid version: inter-reader analysis and correlation with rotator cuff tendinopathy and atrophy in patients with shoulder osteoarthritis. Skeletal Radiol. https://doi.org/10.1007/s00256-020-03386-z
10. Jacxsens M, Van Tongel A, Henninger HB, De Coninck B, Mueller AM, De Wilde L (2016) A three-dimensional comparative study on the scapulohumeral relationship in normal and osteoarthritic shoulders. J Shoulder Elbow Surg 25(10):1607–1615. https://doi.org/10.1016/j.jse.2016.02.035
11. Hartwell MJ, Harold RE, Sweeney PT, Seitz AL, Marra G, Saltzman MD (2021) Imbalance in axial-plane rotator cuff fatty infiltration in posteriorly worn glenoids in primary glenohumeral osteoarthritis: an mri-based study. Clin Orthop Relat Res 479(11):2471–2479. https://doi.org/10.1097/corr.0000000000001798
12. Domos P, Checchia CS, Walch G (2018) Walch B0 glenoid: pre-osteoarthritic posterior subluxation of the humeral head. J Shoulder Elbow Surg 27(1):181–188. https://doi.org/10.1016/j.jse.2017.08.014
13. Walker KE, Simcock XC, Jun BJ, Iannotti JP, Ricchetti ET (2018) Progression of glenoid morphology in glenohumeral osteoarthritis. JBJS 100(1):49–56. https://doi.org/10.2106/jbjs.17.00064
14. Mirzayan R, Donohoe S, Batech M, Suh BD, Acevedo DC, Singh A (2020) Is there a difference in the acromiohumeral distances measured on radiographic and magnetic resonance images of the same shoulder with a massive rotator cuff tear? J Shoulder Elbow Surg 29(6):1145–1151. https://doi.org/10.1016/j.jse.2019.10.020
15. Kleim BD, Hinz M, Geyer S, Scheiderer B, Imhoff AB, Siebenlist S (2022) A 3-dimensional classification for degenerative glenohumeral arthritis based on humeroscapular alignment. Orthop J Sports Med 10(8):23259671221110510. https://doi.org/10.1177/23259671221110512
16. Ricchetti ET, Khazzam MS, Denard PJ, Dines DM, Bradley Edwards T, Entezari V, Friedman RJ, Garrigues GE, Gillespie RJ, Grawe BM, Green A, Hatzidakis AM, Gabriel Horneff J, Hsu JE, Jawa A, Jin Y, Johnston PS, Jun BJ, Keener JD, Kelly JD 2nd, Kwon YW, Miniaci A, Morris BJ, Namdari S, Spencer EE, Strnad G, Williams GR Jr, Iannotti JP (2021) Reliability of the modified Walch classification for advanced glenohumeral osteoarthritis using 3-dimensional computed tomography analysis: a study of the ASES B2 Glenoid Multicenter Research Group. J Shoulder Elbow Surg 30(4):736–746. https://doi.org/10.1016/j.jse.2020.07.013
17. Shukla DR, McLaughlin RJ, Lee J, Cofield RH, Sperling JW, Sánchez-Sotelo J (2019) Intraobserver and interobserver reliability of the modified Walch classification using radiographs and computed tomography. J Shoulder Elbow Surg 28(4):625–630. https://doi.org/10.1016/j.jse.2018.09.021
18. Hopkins CM, Azar FM, Mulligan RP, Hollins AM, Smith RA, Throckmorton TW (2021) Computed tomography and magnetic resonance imaging are similarly reliable in the assessment of

glenohumeral arthritis and glenoid version. Arch Bone Jt Surg 9(1):64–69. https://doi.org/10.22038/abjs.2020.38922.2035
19. Kappe T, Cakir B, Reichel H, Elsharkawi M (2011) Reliability of radiologic classification for cuff tear arthropathy. J Shoulder Elbow Surg 20(4):543–547. https://doi.org/10.1016/j.jse.2011.01.012
20. Iannotti JP, McCarron J, Raymond CJ, Ricchetti ET, Abboud JA, Brems JJ, Williams GR (2010) Agreement study of radiographic classification of rotator cuff tear arthropathy. J Shoulder Elbow Surg 19(8):1243–1249. https://doi.org/10.1016/j.jse.2010.02.010
21. Cohen J (1960) A coefficient of agreement for nominal scales. Educ Psychol Measur 20(1):37–46. https://doi.org/10.1177/001316446002000104
22. Iannotti JP, Jun B-J, Patterson TE, Ricchetti ET (2017) Quantitative measurement of osseous pathology in advanced glenohumeral osteoarthritis. JBJS 99(17):1460–1468. https://doi.org/10.2106/jbjs.16.00869
23. Cabarcas BC, Cvetanovich GL, Gowd AK, Liu JN, Manderle BJ, Verma NN (2019) Accuracy of patient-specific instrumentation in shoulder arthroplasty: a systematic review and meta-analysis. JSES Open Access 3(3):117–129. https://doi.org/10.1016/j.jses.2019.07.002
24. Olaiya OR, Nadeem I, Horner NS, Bedi A, Leroux T, Alolabi B, Khan M (2020) Templating in shoulder arthroplasty - A comparison of 2D CT to 3D CT planning software: a systematic review. Shoulder Elbow 12(5):303–314. https://doi.org/10.1177/1758573219888780
25. Harding GT, Bois AJ, Bouliane MJ (2021) A novel method for localization of the maximum glenoid bone defect during reverse shoulder arthroplasty. JSES Int 5(4):667–672. https://doi.org/10.1016/j.jseint.2021.04.001
26. Olszewski A, Ramme AJ, Maerz T, Freehill MT, Warner JJP, Bedi A (2020) Vault perforation after eccentric glenoid reaming for deformity correction in anatomic total shoulder arthroplasty. J Shoulder Elbow Surg 29(7):1450–1459. https://doi.org/10.1016/j.jse.2019.11.011